Vinicius de Oliveira

Optimal operation strategies for dynamic processes under uncertainty

Doctoral thesis for the degree of philosophiae doctor

Trondheim, April 2016

Norwegian University of Science and Technology
The Faculty of Natural Sciences and Technology
Department of Chemical Engineering

NTNU

Norwegian University of Science and Technology

Doctoral thesis
for the degree of philosophiae doctor

The Faculty of Natural Sciences and Technology
Department of Chemical Engineering

ISBN 978-82-326-1548-3 (printed version)
ISBN 978-82-326-1549-0 (electronic version)
ISSN

Doctoral theses at NTNU, 2016:105

Printed by Skipnes

Summary

The main focus of this thesis is to find implementation strategies for the optimal operation of processes during transients. That is, we do not focus on the algorithms to solve a given dynamic optimization problem, but on how to implement the solution in practice using control. The underlining theme is based on the general idea of finding feedback policies that give acceptable performance even in the presence of model uncertainties and disturbances. By 'acceptable' we mean that important constraints should always be satisfied and the economic performance should be near the optimal. In this thesis we considered different classes of applications, each one with their own particularities and challenges.

The first part of the work deals with the optimal operation of thermal energy storage systems. We consider the optimal operation of energy storage in buildings with focus on the optimization of an electric water heating system. The optimization objective is to minimize the energy costs of heating the water, with the requirement that we should satisfy the uncertain demand at any time. The main complications in this problem are the time varying nature of the electricity price and the unpredictability of the future water demand. First, we present a detailed problem formulation which may also be suitable similar problems. Many insights into the optimization problem formulation are given and guidelines on implementation strategies including feedback control structures are proposed.

Next, we use the hot water system as an example to illustrate our proposed implementation strategy based on hierarchical decomposition of the optimization-control problem. In our approach, economic objectives and control objectives are decoupled using a two-layer cascade feedback structure. We show that the decomposed optimization problem can be written as a simple linear program (LP) which can be solved very efficiently. The main result is that great economical benefits can be obtained at a very low computational cost and suitable for low cost embedded hardware.

Part two of the thesis is dedicated to an intelligent anti-slugging con-

trol system for offshore oil production maximization. Existing anti-slug control systems are not robust and tend to become unstable after some time, because of inflow disturbances or plant dynamic changes, thus, requiring constant supervision and retuning. A second problem is the fact that the ideal setpoint is unknown and we could easily choose a suboptimal or infeasible operating point. Here we present a method to tackle these problems. Our complete control solution is composed of an autonomous supervisor that seeks to maximize production by manipulating a pressure setpoint and a robust adaptive controller that is able to quickly identify and adapt to changes in the plant. Our proposed solution has been tested in a experimental rig and the results are very encouraging. An analysis of the robustness and optimality of different linear controllers for slug mitigation is also carried out in this part of the thesis.

In the last part of the thesis we discuss near-optimal operation strategies using simple feedback control. First, we generalize the neighbouring extremal control design that has been presented in the literature (Gros et al., 2009b) to explicitly handle measurement noise and implementation errors. The benefits of our method are illustrated in a case study where we show that the sensitivity of the controller performance to measurement noise is considerably reduced. Finally, we extended the concept of self-optimizing control (Skogestad, 2000; Alstad and Skogestad, 2007) for the near-optimal operation of transient processes. The main idea is to find a function of the measurements whose trajectory is optimally invariant to disturbances and then track the trajectory using standard feedback controllers. Doing so results in near-optimal economic operation in spite of disturbances without the need for re-optimization. We show that the invariant trajectories can be computed as linear combinations of the measurement vector, where the time-varying combination matrix is easily obtained from optimal sensitivities.

Acknowledgements

This thesis would not have been completed without the help of many people. First of all, I want to thank Prof. Sigurd Skogestad, who spent a great amount of time and energy to support me during these years. His enthusiasm, patience and remarkable talent makes him the ideal supervisor. Without his contributions this thesis would not have been accomplished. Special thanks to my co-supervisor Johannes Jäschke, who has always been very helpful, positive and supportive, even at those difficult times when progress has been slower than we desired.

I would like to thank all my colleagues (past and current) at the Chemical Engineering Department for helping creating such a relaxed and welcoming working environment. Sincere thanks go to my officemates Chriss Grimholt, Sebastian Roll and Vladmiros Minasidis for all the fun moments we had together during this long journey. Thanks to Esmaeil Jahanshahi for introducing me to the interesting world of anti-slug control.

Thanks to my family, for always believing and encouraging me throughout the years. Finally, my biggest thanks to Marcela, for being so understanding and supportive. Thanks to you all.

Vinicius de Oliveira
Trondheim, April 2016

Contents

Chapter 1

Introduction

In this chapter we define the scope of the thesis, motivate the work and put the thesis chapters into perspective. An overview of the thesis and a list of the publications emerging from this thesis are given.

1.1 Motivation and scope

Optimal operation is essential for improved productivity and profitability of process plants. The general economic objective is to achieve maximum profit while meeting environmental, safety and product requirements. During operation of chemical processes we have available degrees of freedom that we want to use in order to optimize the process behaviour. We are here not concerned with the optimization of these systems but rather on how the decisions are implemented. The main challenge in implementing the right decision is the presence of disturbances. These include variations in exogenous variables, such as energy prices, changes in the process dynamics and operating conditions, parameter variations in the system as well as model uncertainties.

For processes whose economics are mainly defined by the steady-state behaviour the concept of self-optimizing control was introduced by Skogestad (2000). Self-optimizing control focus on selecting a set of controlled variables that, when kept at constant setpoints, indirectly result in optimal economic operation in spite of disturbances. Diverse systematic methods are available to find the right variables to control for steady-state problems. Skogestad and Postlethwaite (2005a) proposed the Maximum Gain Rule to select individual measurements. Alstad and Skogestad (2007) presented the Null Space method to select optimal linear combinations of measurements to be controlled. An extension of that work was presented in Alstad et al.

(2009), where measurement noise is also considered. Jäschke and Skogestad (2012) extended the scope of self-optimizing control to polynomial systems.

The focus of this thesis has been on processes where the dynamic behaviour is important in terms of economic performance. Optimal economic operation of many processes may be in general formulated as a dynamic optimization problem. This includes problems that are transient in nature, where the dynamic behaviour must be considered, such as batch operations, grade changes and start-up and shut-down of continuous plants (Biegler, 2010). We have identified the following main cases which are treated in three different parts of this thesis:

- Optimal dynamic use of inventories (storage) to take advantage of time varying electricity prices. Our main case study here is on thermal energy storage in buildings with focus on the hot water system. This is the topic of Part I.

- Operation of dynamic systems where the optimal operation point is at the limit of dynamic infeasibility. Our application is the anti-slug control problem which refers to the problem of stabilizing severe flow oscillations in offshore multiphase pipelines (Jahanshahi et al., 2013). This is the theme of Part II.

- Optimal operation of batch systems under uncertainties. This is presented in Part III of the thesis.

The main focus of this thesis is to find implementation strategies for the optimal operation of dynamic systems. That is, we are not only interested in obtaining the optimal solution to a given dynamic optimization problem, but even more so on the practical implementation (using feedback control), where the important issue is to remain optimal in spite of unknown disturbances. In other words, we are interested in the integration between optimization and control objectives. The overall goal is to find implementation strategies which give acceptable performance in terms of constraint violation and economic loss in the face of disturbances and uncertainties.

In the next subsection we present an illustrative example which is used to highlight the key concepts and challenges that are discussed throughout the thesis.

Motivational example

Consider the problem of driving a hypothetical unidimensional car from a given initial point $x(t_0) = 0$ to a desired final position $x(t_f) = x_{target}$ in

minimum time t_f. The end position is at the edge of a steep cliff so we must ensure that the final velocity is zero, that is $v(t_f) = 0$. The only degree of freedom is the acceleration/breaking force u which is bounded $u_{min} \leq u \leq u_{max}$. The main complicator for this problem is the unknown disturbance d. This disturbance may represent unmodelled forces such as friction and wind resistance. The optimization problem can be formulated as

$$\min_u t_f \tag{1.1}$$

subject to

$$\begin{aligned} &\dot{x} = v \\ &\dot{v} = u + d \\ &u_{min} \leq u \leq u_{max}, \\ &v(t_f) = 0 \\ &x(t_f) = x_{target} \end{aligned} \tag{1.2}$$

Figure 1.1 depicts an optimal solution to the above problem for a nominal case, that is, without uncertainties ($d = 0$). In this example we have $x_{target} = 500$, $u_{max} = 10$ and $u_{min} = -10$. Notice in the bottom plot in Fig. 1.1 that the optimal input trajectory consists of two constraint seeking arcs: first we drive with maximum acceleration ($u = u_{max}$) and then we switch to maximum break force ($u = -u_{max}$) until the car stops right at the edge of the cliff. Because the breaking force is limited, it is necessary to start breaking before we reach the cliff.

Naturally, the optimal control trajectory depends on perfect knowledge of the system's dynamics and disturbances. Figure 1.2 shows the result of implementing the open-loop solution (in blue) in the presence of a small disturbance $d = 0.5$. This disturbance is equivalent to a uncertainty in the control input effectiveness, which is common in practice. For comparison we also show the optimal solution (in red) for the disturbed system. The presence of such a small disturbance makes the open-loop solution unacceptable: we waited too long to start breaking and we are not able to stop in time, resulting in a catastrophic constraint violation. This example shows that even in the simplest cases, some flavour of feedback control is necessary to ensure an acceptable operation. By 'acceptable' we mean that the resulting operation must be feasible and the economic loss small. Nonetheless, it is not always clear what the implementation strategy should be. For instance, we may choose to drive the car slowly so that we have enough time to stop before the cliff, but this may result in a big loss of optimality. If the

maximum expected disturbance is known, we could compute the last safe position to start breaking after full acceleration is applied. This strategy, however, fails in the presence of other unmodelled dynamics or disturbances.

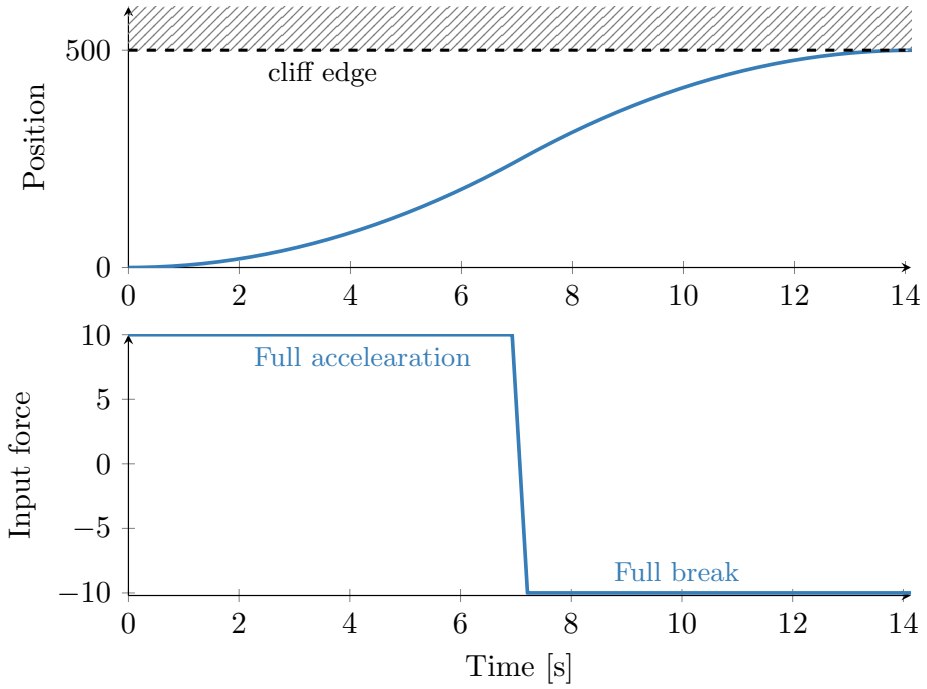

Figure 1.1: Optimal solution without uncertainty ($d = 0$). Under ideal conditions we are able to stop right at the edge of the cliff and we sucessfully finish the trajectory in minimum time.

In general the choice of the control and optimization integration approach is not straightforward. The control objectives are typically related to satisfying constraints and maintaining the system near a desired trajectory or operating point, whereas the optimization objectives are related to economic performance. There are two main paradigms for such an integration.

- **On-line optimization (paradigm 1) :** where the optimization problem is solved in real time with the arrival of new measurements to update the inputs. The inputs may be setpoints to a lower level control layer or the actual physical inputs, such as valve openings.
- **Offline analysis (paradigm 2):** where we use model base offline

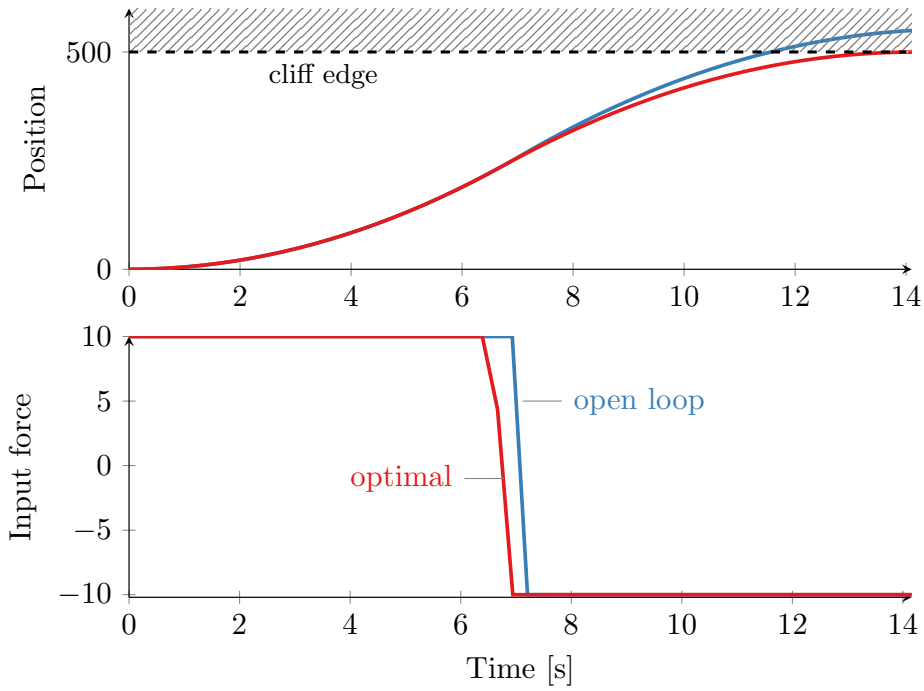

Figure 1.2: Simulation with constant disturbance ($d = 0.5$). The presence of such a small disturbance is enough to yield the open-loop solution unnaceptable: our ficticious car unfortunately falls off the cliff.

optimizations, simulations, physical understanding, etc., to gain valuable insights into the key characteristics of the optimal solution. These insights are then translated into strategies that are implemented online using control. The goal to find a policy that gives near-optimal results without the need for online optimization.

It is worth pointing out that combinations of the two paradigms are possible and, in many cases desirable. By selecting a good control structure using an offline analysis we may be able to simplify considerably the formulation and implementation of the online optimizer. This is discussed in Chapter 3 with application to a domestic hot water system. Paradigm 2 is closely related to the concept of self-optimization control (Skogestad, 2000), where the goal is to find a control structure that gives acceptable operation under all conditions with constant setpoints for the controlled variables. This is the theme of Chapter 8, where we extend the concept of self-optimizing

control to tackle transient problems.

In our car problem, when applying paradigm 1 we would solve the optimization problem (1.1)-(1.2) at every sample time in order to obtain the optimal input force $u(t)$. In addition, an observer would be used to estimate unmeasured variables such as the disturbance d. When using paradigm 2, in an offline stage we would study how the optimal solution of (1.1)-(1.2) is affected by variations in d and try to find a function of the available measurements (e.g. position and speed) whose optimum is insensitive to the disturbance. Then, during operation, online, we would use a simple controller to track this function and if a good "self-optimizing" function is chosen, this will lead to an acceptable performance.

In paradigm 1 we still need to decide on the hierarchical configuration of the overall system. We may opt for merging economic and control objectives into a single layer, where the control actions are obtained directly from the economic optimization solution. An example of such an approach is the so called Economic model predictive control (EMPC) (Ellis et al., 2014). In the thesis, Chapter 4 is devoted to the implementation of an EMPC for a domestic heating system aiming at minimizing electricity bill while respecting operational constraints related to comfort and air purity.

Conversely, we may decompose the overall problem of economic optimization and control into simpler sub-problems by using a cascade feedback structure (Ellis and Christofides, 2014). In this scheme the bottom layer is a regulatory control layer that follow the setpoints specified by an optimizer in the upper layer. The choice of the variables that link the optimization and the control layers is a critical decision and must be analysed for every specific case. The correct choice may simplify the optimization problem formulation and reduce the need for high frequency optimization as we will see in Chapter 3. We may consider this strategy as a combination of paradigms 1 and 2.

Another challenge which becomes evident in the car problem is how to satisfy the constraints (such has the final constraint) in the presence of uncertain dynamics and disturbances. For maximum profitability we usually want to operate the uncertain system near its limits but without violating any operational constraints. Nevertheless, due to uncertainty in the dynamics and changes in the operation condition, such a limit might be unknown a priori. This is the challenge addressed in Chapter 5. Generally speaking, our proposed method attempts to find the most economically beneficial operating point for the system while adapting to dynamic changes to ensure a stable operation. It turns out, in our anti-slug control application the optimal operating point lies at the boundary between stable and unstable

operations, but this limit is unknown and it may change. The job of our proposed control system is to find such a boundary without 'falling from the cliff'. Other examples for which this approach could be applicable include the control of compressors near surge and the operation of airfoil systems near the stability boundary to achieve greater power efficiency in aircraft (Wilson and Robinett, 2013).

1.2 Summary of the chapters in this thesis

In **Chapter 2**, we consider the optimal operation of energy storage in buildings with focus on the optimization of an electric water heating system. We present a detailed problem formulation which may also be suitable similar problems. Many insights into the optimization problem formulation are given and guidelines on implementation strategies including feedback control structures are proposed.

In **Chapter 3**, we use the hot water system presented in Chapter 2 as an example to illustrate our proposed implementation strategy based on hierarchical decomposition of the optimization-control problem. In our approach, economic objectives and control objectives are decoupled using a two-layer cascade feedback structure.

In **Chapter 4**, we discuss the implementation of an EMPC for a domestic heating system aiming at minimizing electricity bill while respecting operational constraints related to comfort and air purity. We also show how to integrate online optimization and self-optimizing control.

In **Chapter 5**, we present the details and results of our innovative adaptive anti-slug control system for offshore oil production maximization.

In **Chapter 6**, we discuss the robust design of baseline (stabilizing) feedback controllers for slug control. This is an important step in the complete anti-slug control system presented in Chapter 5.

In **Chapter 7**, we generalize the neighbouring extremal control design that has been presented in the literature (Gros et al., 2009b) to explicitly handle measurement noise and implementation errors.

In **Chapter 8**, we extend the concept of self-optimizing control to dynamic optimization problems.

Except for Chapter 7, which deals with steady-state optimization, all this thesis is concerned with the optimal operation of systems during transients. In the authors opinion, Chapters 2, 3 and 5 are the main contributions of this PhD work.

1.3 List of publications included in the thesis

Journal Papers

- V. de Oliveira, J. Jäschke and S. Skogestad, **Optimal operation of energy storage in buildings: Use of the hot water system**. *Journal of Energy Storage, vol. 5, 2016.*

- V. de Oliveira, J. Jäschke and S. Skogestad, **Hierarchical control in dynamic optimization of energy storage systems**. *In preparation.*

Patents

- V. de Oliveira, J. Jäschke and S. Skogestad. **An intelligent adaptive anti-slug control system for oil production maximization**.United Kingdom Patent Application No. 1508125.0. Priority date. 13 May 2015.

Peer-Reviewed Conference Papers

- V. de Oliveira, J. Jäschke and S. Skogestad, **Null-space method for optimal operation of transient processes**. *Submitted to the IFAC International Symposium on Dynamics and Control of Process Systems, 2016.*

- V. de Oliveira, J. Jäschke and S. Skogestad, **Neighbouring-Extremal Control for Process Optimization Using Noisy Measurements**. *International Symposium on Advanced Control of Chemical Processes, 2015.*

- V. de Oliveira, J. Jäschke and S. Skogestad, **An autonomous approach for driving systems towards their limit: an intelligent adaptive anti-slug control system for production maximization**. *2nd IFAC Workshop on Automatic Control in Offshore Oil and Gas Production,2015.*

- E. Jahanshahi, V. de Oliveira, C. Grimholt and S. Skogestad, **A comparison between Internal Model Control PIDF, optimal PIDF and robust controllers for unstable flow in risers**, *IFAC World Congress, 2014.*

- V. de Oliveira, J. Jäschke and S. Skogestad, **Dynamic online optimization of a house heating system in a fluctuating energy price scenario,** *IFAC International Symposium on Dynamics and Control of Process Systems, 2013.*

1.4 List of publications not included in the thesis

Journal Papers and Book Chapters

- V. de Oliveira, A. Nicoletti and A. Karimi, **Robust Smith Predictor Design for Uncertain Time-Delay Systems by Convex Optimization,** *Springer Series in Advances in Delays and Dynamics, vol. 4, 2014.*

- J. Marcinichen, J. Olivier, V. de Oliveira and J. Thome, **A review of on-chip micro-evaporation: Experimental evaluation of liquid pumping and vapor compression driven cooling systems and control**, *Applied Energy, 92, 147-161, 2011.*

- V. de Oliveira, A. Trofino and C. J. Hermes, **A switching control strategy for vapor compression refrigeration systems,** *Applied Thermal Engineering, 31, 3914-392, 2011.*

Peer-Reviewed Conference Papers

- M. Sadeghpour, V. de Oliveira and A. Karimi, **A toolbox for robust PID controller tuning using convex optimization,** *IFAC Conference on Advances in PID Control, 2012*

- V. de Oliveira and A. Karimi, **Robust and Gain-Scheduled PID Controller Design for Condensing Boilers by Linear Programming,** *IFAC Conference on Advances in PID Control, 2012*

- V. de Oliveira and A. Karimi, **Robust Smith Predictor Design for Time-Delayed Systems with H_∞ Performance,** *IFAC Joint Conference, Grenoble, France, 2013*

- V. de Oliveira, M. Amrhein, and A. Karimi, **Robust gain-scheduled blending control of the raw-mix quality in cement industries,** *50th IEEE CDC-ECC, Orlando, USA, 2011.*

- V. de Oliveira, A. Trofino and C. J. Hermes, **Applicability of a dual-mode switching control strategy for vapor compression refrigeration systems,** *23th IIR International Congress of Refrigeration - Prague, Czech Republic, August 21-26, 2011.*

- N. Bajcinca, V. de Oliveira, C. Borchert, J. Raisch and K. Sundmacher, **Optimal control solutions for crystal shape manipulation,** *20th European Symposium on Computer Aided Process Engineering - ESCAPE20, Ischia, Naples, Italy June 6-9, 2010.*

Part I

Optimal operation of energy storage systems

Chapter 2

Optimal operation of energy storage in buildings: Use of the hot water system

We consider the optimal operation of energy storage in buildings with focus on the optimization of an electric water heating system. The optimization objective is to minimize the energy costs of heating the water, with the requirement that we should satisfy the uncertain demand at any time. The main complications in this problem are the time varying nature of the electricity price and the unpredictability of the future water demand. In this paper we use the water heating system as an example for formulating a general framework which could easily be applied to similar problems with energy storage capacity. Feasibility and optimality are discussed and the main points are illustrated in the simulation case studies.

Published in the Journal of Energy Storage, vol. 5, 2016.

2.1 Introduction

Recently, considerable attention has been paid to renewable energy sources like wind turbines and photovoltaic parks. These alternative energy sources suffer a major drawback, however, due to their strong dependence on uncontrolled and varying weather conditions. This is an important limitation since the energy production is expected to cover the demand at any given time.

A possible approach for handling these fluctuations in the production is to shift the consumer load to periods where a lot of energy can be produced cheaply. This is referred to as demand side load management (Molderink et al., 2009). Field tests in the USA have demonstrated that such an optimization of domestic energy consumption can significantly reduce load peaks (Hammerstrom, 2007; Faruqui and Sergici, 2010). This can be achieved by manipulating the energy price according to demand information and weather forecasts. Electricity consumers are thus encouraged to consume electricity more prudently in order to minimize their electric bill. The dynamic energy pricing for demand load management is in itself a non-trivial problem and it is currently an active research area. The interested reader may check the literature (Mardavij Roozbehani and Mitter, 2010; Borenstein, 2005; Goudarzi et al., 2011) for more information, as this problem is outside the scope of this work.

Local energy storage in such setting provides several benefits for the consumer without having to adjust their consumption pattern. In particular, it enables

1. Higher peak capacity. For example, one may heat extra hot water in the morning to make sure there is enough water for everyone to have a shower.

2. Taking advantage of varying energy price. Energy can be purchased when prices are low and it can be used when the prices are high. (Since human users typically have a weak response to energy prices (Zhou et al., 2012), automatically controlled consumers are better suited for a variable pricing scenario.)

3. Taking advantage of favourable outdoor conditions (e.g. cooling at night or heating during the day)

Energy storage devices could include hot water tanks, batteries, ice banks, liquid nitrogen, thermal storage building mass thermal capacity and compressed air storage (Zhou et al., 2012).

Recently, there has been significant research activity around the problem of optimal usage of energy storing devices. For example, in van de Ven et al. (2012) the problem of optimizing the end-consumer energy storage policies is considered. The proposed idea is to charge batteries when the electricity price is low and use the stored energy when the price is high. The authors show that the optimal policy has a simple structure based on two threshold levels: if the battery level is below a certain lower threshold value, the optimal policy is to charge it as close to the lower threshold value as possible.

If the battery level lies above some upper threshold value then it is optimal to use the stored energy from the battery instead of purchasing from the grid. The difficulty lies in the computation of the optimal threshold levels which are a function of the varying energy price. However, analytical results can be derived for a few simplified cases, e.g. assuming perfect efficiency for charging and discharging the battery.

Ericson (2009) presented results from a large scale Norwegian project where load control was applied on domestic hot water heaters. The main idea was to disconnect the water heaters from the electricity grid during peak hours in order to reduce the peak load. Electrical consumption of 475 households were investigated over a six month period from November 2003 to May 2004. The results show significant peak shavings in consumption during disconnection of hot water heaters. However, the researchers observed a considerable increased consumption after the reconnection of the heaters, which may have the adverse consequence of causing a new peak in the system.

Henze et al. (2004) consider the optimization of the cooling system in commercial buildings. The authors propose shifting the thermal load by precooling the buildings structure at night, in addition to using *active* storage means such as ice thermal storage. The ultimate goal is to take advantage of ambient conditions and of real-time pricing to maximize the energy cost savings. The simulations show that the cost savings and on-peak demand reductions can be substantial (up to 57% and 50%, respectively) if a good model and accurate weather predictions are used.

Many recent contributions use model predictive control (MPC) solutions for this problem. In Avci et al. (2013) a MPC controller is used to minimize a multi-objective function which trades off energy cost and comfort level in a dynamic real-time pricing scenario. They show that there is a good potential for savings compared to traditional control strategies. Not surprisingly, it is shown that the energy cost increases as the comfort level increases.

In this paper, we focus on the optimization of an electric water heating system which provides hot water for domestic usage. The optimization objective is to minimize the energy costs while obeying some operating constraints. The main idea is to use the heat capacity of the water tank to *store energy* in times when electric power is cheap and use it to match the demand when energy is expensive. The main contribution of this paper is to provide a systematic comparison between different strategies to operate the system. The idea here is to have a better understanding of the potential benefits of using energy storage in this problem. A comparison of the various strategies will be presented. We will distinguish between the following cases:

- *Ideal case*, where the optimal solution is computed assuming perfect knowledge of the future demand. This is a theoretical limit which cannot be achieved in practice, unless the future demand is known exactly.

- *Maximum storage policy*, where we maintain maximum storage in the tank at all times. This is achieved by fixing the tank temperature setpoint T_s and tank volume setpoint V_s at their maximum allowed value. This is the safest policy in terms of avoiding constraint violation caused by unforeseen high demand as it minimizes the risk of not having enough hot water.

- *Simple variable storage policy*, an intuitive money saving strategy in which we buy and store as much energy as possible during the night to be used during the day. The idea is to activate a 'storage mode' during night, when we set the energy storage setpoint E_s to its maximum, and a 'saving mode' during the day when we set E_s to a lower value. This policy is analogous to the work of van de Ven et al. (2012), where the setpoint E_s plays the role of the switching threshold discussed in that paper.

- *Optimal variable storage policy*, where the temperature setpoint T_s and tank volume setpoint V_s are updated at every time step using a moving horizon optimization (MHO) approach. The optimization algorithm relies on a simple forecast model to predict the future demand. A detailed derivation of this method is presented in an accompanying paper (de Oliveira et al., 2016).

Additional contributions of this paper include:

1. A detailed general problem formulation which may also be suitable for different applications involving dynamic optimization, energy storage and variable energy prices.

2. Guidelines about implementation strategies including control structures.

The paper is organized as follows: Section 2 presents the process modelling; Section 3 formulates the optimal control problem; In Section 4, insights into the implementation strategies are given; In Section 5 we detail different strategies for control and optimization of the system; Section 6 details a simulation study comparing various approaches. Section 7 presents a discussion on the subject and Section 8 concludes the paper.

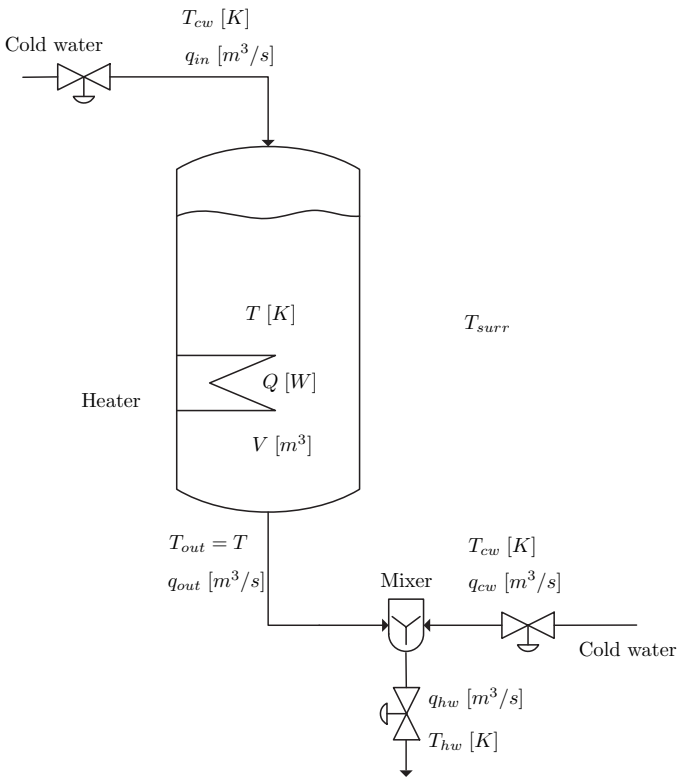

Figure 2.1: Simplified process flow scheme

2.2 Process model for hot water storage tank

The process we are dealing with consists of a heater which provides hot water for domestic usage. A simplified process flow scheme is shown in Figure 2.1 where the important notation is presented. The system includes a cold water source, a thermally insulated tank, a heating coil with adjustable power and control valves that regulate the cold water inflow q_{in} and the hot water outflow q_{out}. A somewhat unusual feature of this system is that the hot water that leaves the tank (q_{out}) is mixed with a cold water stream (q_{cw}) from the same water source. This extra mixer is to allow extra flexibility and implies that the water in the storage tank ($T_{out} = T$) can be heated to a higher temperature than the hot water to the consumer (T_{hw}).

We defined the tank as our control volume and derive a dynamic model from mass and energy balances for the water in the tank. The mass balance for the tank is

$$\frac{d(\rho V)}{dt} = \rho_{in} q_{in} - \rho_{out} q_{out} \qquad [kg/s] \tag{2.1}$$

where $V\,[m^3]$ is the volume of the tank. We will assume constant fluid density ($\rho = \rho_{in} = \rho_{out}$). Assuming constant pressure and no mechanical work and neglecting kinetic and potential energy, the energy balance for the tank becomes (e.g, Skogestad (2009))

$$\frac{dH}{dt} = h_{in} - h_{out} + Q - Q_{loss} \qquad [J/s] \tag{2.2}$$

where $Q_{loss}\,[J/s]$ is the heat loss to the surroundings, $H\,[J]$ is the enthalpy of the system, $h_{in}\,[J/s]$ and $h_{out}\,[J/s]$ is the enthalpy of the streams and $Q\,[J/s]$ is the added power. The standby heat loss from the heater to the surroundings is

$$Q_{loss} = UA(T - T_{surr}) \tag{2.3}$$

where $UA\,[W/K]$ is the heat transfer constant and T_{surr} is the temperature of the surroundings. Assuming constant heat capacity c_p, no phase change and perfect mixing ($T_{out} = T$), the enthalpies are given by (Skogestad, 2009)

$$H = \rho V c_p (T - T_{ref}) \qquad [J] \tag{2.4}$$

$$h_{in} = \rho q_{in} c_p (T_{cw} - T_{ref}) \qquad [J/s] \tag{2.5}$$

$$h_{out} = \rho q_{out} c_p (T - T_{ref}) \qquad [J/s] \tag{2.6}$$

where $T_{ref}\,[K]$ is a fixed reference temperature, $q\,[m^3/s]$ is the flowrate and T_{cw} is the temperature of the cold water from the network. Combining equations (2.1) and (2.2), with the assumption of constant c_p and ρ, the dynamic model of the tank becomes

$$\frac{dV}{dt} = q_{in} - q_{out} \tag{2.7a}$$

$$\frac{dT}{dt} = \frac{1}{V}\left[q_{in}(T_{cw} - T) + \frac{Q - Q_{loss}}{\rho c_p}\right] \tag{2.7b}$$

where T is the tank water temperature and T_{cw} is the temperature of the inlet flow. Note that T_{ref} drops out of the equations.

Similarly, we may write mass and energy balances for the mixer system, which is assumed to be a static process. The mass balance is given by

$$q_{hw} = q_{out} + q_{cw} \tag{2.8}$$

The steady sate energy balance for the mixer is given by

$$h_{hw} = h_{cw} + h_{out} \qquad [J/s] \tag{2.9}$$

where h_{cw} and h_{hw} are the enthalpies of the cold and hot water streams, which are defined as

$$h_{cw} = \rho q_{cw} c_p (T_{cw} - T_{ref}) \tag{2.10}$$
$$h_{hw} = \rho q_{hw} c_p (T_{hw} - T_{ref}) \tag{2.11}$$

Rearranging (2.9) gives the hot water temperature

$$T_{hw} = \frac{q_{out} T + q_{cw} T_{cw}}{q_{hw}} \tag{2.12}$$

2.2.1 Energy storage and demand

In this subsection we introduce some terms that will be useful for analysis. We define the energy stored in the tank relative to the current cold water supply temperature (T_{cw}) as

$$E = \rho c_p V (T - T_{cw}) \; [J] \tag{2.13}$$

We define the power demand at any given time as

$$Q_{\text{demand}} = \rho c_p q_{hw} (T_{hw} - T_{cw}) \qquad [\text{J/s}] \tag{2.14}$$

This is the power we would need to supply at any given time if there were no energy storage. Upon combining (2.2) and (2.9) we obtain the overall energy balance of the combined tank-mixer system

$$\frac{dH}{dt} = h_{in} + h_{cw} - h_{hw} + Q - Q_{loss} \tag{2.15}$$

By introducing E and Q_{demand}, the energy balance can be written in the following alternative form (see Appendix A for derivation)

$$\frac{dE}{dt} = Q - Q_{\text{demand}} - Q_{loss} - \rho V c_p \frac{dT_{cw}}{dt} \tag{2.16}$$

which will be useful for analysis of the system. Note that for the case with constant cold water supply temperature ($\frac{dT_{cw}}{dt} = 0$), which is also assumed in the case study, we simply get

$$\frac{dE}{dt} = Q - Q_{\text{demand}} - Q_{loss} \tag{2.17}$$

that is, the change in the stored energy is the difference between the current heating ($Q - Q_{loss}$) and current use Q_{demand}. It is also relevant to define the maximum energy capacity as

$$E_{max} = \rho c_p V_{max} (T_{max} - T_{cw}) \tag{2.18}$$

and the minimum energy amount that needs to be satisfied at all times as

$$E_{min} = \rho c_p V_{min}(T_{min} - T_{cw}) \tag{2.19}$$

The bounds for volume and temperature V_{min}, V_{max}, T_{min} and T_{max} are discussed in section 2.3.2. For analysis it will be helpful to define the scaled stored energy

$$\bar{E}(t) = \frac{E(t) - E_{min}}{E_{max} - E_{min}} \tag{2.20}$$

which lies between $\bar{E}_{min} = 0$ and $\bar{E}_{max} = 1$.

2.3 Problem formulation

2.3.1 Independent variables

Control degrees of freedom

From Fig. 2.2, the system has four independent variables, namely, Q, q_{cw}, q_{hw} and q_{in}. However, as discussed next, two of these variables (q_{hw} and q_{cw}) are used to satisfy demand requirements on the hot water flow and temperature, respectively. The remaining two degrees of freedom (decision variables) for control and optimization are the power input Q and the cold water inlet flow q_{in}.

Disturbances

The hot water flow rate, q_{hw}, and the hot water temperature setpoint, $T_{hw,s}$ are set by the user and are considered disturbances from a control point of view. We assume perfect temperature control ($T_{hw} = T_{hw,s}$) whenever feasible. By 'whenever feasible' we mean whenever the tank temperature is above the delivery setpoint, $T \geq T_{hw,s}$. In this case, the flows q_{out} and q_{cw} are given by (2.8) and (2.12) with $T_{hw} = T_{hw,s}$. For the case when $T < T_{hw,s}$, we cannot achieve the desired setpoint and we set $q_{cw} = 0$ in order to maximize the delivery temperature T_{hw}, and we get $q_{out} = q_{hw}$ and $T_{hw} = T$.

The main disturbances for the optimization are related to the user demand ($T_{hw,s}$ and q_{hw}), the cooling water temperature (T_{cw}) and the price of electricity (p) and can be regarded as stochastic variables. The cold water temperature (T_{cw}) can vary significantly in the long term (e.g. from summer to winter), but this variation is not important in our time scale (which is from minutes to hours). From an operational point of view, the effect of changes in both q_{hw} or $T_{hw,s}$, is a change in the power demand Q_{demand}.

Therefore, for simplicity, we here assume that $T_{hw,s}$ is constant and consider disturbances in the hot water demand, q_{hw}. In the case study we assume T_{cw} is constant.

2.3.2 Constraints

The operation of the system should respect constraints related to physical limitations, safety and specifications. Firstly, in terms of inputs, the heating power and water inflows are limited, so that

$$0 \leq Q \leq Q_{max} \tag{2.21}$$

$$0 \leq q_{in} \leq q_{max} \tag{2.22}$$

In terms of output constraints, the temperature of the water should be bounded above (T_{max}) for safety reasons and indirectly bounded below ($T_{hw,s}$) to guarantee that the desirable temperature of the hot water is achievable. Naturally, the volume is bounded by the size of the tank. Therefore, we have

$$T_{min} \leq T \leq T_{max} \tag{2.23}$$

$$V_{min} \leq V \leq V_{max} \tag{2.24}$$

where $T_{min} = T_{hw,s}$.

2.3.3 Optimal control problem formulation

In its simplest form, the objective we would like to minimize is the future energy cost

$$J = \int_{t_0}^{t_f} p(t)Q\,dt \tag{2.25}$$

where $p(t)$ is the time-varying electricity prices, $Q(t)$ is the power we buy at time t, t_0 is the initial time and t_f is the final time. In addition, we want to satisfy the operational constraints (2.21), (2.22), (2.23) and (2.24) and we have to satisfy the process dynamics (2.7). Notice that the process dynamics introduce nonlinearity into the optimization problem, which makes the problem more difficult to solve.

2.4 Insights into the optimal solution

In this section we will present some properties of the solution that can be used to simplify the optimization problem. In addition, these insights will be used to derive simple implementation strategies for this system.

2.4.1 Ideal liquid level

When a target for the energy storage E is specified (e.g. by an optimization algorithm) a decision on the appropriate values for T and V that achieve the given energy storage needs to be made. This is because of the non-uniqueness in the energy storage $E = \rho c_p V(T - T_{cw})$ in terms of temperature and volume. In practice, to reduce the heat loss, we want to keep the temperature T as low as possible, which for a given energy storage (E) is achieved by maximizing the tank filling. We then have the following important insight:

For a given energy storage E it is optimal to keep the liquid V in the tank as large as possible to minimize energy losses.

This means that we will keep $V = V_{max}$ as long as the temperature in the tank T is above the hot water setpoint $T_{hw,s}$. When the temperature T reaches $T_{hw,s}$ we may have to reduce the refilling cold water, which means that V will drop below V_{max}. However, note that for safety reasons we always have to keep $V \geq V_{min}$.

2.4.2 Initial condition and terminal state constraint

The electricity price tends to be at its lowest during night and it typically peaks in the morning when the demand is high. The hot water demand profiles show a similar behaviour, with demand peaking early in the morning. Based on this observation we have the following insight

> *It is optimal to have maximum energy stored ($V = V_{max}$ and $T = T_{max}$) late in the night.*

This is an important insight because it means that we can always consider a 24 hours optimization horizon, even when the actual horizon (t_f) is longer. For an optimization horizon of 24 hours this implies that we should have

$$T(t_0) = T(t_0 + 24h) = T_{max} \tag{2.26}$$
$$V(t_0) = V(t_0 + 24h) = V_{max} \tag{2.27}$$

where the initial time t_0 should be appropriately chosen. For example, it could be some time after midnight. This suggests that the optimization of every 24-hours interval may be performed independently because the terminal constraints decouple the optimization problems of two consecutive days.

2.5 Solution approaches

In this section we will describe in more details the different approaches that will be compared.

2.5.1 The ideal solution

The solution to the optimization problem (2.25) requires the characterization of future price $p(t)$ and demand $q_{hw}(t)$ for the horizon of interest. In the ideal case, we assume perfect knowledge of the future demand q_{hw}. The term *ideal* refers to the fact that this assumption is generally not satisfied and this solution should be regarded as a theoretical limit. The results obtained in this case are very useful to benchmark the performance of any other policy.

2.5.2 Maximum storage policy

This is the simplest policy, where we maintain maximum energy storage in the tank at all times. This is achieved by fixing the tank temperature setpoint T_s and tank volume setpoint V_s at their maximum allowed value. The control structure that can be used is shown in Fig. 2.2. This is the safest policy in terms of avoiding constraint violation caused by unexpectedly high demand, but it does not seek to reduce the electricity costs.

2.5.3 Simple variable storage policy

The observations and insight presented in Section 2.4.2 suggests a simple money-saving strategy in which we attempt to store as much energy as possible during the night. Therefore, the idea is to manipulate the energy storage setpoint E_s using a simple time-based feedforward rule

$$\text{Simple policy: } \begin{cases} E_s = E_{max} & \text{during night (storage mode)} \\ E_s = E_{min} + E_{\text{backoff}} & \text{during day (saving mode)} \end{cases} \tag{2.28}$$

Where the positive constant E_{backoff} is a backoff from the constraint to reduce the risk of frequent constraint violation caused by large demand during the day. The backoff should be adjusted such that the amount of constraint violations is acceptable for the given case. Using $E_s = E_{max}$ at night accomplishes two things: takes advantage of more favourable electricity prices at night and it anticipates for a high consumer demand in the morning. The main problem here is to determine the most beneficial times to switch

between the setpoints. One approach is to use historical price data to compute the time interval with the lowest price in average. Such time interval should be long enough to ensure a full tank with maximum temperature before entering the 'saving mode'.

Simple policy: temperature and volume setpoints

For a practical implementation using control it is convenient to know what the simple policy (2.28) means in terms of temperature and volume setpoints. During 'storage mode' we obviously have $T_s = T_{max}$ and $V_s = V_{max}$. On the other hand, during 'saving mode' we need to use the insight in Section 2.4.1 to compute the setpoints which for small backoff (E_{backoff}) becomes

$$\begin{aligned} T_s &= T_{hw,s} \\ V_s &= \frac{E_{min} + E_{\text{backoff}}}{\rho c_p (T_{hw,s} - T_{cw})} = V_{min} + V_{\text{backoff}} \end{aligned}$$

where the constant $V_{\text{backoff}} = \frac{E_{\text{backoff}}}{\rho c_p (T_{hw,s} - T_{cw})}$ is non-negative. When the backoff E_{backoff} is large enough we will have $V_s = V_{max}$ and the temperature setpoint needs to be greater than the lower bound ($T_s > T_{hw,s}$).

After switching from one mode to another, there will always be a transient period where we are not meeting the energy storage setpoint E_s. During the transition from storing to saving mode (night to day) we don't want to add any power Q because of the high price in this period. In addition, to reduce heat losses we should let the temperature T drop to the setpoint T_s before we start reducing the volume to the new setpoint. This can be easily achieved by keeping $V_s = V_{max}$ while $T > T_{hw,s}$ and only when the temperature reaches the new setpoint ($T = T_{hw,s}$) we switch the volume setpoint to the desired 'saving mode' level ($V_s = V_{min} + V_{\text{backoff}}$).

On the other hand, during the transition from day to night operation we should first increase the tank level until $V = V_{max}$ and then we start increasing T to reduce losses. This can be achieved by setting $Q = Q_{max}$ while using the water refilling to keep $T = T_{hw,s}$ until the tank is full ($V = V_{max}$). At this point then switch to the structure in Fig. 2.2 for the night operation.

Simple policy: Implementing insights using control

The policy during 'storage mode' can be implemented using feedback control:

- Use the water refilling (q_{in}) to keep V at constant setpoint V_{max}.
- Use the power input (Q) to control T at constant setpoint T_{max}.

Figure 2.2 depicts the control structure for this case. During 'saving mode' (after the transient) a similar structure can be used. However, for large disturbances the temperature controller might saturate ($Q = Q_{max}$) and it is not advantageous to have $V = V_s = V_{min} + V_{\text{backoff}}$ as it will force T to drop below $T_{hw,s}$ and we should let V drop. A simple way to achieve this is to use split range control as shown in Fig. 2.3. The basic idea is that a single controller uses both the power input Q and the level setpoint V_s to control the temperature when the setpoint is $T_s = T_{hw,s}$. The temperature controller computes a virtual control action u which is translated to values for Q and V_s according to a defining function as depicted in Fig. 2.4. When the volume setpoint reaches the lower bound $V_s = V_{min}$ the temperature control is lost and T drops below $T_{hw,s}$.

2.5.4 Optimal variable storage policy

The main idea here is to use a moving horizon optimization (MHO) scheme to solve the problem. At each time sample a model-based dynamic optimization problem with horizon h is solved using the information that is currently available. However, only the first portion of the optimal profile corresponding to $t \in [t_0, t_0 + \Delta t]$ is implemented, where t_0 is the initial time and Δt is the sample time. Within this framework we find two different implementation philosophies:

- **Single layer strategy** in which optimization and control are integrated; Here, optimization problem (2.25) is solved using a moving horizon approach and the optimal inputs (q_{in} and Q) are re-computed directly (by the optimizer) at every time sample. This is, in theory, the optimal approach. However, it requires high computational power as the full optimization problem needs to be solved at every time sample. In the literature this strategy is sometimes called economic model predictive control (Ellis et al., 2014).
- **Two level strategy** where the optimization problem is decomposed in two simpler problems where the economic objectives are decoupled from the control objetives.

The second strategy is our preferred and is the approach used in this paper. The basic idea is to decompose the overall problem of economic optimization and control (Eq. (2.25)) into simpler sub-problems by using a cascade

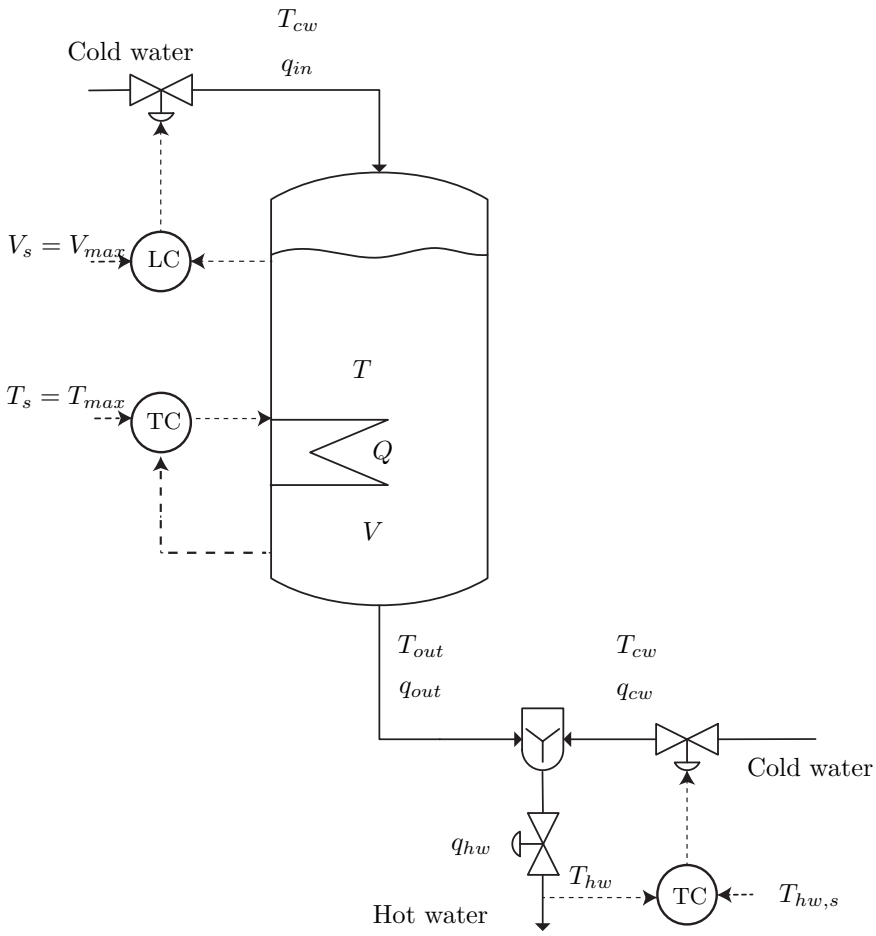

Figure 2.2: Proposed control structure when $T_s = T_{max}$ and $V_s = V_{max}$ (Simple policy (2.28) during night).

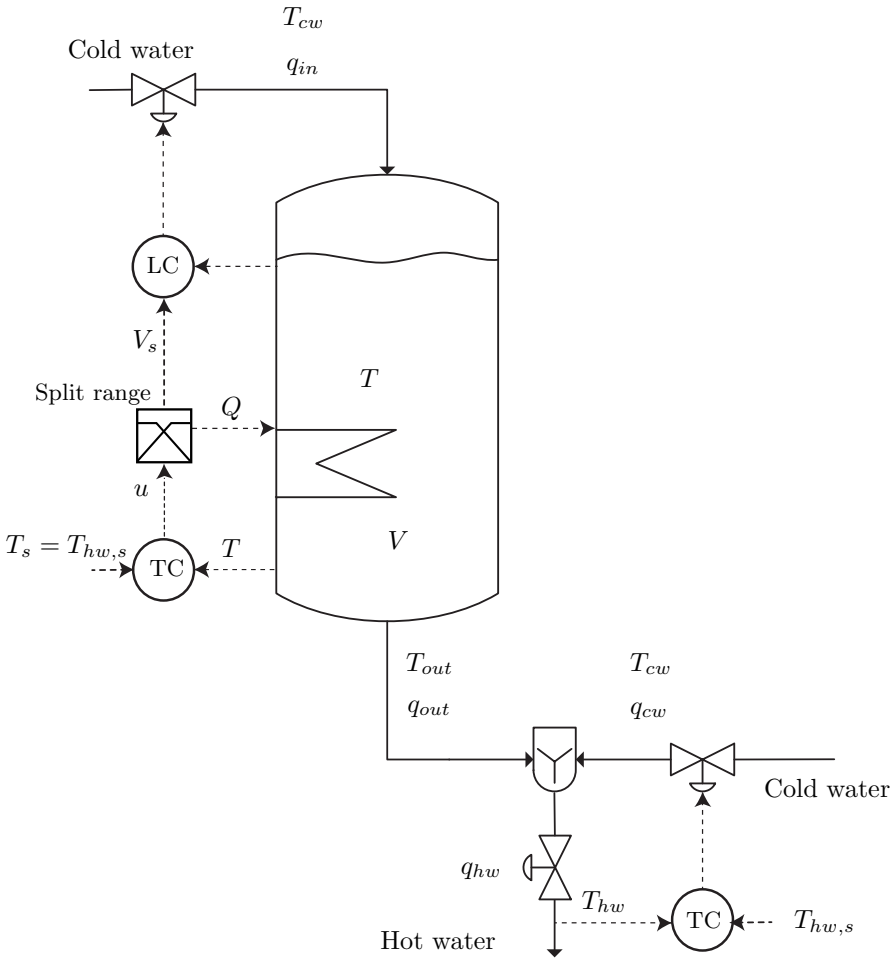

Figure 2.3: Split range control structure, used when $T_s = T_{hw,s}$ and V_s may vary between $V_{min} + V_{\text{backoff}}$ and $Vmin$; see Fig. 2.4. (Simple policy (2.28) during day). The lower temperature controller, where extra cold water is mixed in, is not active during normal day operation. In the transition period between night (Fig. 2.2) and day (Fig. 2.3) operation, we set $Q = 0$ and first let T_{out} drop from T_{max} to $T_{hw,s}$ (with $V_s = V_{max}$) and then set $q_{in} = 0$ and let V drop from V_{max} to $V_{min} + V_{\text{backoff}}$.

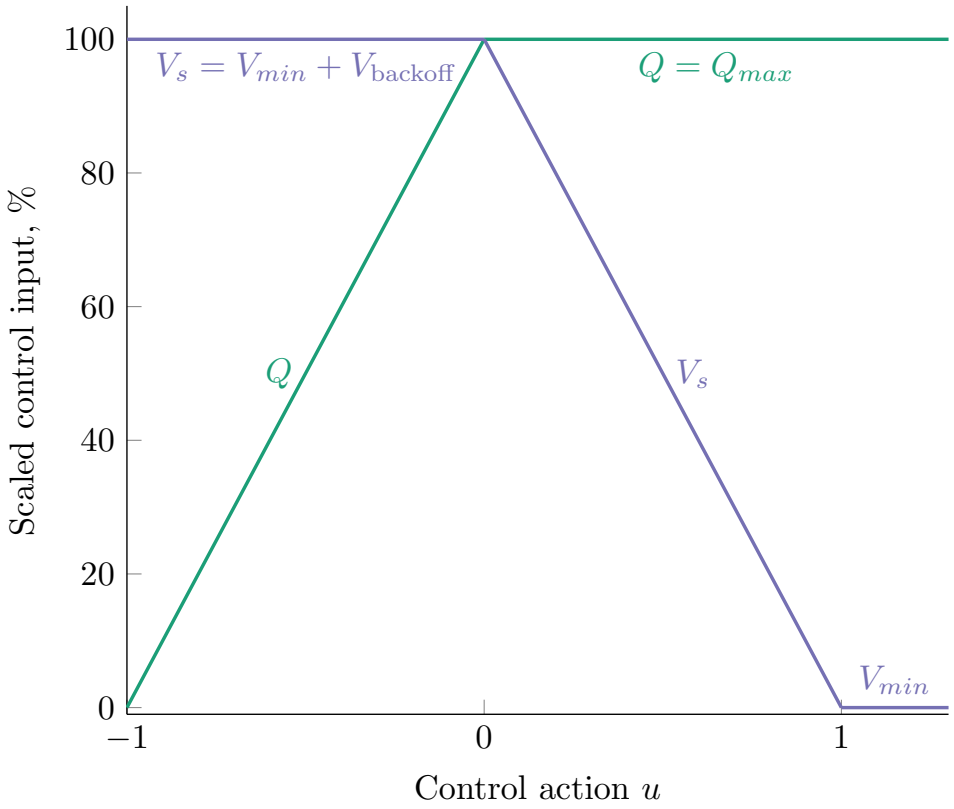

Figure 2.4: Simple representation of a split-range control where both the power Q and the level setpoint V_s are used to control the temperature when the setpoint is $T_s = T_{hw}$. Note it is not necessary to have $u = 0$ as the point where you switch; this value may be used to equalize the scaled process gains for the two inputs.

feedback structure. In this scheme the bottom layer is a regulatory control layer that follow the set-points specified by an optimizer in the upper layer. In our problem the regulatory control layer is similar to that of Fig. 2.2 and the task of the optimizer is to update the setpoints T_s and V_s. Our idea is to write a simplified optimization problem in terms of the energy storage E only and then translate the optimal energy level E_{opt} into setpoints V_s and T_s.

A detailed derivation of this method is presented in the accompanying paper de Oliveira et al. (2016). In de Oliveira et al. (2016) it is shown that the remaining optimization problem for the upper layer can be written as a simple linear program (LP) which can be solved very efficiently at a low computational cost.

An important factor for the success of this optimization scheme is to have relevant information about the user demand and the future price. An idea is to construct a demand model based on the empirical distribution of hot water consumption for every time step using historical data. This model can be updated online as new measurements become available, making it possible to adapt to new consumption patterns when necessary. However, our simulation studies suggest that even simpler models (e.g. assume constant demand) can give satisfactory results if the optimization problem is resolve frequently enough. For simplicity, we will assume the electricity price is known 24h in advance.

As in the simple policy (2.28), it may be necessary to include a backoff E_{backoff} from the constraint in order to reduce the probability of breaking the constraints due to large disturbances. The idea is to shift the current desired energy level E_s (computed by the optimizer) if it is too close from the boundary E_{min} so that $E_s \geq E_{min} + E_{\text{backoff}}$.

2.6 Case Study

In this section we will show a simulation example of the methodology presented in the previous section. The idea here is to have a better understanding of the potential benefits of using energy storage in this problem. A comparison of the various strategies will be presented.

2.6.1 Electricity prices

For simulation and optimization we used the electricity price data available in the archives of Nord Pool spot market (NordPoolSpot, 2014). A sample of the electricity price for the first 10 days of February, 2012 in Trondheim,

Norway is shown in Fig. 2.5. Although Norway currently does not use real-time pricing for the end-user, the spot prices provide a reasonable real-time pricing estimates. The resolution of the price data is one hour.

2.6.2 Realistic hot water demand

For a realistic comparison, we emulate hot-water flow demand (q_{hw}) profiles based on the empirical probability distributions published by Jordan and Vajen (2001). The consumption profiles have a resolution of one minute and correspond to a single family house with a mean load volume of 350 litres per day. An example of a consumption profile is depicted in Fig. 2.5, where twenty unique hot-water profiles were generated. For simplicity, we will assume constant temperature setpoint $T_{hw,s}$ and cold water temperature T_{cw}.

2.6.3 Heat loss

The typical heat loss from a domestic hot water tank is approximately $0.1kWh/h$ at a temperature of 75°C (Ericson, 2009). For a room temperature $T_{surr} = 25$°C it follows from (2.3) that the heat transfer constant (UA) for domestic water heaters is approximately

$$UA = \frac{Q_{loss}}{T - T_{surr}} = \frac{0.1}{50} = 0.002 \quad [kW/K] \tag{2.29}$$

which we assume constant throughout the simulations. Additional important parameter values for our case study are presented in Table 4.2.

Table 2.1: Parameters for case study

Parameter	Description	Value	Unit
Q_{max}	Maximum power	5	kW
Q_{min}	Minimum power	0.0	kW
T_{max}	Temperature upper bound	90	°C
V_{max}	Volume upper bound	150	l
V_{min}	Volume lower bound	50	l
T_{cw}	Cold water temperature	5	°C
T_{hw}^{sp}	Hot water temperature	50	°C
c_p	Heat capacity of the water	4.19	kJ/kg/K
UA	Heat transfer constant	0.002	kW/K
T_{surr}	Room temperature	25	°C

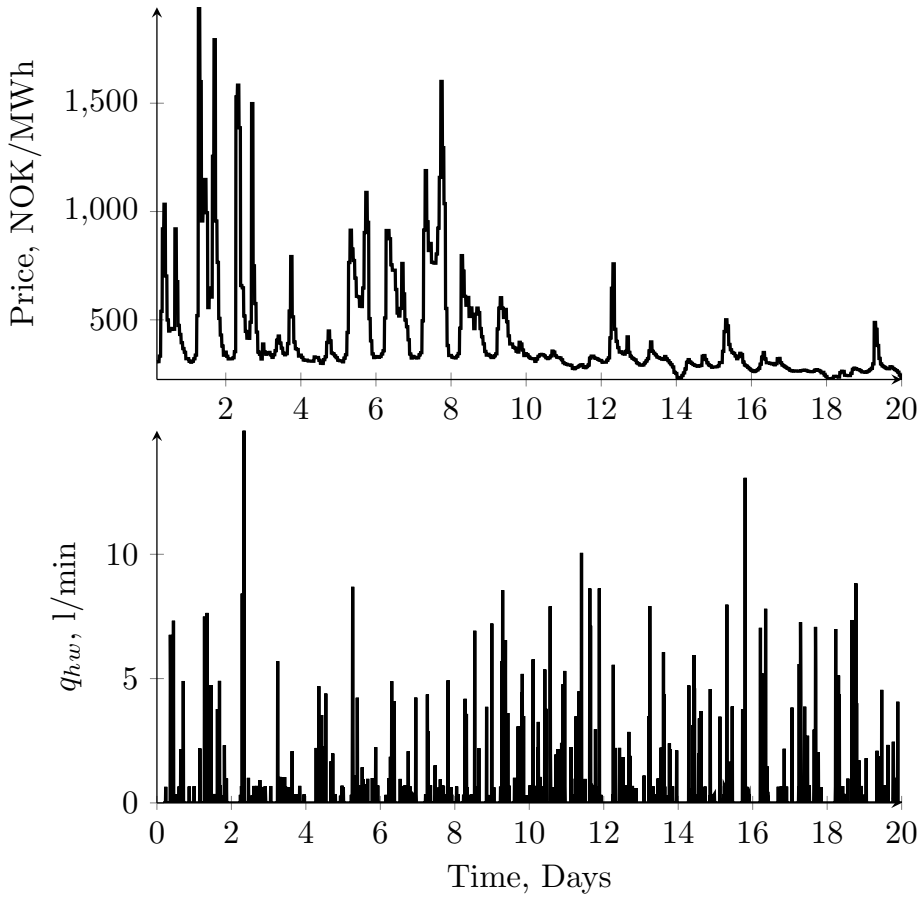

Figure 2.5: Electricity price and hot water demand.

2.6.4 Ideal case

To compute the ideal solution, we discretize the optimal control problem using orthogonal collocation in a simultaneous approach (Biegler, 1984). In this approach, the differential equations are converted to algebraic ones by orthogonal collocation which should be satisfied only at the solution of the optimization problem (Biegler, 1984). The key characteristic here is that both states and manipulated variables profiles are approximated, with the same accuracy, by orthogonal polynomials, resulting in a large scale nonlinear programming problem (NLP). An interesting characteristic of this method is that it can efficiently handle problems with constraints on states and control inputs.

We formulate the problem in Matlab and solve it using the sparse NLP solver SNOPT (Gill et al., 2002). This solver employs a sparse SQP algorithm with quasi-Newton approximations to the Hessian. Gradient information is obtained using a symbolic differentiation approach. The interface between Matlab and SNOPT is handled by the optimization environment TOMLAB.

The optimization for every day is carried out independently, where we consider the initial time $t_0 = 4$h in the morning and a horizon $h = 24$ hours. The tank is always initially full ($E(t_0) = E_{max}$) and we impose the terminal constraint $E(t_f) = E_{max}$. The penalty terms p_1^* and p_2^* were adjusted so that a constraint violation ($T_{hw,s} - T$) of 20 degrees results in a compensation of $p^*(T) = 2$ NOK/kWh, slightly above the highest electricity price observed.

2.6.5 Simple variable storage policy

The main decision in the design of the simple policy (2.28) is the time to switch the temperature setpoints. The duration of the 'storage mode' period (Δt_{night}) should be long enough to ensure that maximum storage energy ($E = E_{max}$) can always be reached at the end of the interval. This value depends on the size of the tank, the maximum water inflow rate and the installed electric power. After determining the minimum duration Δt_{night} we can use historical price data to determine the period of the day with duration Δt_{night} with the lowest price in average. In this case study we have chosen to activate the 'storage mode' only from 2 am to 6 am. In this example, we have chosen the backoff level $E_{\text{backoff}} = 0.2(E_{max} - E_{min})$, which corresponds to $V_{\text{backoff}} = 50$ l.

2.6.6 Optimal variable storage policy

As in the ideal solution, we include the terminal constraint $E(t_f) = E_{max}$ into our optimization problem. This suggests a shrinking horizon approach where the optimization horizon h is periodically decreased according to

$$h_k = h_{k-1} - \Delta t \tag{2.30}$$

where Δt is the time between two consecutive optimizations. When $h_k = \Delta t$ we have to reset it to the initial horizon h_0. The initial horizon is chosen as $h_0 = 24$ h. The electricity price changes every hour so we discretize the optimization problem with sample time $\Delta t_o = 1$h. Note that Δt_o may differ from the time between consecutive optimizations Δt. In that case, we may need to vary the size of the first step of the discretized problem in order to synchronize with price variations. To estimate hot water consumption we

used the simplest model where the predicted flow $\bar{q}_{hw}$ is assumed constant throughout the day. Here we have chosen $\bar{q}_{hw} = 0.2431$ l/min to match the daily average consumption of 350 l/day. The backoff level E_{backoff} was chosen the same as in the simple policy (2.28).

2.6.7 Simulation results

Figures 2.7 and 2.8 show a comparison between the costs achieved by the various strategies when subjected to the disturbances in price and demand shown in Fig. 2.5. The figure includes the result for the optimal variable storage policy with time between consecutive optimizations $\Delta t = 5$ min. The first thing to notice from these results is that all methods give substantial savings compared to the maximum storage policy. The optimal variable storage approach results in close-to-ideal performance even with very limited information about the demand available to the optimizer. More remarkable is the performance of the simple variable storage policy. Without any optimization algorithm or information about the price or demand it is able to give results comparable to that of the optimization-based approach. This finding should encourage practitioners to implement such simple polices to manage their energy storage units even when limited resources for advanced computer control are available.

The behaviour of the different methods can be analysed by looking at the tank volume and temperature in Fig. 2.9. We chose to show only the first three days to facilitate the visualization. Information about price and demand for the first three days is repeated in Fig. 2.6. The simple variable storage policy, the optimal variable storage and the ideal solution show very similar temperature trends. However, they differ in terms of volume. During the day, both the optimal and the simple variable storage policy try to keep the volume above a certain level $V_s = V_{min} + V_{\text{backoff}}$ which is function of the backoff E_{backoff}. On the other hand, the ideal case is able to bring the volume close to the limit V_{min} without violating constraints.

The information of temperature and volume can be summarized by the energy levels E given by the different approaches, as shown in Fig. 2.10. The scaling is done according to (2.20) to ease the analysis. Because of the perfect knowledge of the demand the ideal solution is able to take maximum advantage of price variations by letting the energy levels drop close to minimum. This is in contrast with the simple and the optimal variable storage policies, which enforce an additional buffer to ensure feasibility. In addition, the knowledge of future price allows the optimization-based approaches to buy cheaper energy in advance. This behaviour can be exemplified in the first and third days as seen in Fig. 2.10. Nonetheless, all strategies show

similar behaviour during the night, when they seek to maximize the stored energy.

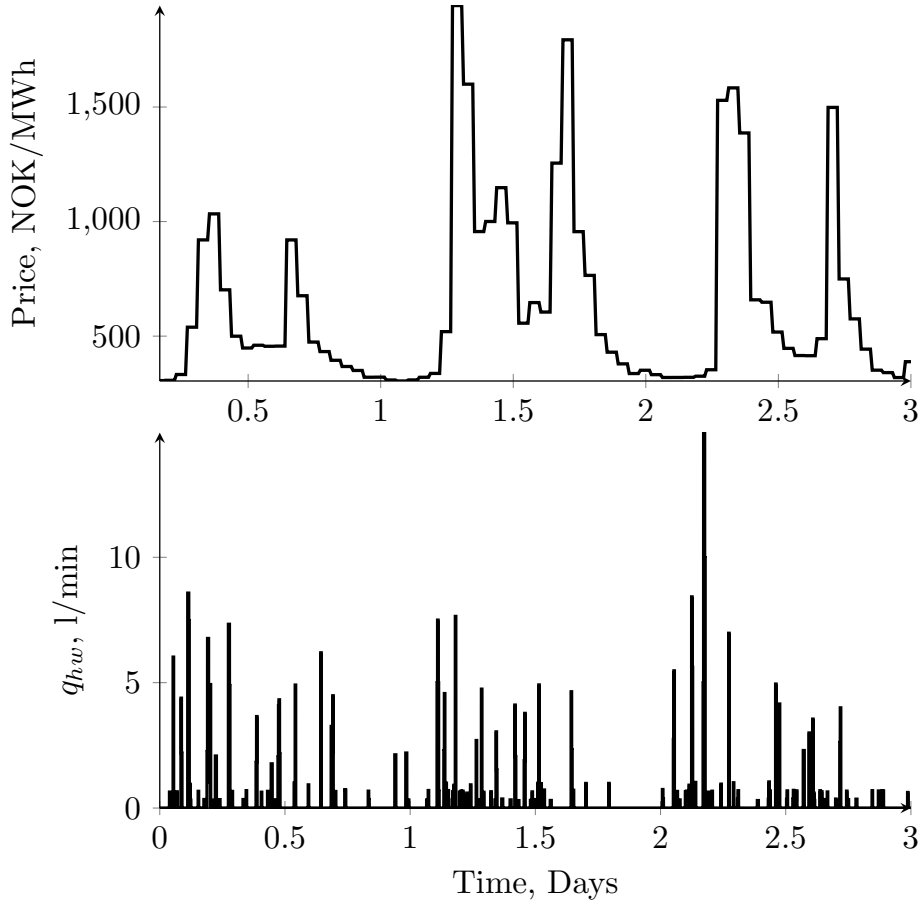

Figure 2.6: Electricity price and hot water demand. First three days.

2.7 Discussion

2.7.1 Choice of the method

We presented several strategies for operation of the water heater aiming at taking advantage of the flexibility given by the energy storage. The simple variable storage policy (2.28) gives big savings compared to the maximum storage policy, with performance comparable to that of more complex

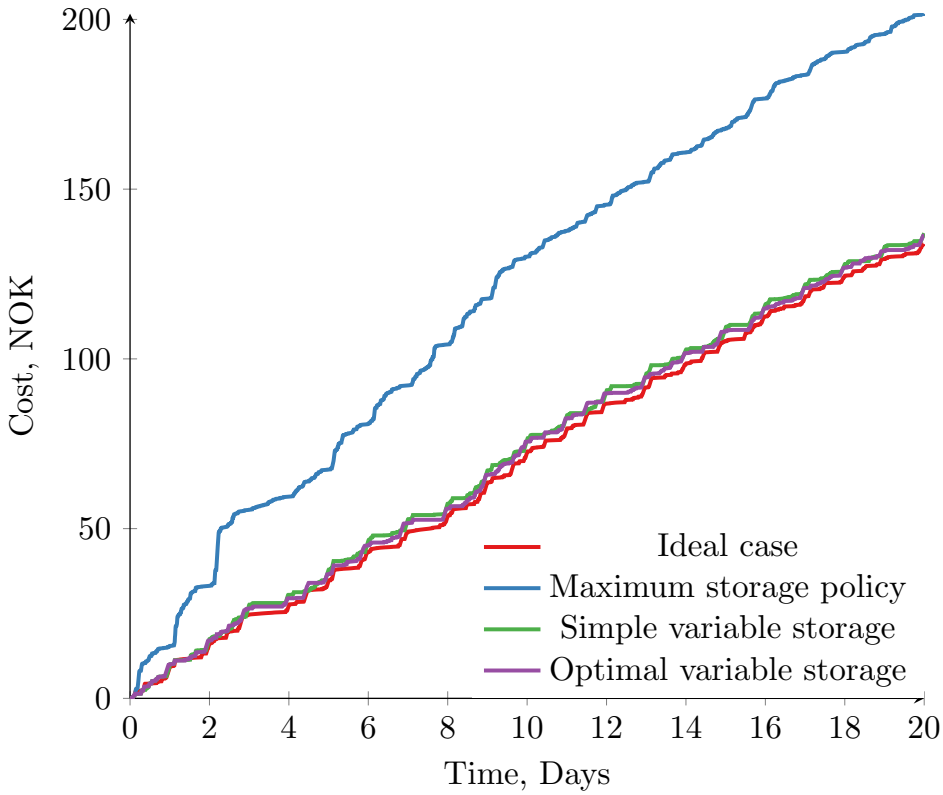

Figure 2.7: Accumlated cost for the different strategies.

optimization-based approaches. However, the question of whether or not the increased complexity and computational load in the optimal variable storage policy is justified will depend on the specific case. In scenarios in which the time intervals with the lowest price vary considerably from day to day we can expect the optimization-based method to be more beneficial. This is because the performance of the simple policy (2.28) is sensitive to our definition of 'day' or 'night'.

The ideal solution has two fundamental advantages compared to other approaches: knowledge of the future price, which allows it to buy cheaper energy in advance; and its perfect knowledge of the demand, which makes it possible to operate closer to feasibility limits. Although perfect knowledge of future demand is not realistic for this problem, there might be cases where the demand is more predictable, for instance, when the demand is linked to a contract between supplier and consumer.

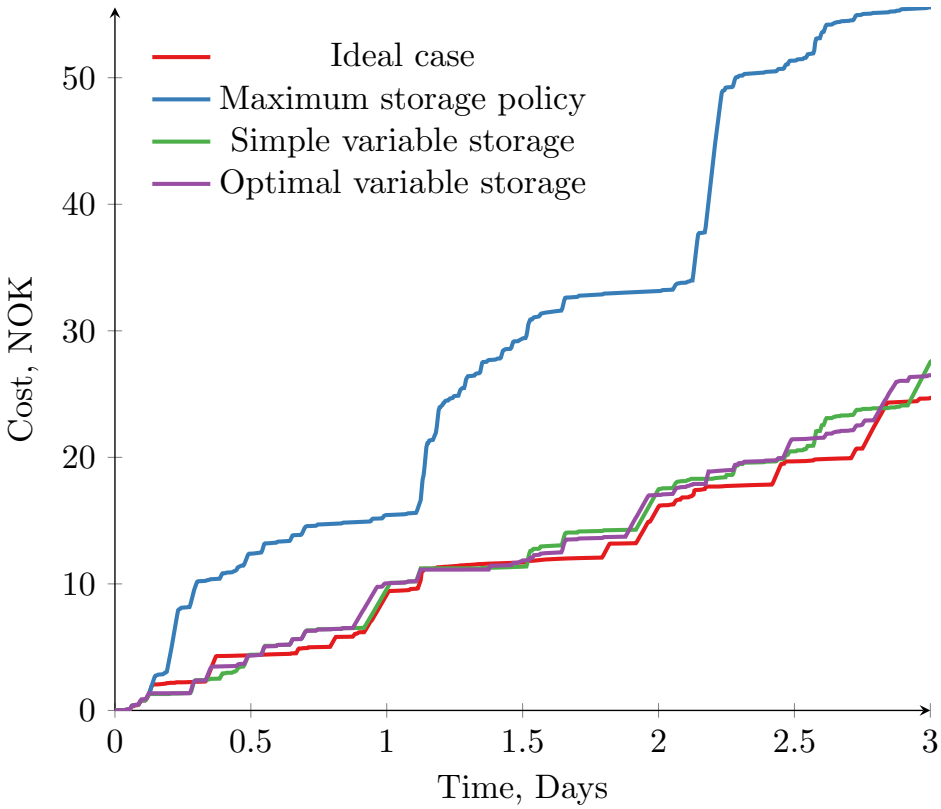

Figure 2.8: Accumlated cost for the different strategies. First three days.

2.7.2 Power consumption

Figure 2.11 shows the hourly average of 20 days of electric power consumption. The figure shows the reduction of electricity consumption during the peak hours by using an appropriate strategy. Notice that the total consumption is equal in both cases, but in the ideal case we are able to shift the load to a more beneficial period. During the peak hours in the morning (from 6am to 10am) we are able to reduce the average consumption from 1.3 kW to 0.43 kW. This indicates that the flexibility given by the thermal energy storage capacity of water heaters can be a good allied for reducing the peak demand in the electricity grid.

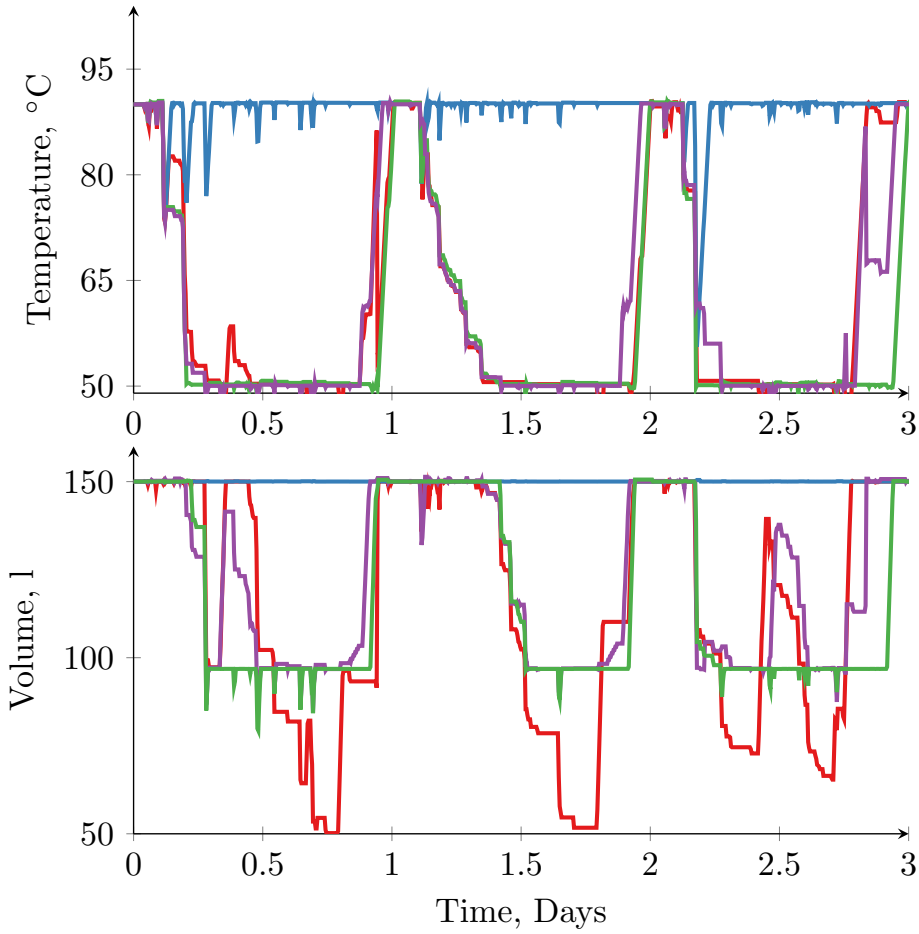

Figure 2.9: Tank volume and temperature. Red lines: ideal case. Green lines: simple variable storage policy. Blue lines: maximum storage policy. Violet lines: optimal variable storage policy.

2.7.3 Design considerations: benefits of increasing storage size

The amount of savings that can be achieved strongly depends on the storage capacity. Ideally we would like to have enough capacity so that all the demand during high price period can be supplied with energy purchased at the lowest price. The electricity price may show large variations within a day where the price is usually the lowest during the first hours. Therefore, an appropriate tank capacity should exceed the average daily consumption

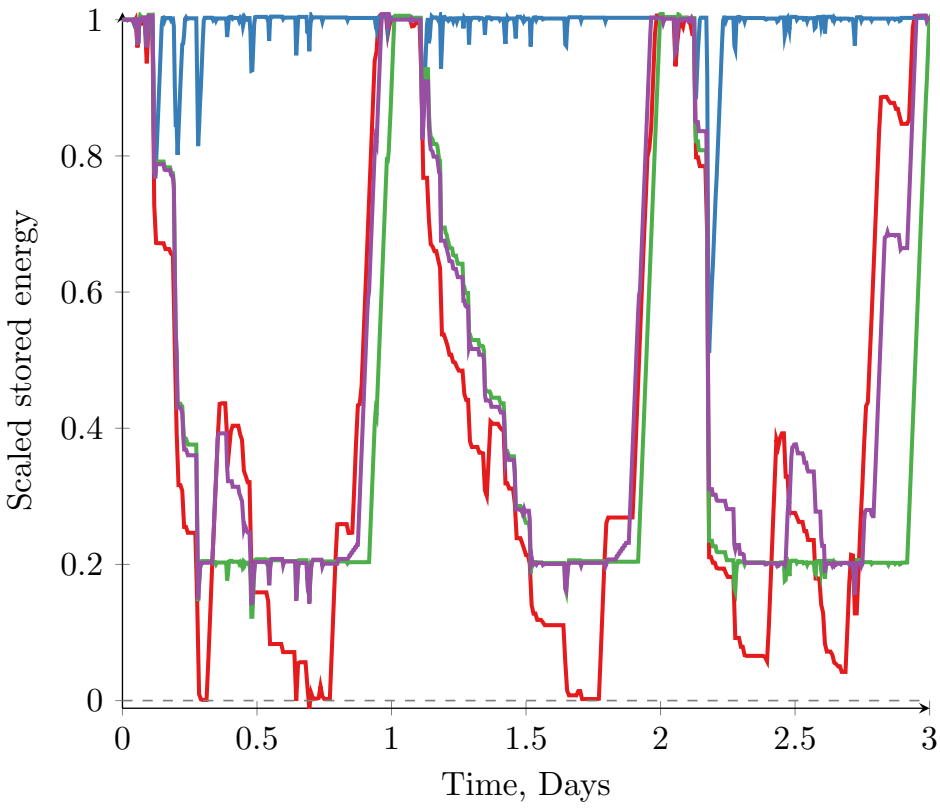

Figure 2.10: Energy level E (scaled) currently stored in the tank for the different strategies. The scaling is such that E_{max} when scaled equals one and E_{min} scaled equals zero. Red line: ideal case. Green line: simple variable storage policy. Blue line: maximum storage policy. Violet line: optimal variable storage policy..

of the household.

In order to study this aspect of the problem we have computed ideal solutions to the optimization problem for a specific day where we varied the maximum tank capacity (V_{max}) from 60 to 600 liters but kept the same price and demand profiles. The chosen price and demand profiles represent the first day shown in Fig. 2.5. Figure 2.12 depicts the optimal savings with respect to the maximum storage policy for different capacities. The savings obtained by the simple variable storage policy are also shown. The saving

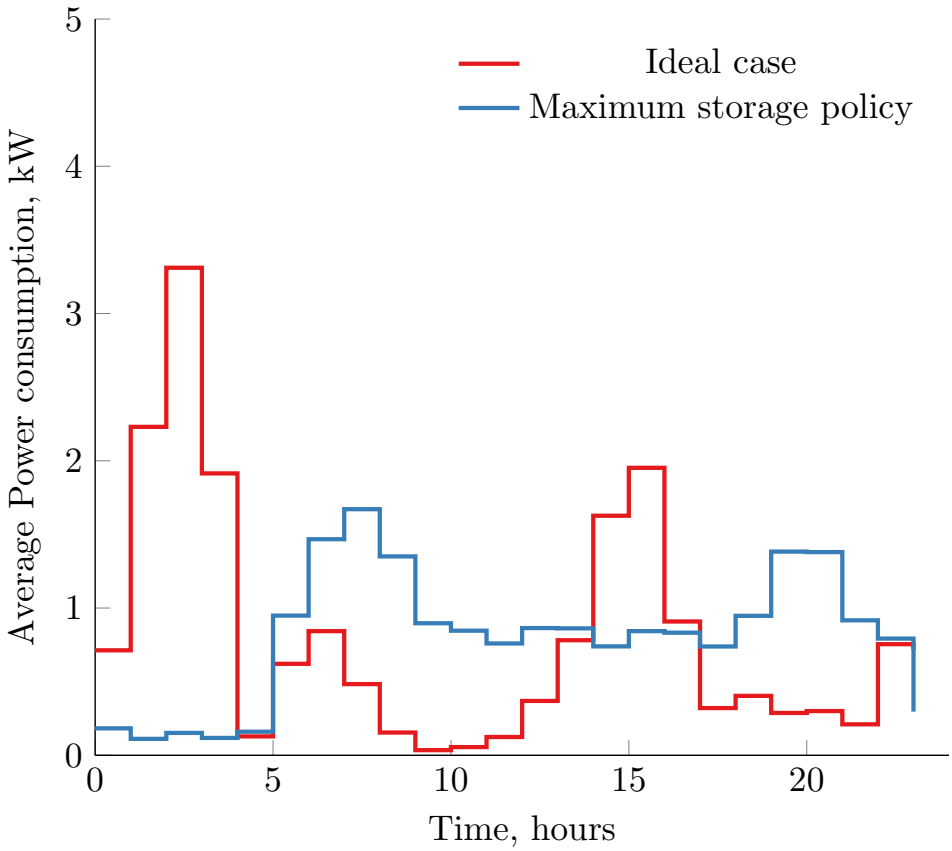

Figure 2.11: Power consumption by hour of the day. Average of 100 days. Comparison between ideal and base cases. The figure shows the reduction of electricity consumption during the peak hours (morning and afternoon).

is defined as follows

$$\text{Saving} = \frac{J^*_{\text{base}} - J^*_{\text{method}}}{J^*_{\text{base}}} \times 100 \tag{2.31}$$

where J^*_{base} is the cost (including the penalty as in (2.25)) for the maximum storage policy and J^*_{method} is the cost for a particular approach.

The study showed that there is a substantial benefit in increasing the tank size. For small tank capacities (below 100 liters) the simple variable storage policy performs worse than the maximum storage policy because of frequent constraint violations. In these cases the simple policy is not storing

enough energy to handle the demand variations. However, for large capacities the simple policy performs very well and eventually becomes optimal.

Another interesting conclusion is that the savings flatten out for capacities above a certain level. The tank size after which the savings flattens out depends on the size of the demand for a given day. The total demand for this period in terms of energy is given by

$$E_{\text{demand}} = \int_{t_0}^{t_0+24} Q_{\text{demand}}(t)dt \tag{2.32}$$

For the ideal case there is not benefit in increasing the tank size when $E(t_0) = E_{\text{demand}} + E_{min}$. If we assume $E(t_0) = E_{max}$ we can compute the ideal tank volume using $V_{opt} = \frac{E_{\text{demand}}+E_{min}}{\rho c_p(T_{max}-T_{cw})}$. For this particular day $V_{opt} = 272$ liters. The ideal tank size for the simple variable storage policy can be computed in a similar way. The only difference is that we need to take the backoff E_{backoff} into consideration so $V_{opt} = \frac{E_{\text{demand}}+E_{min}+E_{\text{backoff}}}{\rho c_p(T_{max}-T_{cw})}$. In this case the ideal tank size for the simple policy is $V_{opt} = 297$ liters.

2.7.4 Alternative applications

The methodology and insights presented in this paper could help solving other problems involving energy storage. An example is a district heating system with storage capacity. Although these systems are typically closed, in which the volume of the heating medium is constant, there might be a possibility of manipulating volume and temperature at different parts of the system if more than one storage tanks are in place. This would allow a straightforward application of the strategies presented here.

The simple policy (2.28) or the optimal variable storage policy could be directly used to control home batteries, which can help electricity consumers avoid paying peak rates.

2.7.5 Comments on the modelling assumptions

In the derivation of the dynamic model we made use of the simplifying assumption of perfect mixing in the tank. This assumption is unlikely to hold for domestic hot water systems, where vertical thermal stratification is often observed (Khalifa et al., 2009; AI-Nimr, 1994). Nevertheless, this assumption does not affect the actual results in terms of operating policies. This is because the standby losses to through the walls are approximately the same whether we consider an homogeneous temperature or a vertical temperature of the water in the tank. In addition, the economical performance depends mainly on the relation between the power that we supply

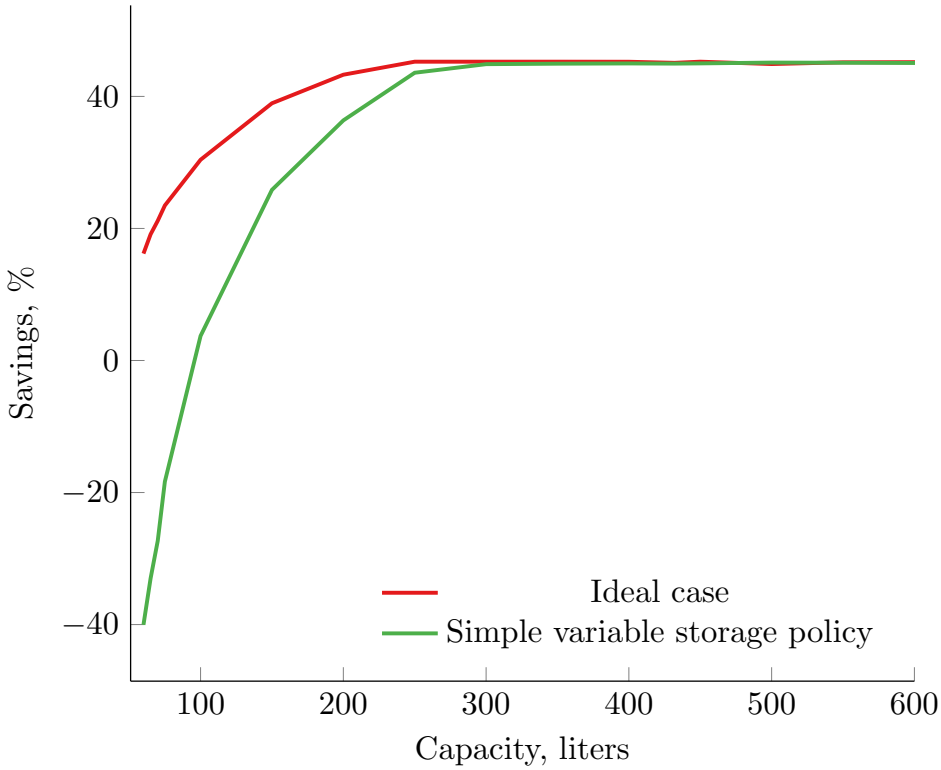

Figure 2.12: Trade-off study showing the benefits of increased storage capacity for a specific day. The savings are relative to the maximum storage policy. The nominal capacity for the case study is 150 liters.

(Q) and remove (Q_{demand}) and the current energy stock (E), and is not affected by the temperature distribution in the tank.

2.8 Conclusion

In this paper we discussed the optimal operation of the water heater system. We aimed at presenting a problem formulation that is sufficiently general to be used in similar problems that include energy storage and variable energy price and uncertain demand. The goal is to exploit the flexibility given by the energy storage capacity to take advantage of varying electricity prices. We showed that the economical benefits of energy storage can be large for the consumer, and they increase with the storage capacity. In

addition, we showed that such strategies can help reducing the power consumption during peak hours, which will benefit the electricity producers. We presented several alternatives strategies for operation of the system and we showed that simple policies can give very good performance when compared to more complex, optimization based approaches. This finding should encourage practitioners to implement such simple polices to manage their energy storage units even when very limited resources are available.

Acknowledgements

This work was partially supported by the Danish Council for Strategic Research (contract no. 11-116843) within the *Programme Sustainable Energy and Environment*, under the EDGE (Efficient Distribution of Green Energy) research project.

Chapter 3

Hierarchical control structure for dynamic optimization of energy storage systems

We consider the dynamic optimization of thermal energy storage systems in a fluctuating energy price scenario with uncertain time-varying demand. We will focus on a domestic hot water system as a case study. For this problem we propose an implementation strategy based on hierarchical decomposition of the optimization-control problem. The economic objectives and control objectives are decoupled using a two-layer cascade feedback structure. We show that the decomposed optimization problem can be written as a simple linear program (LP) which can be solved very efficiently. The main result is that great savings can be obtained at a very low computational cost and suitable for low cost embedded hardware.

3.1 Introduction

Local energy storage technologies are beneficial for electricity consumers as they enable taking advantage of electricity price and environmental conditions variations and enable higher peak capacity (de Oliveira et al., 2015). Thus, energy storage gives the user more degrees of freedom which can be exploited to yield optimal economical performance. In particular, this flexi-

bility means that energy consumption can be shifted temporally, so that an optimal objective can be achieved. The optimal operation of such systems is dynamic in nature due to the time-varying behaviour of the energy price and demand. Thus, a dynamic optimization scheme is needed to compensate these variations while minimizing the energy cost.

A popular approach to solve such problems is economic model predictive control (EMPC) (see for instance Ellis et al. (2014)) where the economic optimization and the control (tracking) problems are solved simultaneously at each sample time in one single control layer. Although EMPC is theoretically the optimal strategy, it has some important practical drawbacks. Considering that EMPC must use a sufficiently large prediction horizon to account for a time-varying economic cost, the optimization problem may be difficult to solve fast enough to control the system in real-time. Additionally, compared to traditional hierarchical control strategies, EMPC requires more detailed and complex models are in order to ensure that the constraints are satisfied, which makes the problem more difficult to be solved efficiently. Finally, it can be difficult to balance the two different objectives of optimal economics and desired dynamic control performance, including robustness and stability in a single controller.

In this paper we propose a hierarchical optimization/control structure for the optimal operation of storage systems where the problem is decomposed into an upper layer, responsible for the economic (real-time) optimization, and a feedback control control layer that follows setpoints computed by the upper layer. As a case study we consider the optimization of an electric water heating system which provides hot water for domestic usage. The main idea is to use the heat capacity of the water tank to *store energy* at times when electric power is cheap and use it to match the demand when energy is expensive.

In this paper we formulate a simplified optimization problem in terms of the energy storage E (the optimization degree of freedom) only and then translate the optimal energy level into volume and temperature setpoints (the controlled variables for the regulatory layer). We define the energy storage as

$$E = \rho c_p V (T - T_{cw}) \tag{3.1}$$

where V is the water volume in the tank, T is water temperature in the tank, T_{cw} is the temperature of the cold refilling water from the network, ρ is the water density and c_p is the heat capacity of the water. It turns out the reformulated optimization problem in terms of E is linear, which greatly facilitates the numerical solution of the problem.

In order to make our approach applicable to other problem areas, it is

necessary to distil the key elements and ideas which enable us to simplify our problem.

1. *Choice of the right decision variables for the optimization problem.* In this case the transformation to stored energy E allows the formulation of a linear program.

2. *Use of time-scale separation.* By selecting appropriate decision variables and by introducing a feedback control layer running in a faster time scale it is possible to reduce computational the load of the optimization problem.

3. *Use of process insight* to reformulate the problem such that it becomes simple.

4. *Make use of Periodic behaviour* of the system to reduce the size of the infinite time horizon dynamic optimization problem by decomposing it into smaller independent sub problems that are solved sequentially.

By carefully examining the problem and exploiting the key elements above, we can achieve significant benefits, for optimizing the operation e.g. a domestic hot water system in a smart grid environment. In particular:

- Minimum modelling efforts are needed.
- Decisions about how to handle constraints on temperature and volume can be decoupled from the economic optimization problems.
- The lower control layer ensures feasibility of the output constraints whenever it is possible. This implies that it is not necessary to resolve the optimization at each sample time, but instead depending on the nature of the price and demand variations.
- We show that the decomposed optimization problem can be written as a simple linear program (LP) which can be solved very efficiently. The main result is that great savings can be obtained at a very low computational cost, making it suitable for low cost embedded hardware.

We believe that our framework can be used as a starting point to solve similar problems involving energy storage systems, such as district heating systems. Moreover, we hope that the development of these low-cost solutions will allow the widespread use of energy storage systems, which in term helps the integration of renewable energy sources into the grid.

The chapter is organized as follows: Section 3.2 presents the process models and introduces relevant notation; Section 3.3 formulates the optimal control problem; In Section 3.4, the proposed method is detailed; Section 3.5 details a simulation study comparing various approaches. Discussions and conclusions are presented in Section 3.6 and Section 3.7, respectively.

3.2 Process description

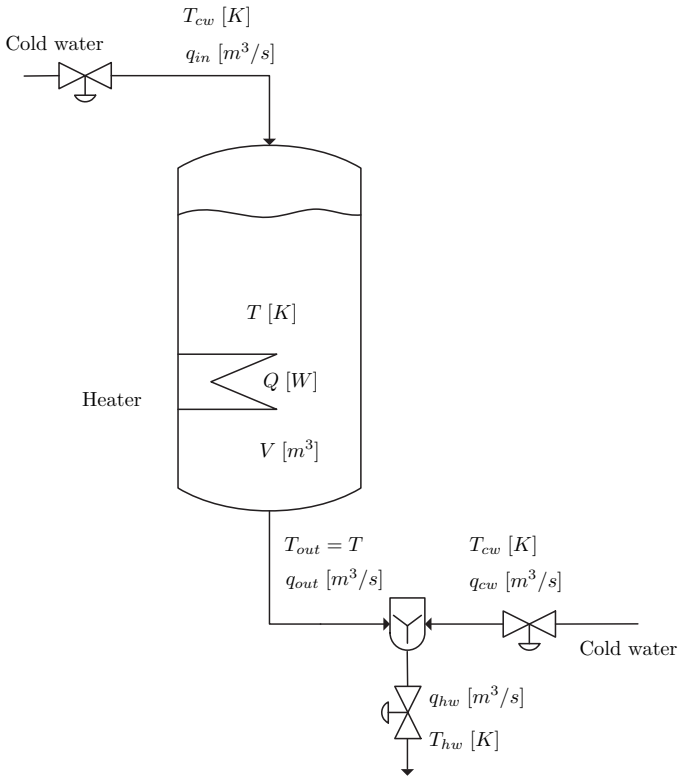

Figure 3.1: Simplified process flow scheme

The process we are studying in this paper consists of a heater that provides hot water for domestic usage. This is the same application considered in de Oliveira et al. (2015). A process flow scheme is shown in Figure 3.1 where the important notation is presented. The system includes a cold water source, a thermally insulated tank, a heating coil with adjustable power and control valves that regulate the cold water inflow q_{in} and the hot water outflow q_{out}. A somewhat unusual feature of this system is that the hot

water that leaves the tank (q_{out}) is mixed with a cold water stream (q_{cw}) from the same water source. This extra mixer is introduced to allow for extra flexibility because the water in the tank can be heated to a higher temperature than the hot water to the consumer (T_{hw}).

3.2.1 Energy storage and demand

In this subsection we introduce some terms that will be useful for analysis. We define the energy stored in the tank relative to the current cold water supply temperature (T_{cw}) as

$$E = \rho c_p V (T - T_{cw}) \; [J] \tag{3.2}$$

We define the energy demand at any given time as

$$Q_{\text{demand}} = \rho c_p q_{hw} (T_{hw} - T_{cw}) \qquad [\text{J/s}] \tag{3.3}$$

This is the energy we would need to supply at any given time if there were no energy storage. The dynamics of the energy storage E can be written as (see the accompanying paper (de Oliveira et al., 2015) for derivation)

$$\frac{dE}{dt} = Q - Q_{\text{demand}} - Q_{loss} \tag{3.4}$$

that is, the change in the stored energy is the difference between the net current heating ($Q - Q_{loss}$) and current use Q_{demand}. In some cases, because the insulation of the tank, the heat loss may be neglected ($Q_{loss} = 0$) resulting in the simple dynamics

$$\frac{dE}{dt} = Q - Q_{\text{demand}} \tag{3.5}$$

The assumption of zero heat loss is made here to further simplify the optimization problem formulation.

3.3 Problem formulation

In this section the original optimization problem formulation is presented. Here, the operational constraints as well as the optimization objectives are defined.

3.3.1 Independent variables

Control degrees of freedom

From Fig. 3.5, the system has four independent variables, namely, Q, q_{cw}, q_{hw} and q_{in}. However, as discussed next, two of these variables (q_{hw} and q_{cw}) are used to satisfy given demand requirements on the hot water flow (q_{hw}) and temperature (T_{hw}), respectively. The remaining two degrees of freedom which can be used to optimize the system with respect to economics are the power input Q and the cold water inlet flow q_{in}.

Disturbances

The hot water flow rate, q_{hw}, and the hot water temperature setpoint, $T_{hw,s}$ are set by the user and are considered disturbances from a control point of view. The hot water temperature T_{hw} is controlled by manipulating q_{cw} while the flow rate q_{hw} is controlled using q_{out}. The main disturbances for the optimization are related to the user demand q_{hw} and the price of electricity p. The cooling water temperature T_{cw} and hot water temperature setpoint $T_{hw,s}$ are assumed constant.

3.3.2 Constraints

During operation the system must respect constraints related to physical limitations, safety and specifications. Firstly, in terms of inputs, the heating power and water inflows are limited, so that

$$0 \leq Q \leq Q_{max} \tag{3.6}$$
$$0 \leq q_{in} \leq q_{max} \tag{3.7}$$

In terms of output constraints, the temperature of the water is be bounded above by T_{max} for safety reasons and indirectly bounded below by $T_{hw,s}$ to guarantee that the desirable temperature of the hot water is always achievable. Naturally, the volume is bounded by the size of the tank. Therefore, we have

$$T_{min} \leq T \leq T_{max} \tag{3.8}$$
$$V_{min} \leq V \leq V_{max} \tag{3.9}$$

where $T_{min} = T_{hw,s}$.

3.3.3 Optimization objective

The operational objective is to minimize the energy costs

$$J = \int_{t_0}^{t_f} p(t)Q(t)\,dt \tag{3.10}$$

where $p(t)$ is the time-varying electricity prices, t_0 is the initial time and t_f is the final time. In addition, we want to satisfy the constraints (3.6), (3.7), (3.8) and (3.9) and the process dynamics.

3.4 A hierarchical control approach for real time dynamic optimization

As stated earlier, for online optimization there are two different implementation philosophies:

- **Single layer strategy (EMPC)** in which optimization and control are integrated; Here, the optimization problem (3.10) is solved using a moving horizon approach and the optimal inputs (q_{in} and Q) are recomputed directly (by the optimizer) at every time sample. This is, in theory, the optimal approach. However, it requires high computational power as the full optimization problem needs to be solved at every time sample.

- **Two level strategy** where the optimization problem is decomposed in two simpler problems where the economic objectives are decoupled from the control objetives.

The second strategy is our preferred and will be further detailed in this section. The basic idea is to decompose the overall problem of economic optimization and control (Eq. (3.10)) into consistent and simple subproblems by using a cascade feedback structure. In this scheme the bottom layer is a regulatory control layer that follow the set-points specified by an optimizer in the upper layer. The idea is exemplified in Fig. 3.2 where K is the regulatory controller and H is the controlled variable (CV) selection matrix. All the measured quantities are represented by the variable y while c are the controlled variables. We will show that, because of this decomposition, the remaining optimization problem for the upper layer can be written as a simple linear program (LP) which can be solved very efficiently at a low computational cost. The LP is solved online using a model predictive control (MPC) approach. The basic differences between the EMPC and the

proposed two-layers approach for our problem is depicted in Fig. 3.3 and Fig. 3.4. In the remaining of the section we will detail this idea.

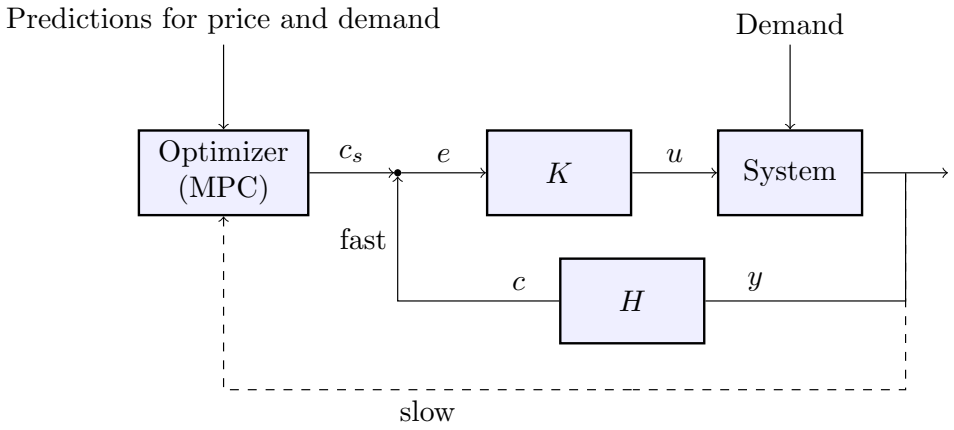

Figure 3.2: Hierarchical control structure

In order to successfully apply the hierarchical approach we follow these main steps:

1. Define the problem formulation (economic objective, constraints and decision variables) for the optimizer (upper layer).

2. Choose the controlled variables c that are used to link the two layers.

3. Design a robust regulatory control layer for tracking the reference c_s.

A key requirement for the hierarchical approach is a time scale separation between the layers. The optimization layer updates the setpoints at every Δt time units, while the control layer updates the control inputs every Δt_c time units, where $\Delta t_c << \Delta t$. We assume here that the control layer reaches steady state in less than Δt time units.

In the sequel we will discuss the details of step 1 and step 2. In addition, we will present other important elements in this framework. The first element is the demand model, which is central in the optimization scheme. Another important aspect is the use of back-off for the setpoints, which is necessary to minimize the risk of violating the constraints caused by unexpected high demand. This is important due to the stochastic nature of the hot water consumption. At the end of this section we will propose simple strategies for implementation of these elements.

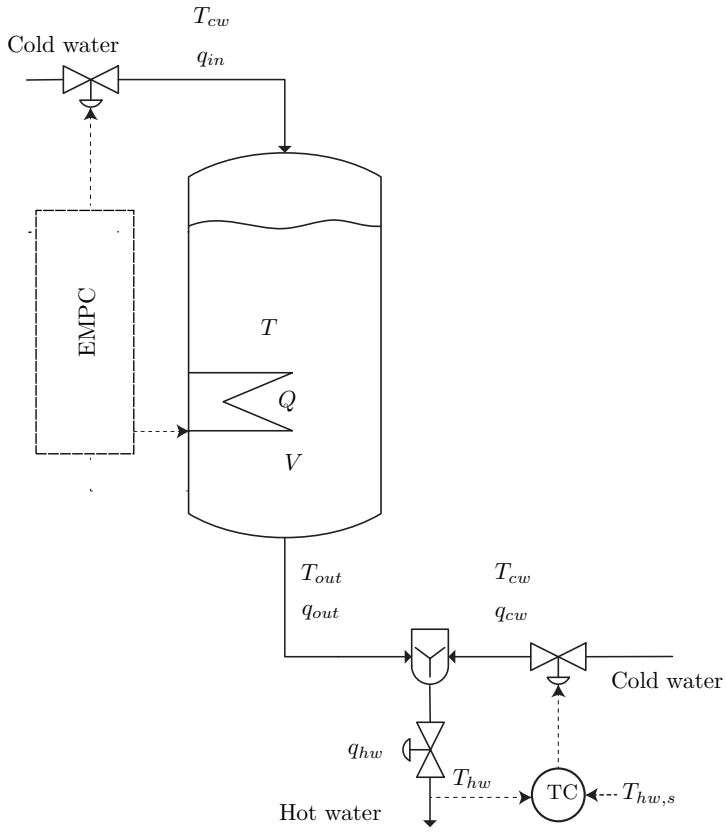

Figure 3.3: Schematic of the process controlled by EMPC. The optimization and control objectives are combined into one layer, which manipulates the degrees of freedom (Q and q_{in}) of the system directly.

3.4.1 Problem formulation for the optimization layer (step 1)

We consider the simple alternative energy balance (3.5). We would like to have a discrete-time formulation to facilitate implementation and solution of the optimal control problem. Considering that the optimization problem is discretized with sampling time Δt_o, the model can be written in discrete time domain using an Euler discretization as:

$$E_{k+1} = E_k + \Delta t_o(Q_k - Q_{k,\text{demand}}) \tag{3.11}$$

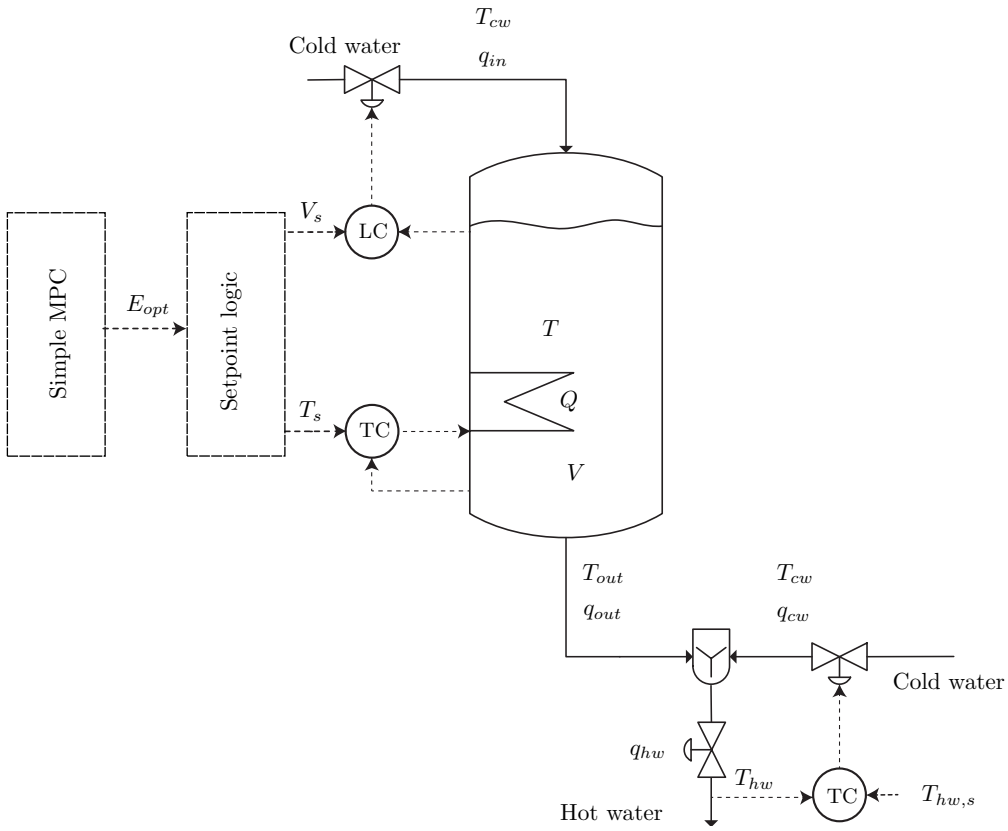

Figure 3.4: Schematic of the process controlled by the proposed approach. The control and the optimization objectives are decoupled.

where k is the current time step; and we assume a constant heat input Q_k and energy demand $Q_{k,\text{demand}}$ during the interval Δt_o. This means that we consider an average demand for the each time interval. Note that the sampling time Δt_o used to discretize the optimization problem may differ from the time between two consecutive optimizations Δt.

At every sample time Δt we attempt to minimize the following cost

$$J_N = \sum_{k=0}^{N-1} p_k Q_k \Delta t_o \tag{3.12}$$

subject to the dynamics (3.11) and the constraints $0 \leq Q \leq Q_{max}$ and $E_{min} \leq E \leq E_{max}$ where N is the horizon length given in sample times.

The constraints on the energy storage E are defined as

$$E_{max} = \rho c_p V_{max}(T_{max} - T_{cw}) \tag{3.13}$$

and

$$E_{min} = \rho c_p V_{min}(T_{min} - T_{cw}) \tag{3.14}$$

Soft-constraints

For unexpected large disturbances it may happen that the energy level E drops below the minimum E_{min}. Therefore, to avoid feasibility problems we can use a formulation based on soft-constraints. In this case the cost function becomes

$$J_N = \sum_{k=0}^{N-1} p_k Q_k \Delta t_o + \sum_{k=1}^{N} \mu[\varepsilon_k]^- \tag{3.15}$$

where $\varepsilon_k \equiv E_k - E_{min}$ and we make use of the notation $[y]^- = \max(0, -y)$. The penalty parameter μ is a positive scalar constant. The linear penalty function is chosen because it is exact in the sense that minimizing (3.15) also minimizes the original cost function (3.12) provided that μ is large enough and that the original problem is feasible (Nocedal and Wright, 2006).

Terminal state constraint and optimization horizon size

The electricity price tends to be the lowest during night when the overall electricity consumption is reduced, and it peaks in the morning when the demand is high. The hot water demand profile shows a similar behaviour, where the demand peaks early in the morning. Based on this observation we have the following insight

> *It is optimal to have maximum energy capacity stored ($E = E_{max}$) late in the night.*

This means that a final constraint $E_N = E_{max}$ may be included in the optimization problem. This constraint reduces the dimension of the problem because it decouples the optimization problem of two consecutive days. In addition, the insight suggests that a shrinking horizon approach may be used where N is reduced at every step as we approach the end of the 24h horizon. After the end of the horizon is reached ($N = 1$), a new optimization day starts and the problem should be reset with a full 24h horizon.

Eliminating the heat input from the decision variables

The formulation with the heat input Q as the decision variable may require short discretization time Δt_o in order to allow for fast changes in the manipulated variable. However, we can redefine the optimization problem using the energy levels E_k as the only decision variables. This is done by rearranging equation (3.11) and using the following expression

$$Q_k = (E_{k+1} - E_k)/\Delta t_o + Q_{k,\text{demand}} \tag{3.16}$$

in the optimization problem formulation. $Q_{k,demand}$ must be computed using an appropriate forecast model as discussed later. This results in the following moving horizon LP:

$$\min_{E} J_N = \sum_{k=0}^{N-1} p_k[E_{k+1} - E_k + \Delta t_o Q_{k,\text{demand}}] + \sum_{k=1}^{N} \mu[\varepsilon_k]^-$$

subject to:

$$E_{min} - \varepsilon_k \leq E_k \leq E_{max} \tag{3.17}$$
$$0 \leq (E_{k+1} - E_k)/\Delta t_o + Q_{k,\text{demand}} \leq Q_{max} \tag{3.18}$$
$$E_N = E_{max} \tag{3.19}$$

Here, $k = 0$ is the current time and E_0 is the current state measurement. Notice that our decision variable is the ideal energy levels E_k at each time step. One of the main advantages of this formulation is that it results in a linear programming problem (LP) which can be solved very efficiently compared and is suitable for low cost hardware.

Comments on the cost function and the sampling time

Assuming feasibility for the entire horizon ($\varepsilon = 0$) we can rewrite the cost function as

$$J = \left[\sum_{k=1}^{N-1} E_k(p_{k-1} - p_k)\right] + \left[\sum_{k=0}^{N-1} p_k \Delta t_o Q_{k,\text{demand}}\right] + E_N p_{N-1} - E_0 p_0 \tag{3.20}$$

This allows us to draw some interesting insights about the optimization problem. We see that for a constant price scenario the first term in the right-hand side is zero and thus the total cost is fixed by the problem parameters

(the initial condition (E_0), the final state constraint E_N and the demand profile $Q_{k,\text{demand}}$) and does not depend on the decision variables. This implies that any solution that satisfies all the constraints is indeed optimal.

For a time-varying price scenario, the first term in (3.20) becomes relevant from which we get another important insight: there is no economical benefit in discretizing the optimization problem with sampling time Δt_o smaller than the update frequency of the energy price p_k. For instance, if the prices are updated in an hourly basis, there will be no economic benefits in choosing $\Delta t_o = 10$ min, since variations in E_k within the hour will not affect the total cost. This indicates that we can choose $\Delta t_o = 1$ hour, fact that greatly reduces the computational burden. Nevertheless, when large discretization time Δt_o is used we might be dynamically infeasible. That is, we might violate the constraint for a short period, even though we have $E_k \geq E_{min}$ at the end of the time interval k. This is because the peak demand gets average out when large sampling times Δt_o are used. This restriction may become important when the size of the demand is large compared to the tank capacity.

On the other hand, a short time between optimizations (Δt) can be very beneficial. Since the demand is very uncertain, short Δt provides fast feedback from the current state to the optimization algorithm allowing it to improve its solution based on updated information. Nevertheless, Δt should be bounded below to ensure a time-scale separation between the optimization and the control layer.

3.4.2 Computation of the back-off

Generally is not possible to ensure $E \geq E_{min}$ at all times because of the high uncertainty and stochastic nature of the demand profile. To decrease the probability of violating the constraints we may back off from the constraint if the current desired energy level E_s (computed by the MPC) is too close from the boundary E_{min}. A straightforward approach is to enforce an additional energy buffer ΔE_{buffer} so that $E_s \geq E_{min} + \Delta E_{buffer}$. The energy buffer level should be adjusted such that the amount of constraint violations is acceptable for the given case.

3.4.3 Selection of the controlled variables (step 2)

The solution of the LP problem presented above gives the optimal energy levels E_s at every time step but does not tell us directly what the control inputs should be. Using the fact that $E = \rho c_p V(T - T_{cw})$ we see that the tank temperature T and volume V are suitable candidates for controlled

variables. However, there are infinite combinations of level V and temperature T that result in a specific energy level E at any given time, indicating non-uniqueness in the choice of the setpoint values for the control layer. To minimize energy losses, which have not been included in the model, we would like to minimize the temperature T, which is achieved by having V_s at its maximum feasible value (V_{ub}). For a given energy level E, the maximum feasible is the highest allowed volume in the tank that still ensures $T \geq T_{hw,s}$ whenever this is possible. Thus, it follows from the definition of E that the desired temperature setpoint can be obtained from

$$T_s = \frac{E_s}{\rho c_p V_{ub}} + T_{cw} \tag{3.21}$$

3.4.4 Regulatory control

The control objective can be achieved by the regulatory control layer structure shown in Figure 3.5 where we use the water refilling (q_{in}) to control V and use the heat input (Q) to control T. However, for large disturbances the temperature controller might saturate ($Q = Q_{max}$) and, when $T_s = T_{hw,s}$, it is not advantageous to have $V = V_s$ as it will force T to drop below $T_{hw,s}$ and we should let V drop. A simple way to achieve this is by the split range control structure shown in Fig. 3.6. The basic idea is that a single controller uses both the power input Q and the modified level setpoint V_s^* to control the temperature when the setpoint is $T_s = T_{hw,s}$. The modified level setpoint lies within the lower bound V_{min} and the setpoint computed by the optimizer layer V_s, that is $V_{min} \leq V_s^* \leq V_s$. The temperature controller computes a virtual control action u which is translated to values for Q and V_s^* according to a defining function as depicted in Fig. 3.7. To ensure that the control loop gains do not change with V_s, we could vary the upper bound for the virtual control action u according to the current value V_s.

3.4.5 Constructing a demand model

An important factor for the success of this approach is to have relevant information about the user demand. An approach is to construct a demand model based on the empirical distribution of hot water consumption for every time step using historical data. This model can be updated online as new measurements become available, making it possible to adapt to new consumption patterns when necessary.

A simple idea is to compute the average demand $\bar{Q}_{\text{demand}} = \rho c_p q_{hw}(T_{hw} - T_{cw})$ for every time interval (for example, for every hour of the day) using

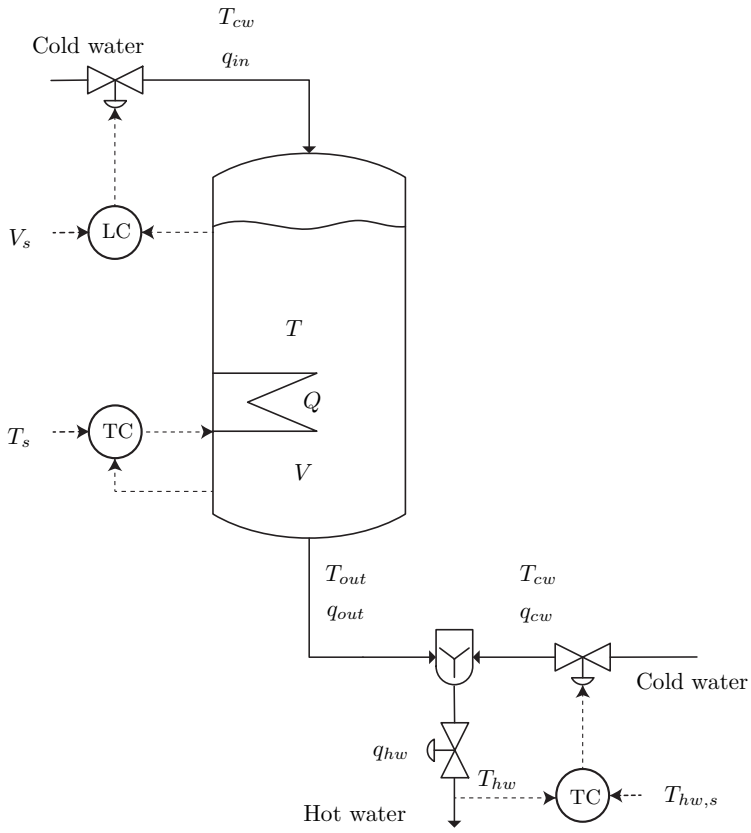

Figure 3.5: Regulatory control structure, used when $T_s > T_{hw,s}$.

the available data. Note that we require measurements of the hot water flow q_{hw}, the hot water temperature T_{hw} and the cold water temperature T_{cw}. Parameters ρ and c_p can be considered constant. The estimates $\bar{Q}_{\text{demand}}$ can be updated online using a day-to-day update rule based on, for example, an exponential moving average filter. For every time interval in which we discretized the day we have a day-to-day update rule in the form

$$\bar{Q}_{\text{demand}} = \alpha Q_{\text{meas, demand}} + (1-\alpha)\bar{Q}_{\text{previous, demand}} \tag{3.22}$$

where $\alpha \in (0,1)$ is the discount factor, $Q_{\text{meas,demand}}$ is the measurement of the demand for the current day, and $\bar{Q}_{\text{previous,demand}}$ is the previous estimate for the demand.

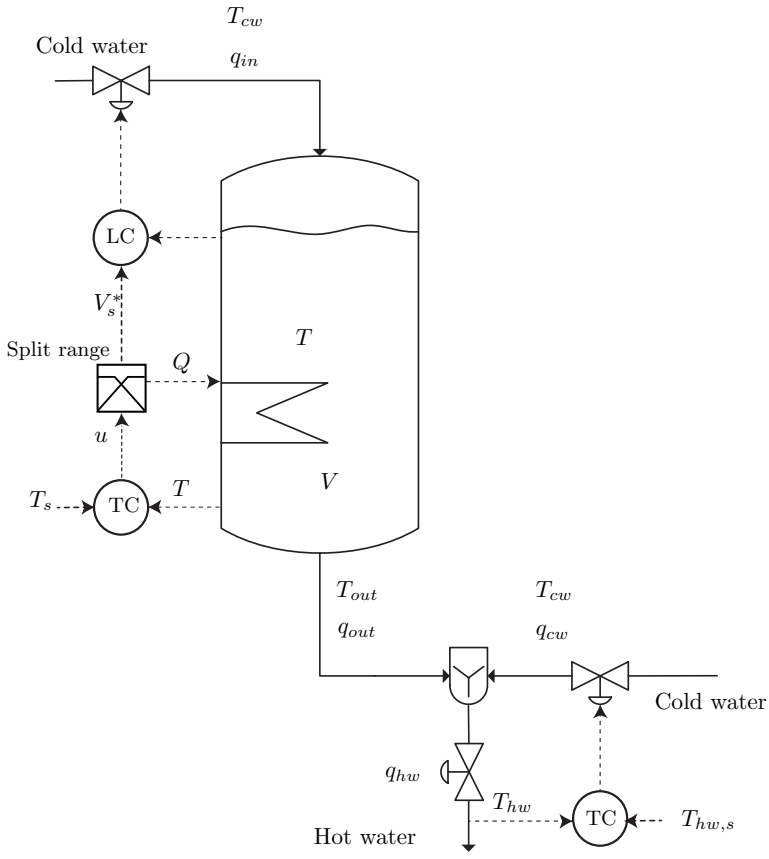

Figure 3.6: Split range control structure, used when $T_s = T_{hw,s}$.

3.5 Case Study

In this section we show a simulation example of the methodology presented in the previous sections. The idea here is to have a better understanding of the potential benefits of using energy storage in this problem. A comparison of the various strategies will be presented.

3.5.1 Electricity prices

For simulation and optimization we used the electricity price data available in the archives of the Norwegian Nord Pool spot market (NordPoolSpot, 2014). A sample of the electricity price for the first 10 days of February, 2012 in Trondheim, Norway is shown in Fig. 3.9. Although Norway currently

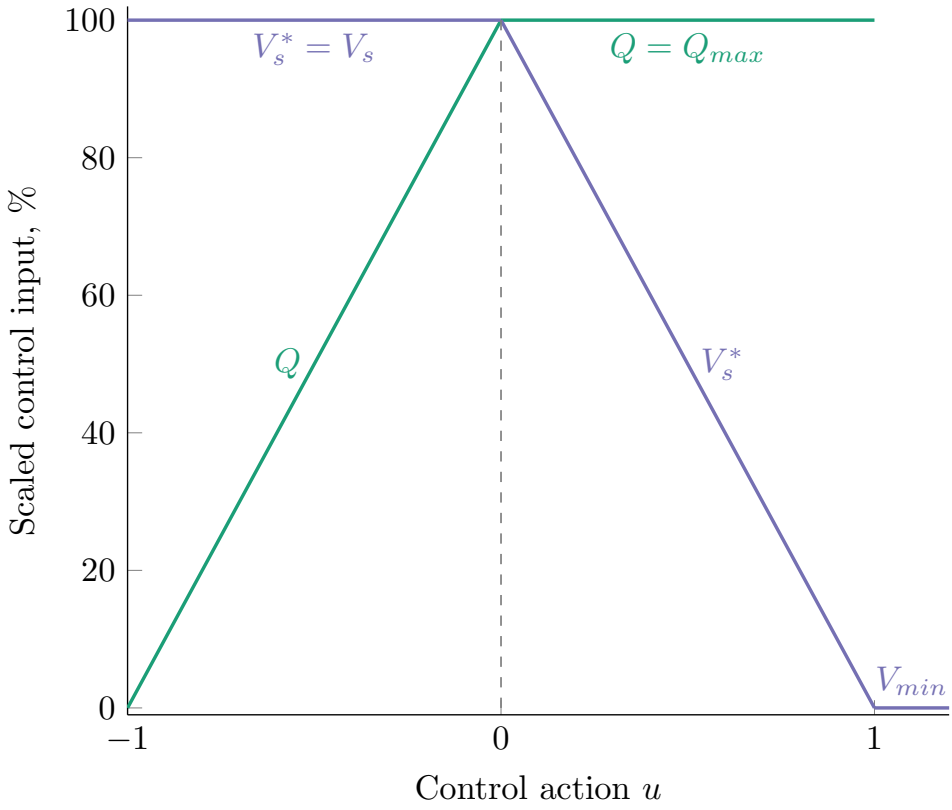

Figure 3.7: Simple representation of a split-range control where both the power Q and the modified level setpoint V_s^* are used to control the temperature when the setpoint is $T_s = T_{hw}$.

does not use real-time pricing for the individual end-user, the spot prices provide a reasonable real-time pricing estimates. The resolution of the price data is one hour.

3.5.2 Realistic hot water demand

For a realistic comparison, we emulate hot-water flow demand (q_{hw}) profiles based on the empirical probability distributions published by Jordan and Vajen (2001). The consumption profiles have a resolution of one minute and correspond to a single family house with a mean load volume of 350 litres per day. An example of a consumption profile is depicted in Fig. 3.9, where twenty unique hot-water profiles were generated. For simplicity, we will assume constant temperature setpoint $T_{hw,s}$ and cold water temperature

T_{cw}. In addition, we neglect heat losses ($Q_{loss} = 0$). Additional parameter values for our case study are presented in Table 4.2.

Table 3.1: Parameters description

Parameter	Description	Value	Unit
Q_{max}	Maximum power	5	kW
Q_{min}	Minimum power	0.0	kW
T_{max}	Temperature upper bound	90	°C
V_{max}	Volume upper bound	150	l
V_{min}	Volume lower bound	50	l
T_{cw}	Cold water temperature	5	°C
T_{hw}^{sp}	Hot water temperature	50	°C
c_p	Heat capacity of the water	4.19	kJ/kg/K
Q_{loss}	Heat loss	0	kW

3.5.3 Demand models

In order to construct our demand model in terms of Q_{demand} we generate thirty unique flow q_{hw} profiles based on distributions given in Jordan and Vajen (2001) with a duration of 24h each. Then, we compute the average demand $\bar{Q}_{demand}$ for every time interval of the day. Here we chose to discretize the day in a hourly basis ($\Delta t = 1$ h), and therefore we computed 24 averages $\bar{Q}_{k,demand}$. For comparison we also constructed a very simple demand model where we assume constant demand throughout the day. Figure 3.8 shows examples for these models. Both models are used to estimate the expected consumption in the MPC algorithm.

3.5.4 Ideal case (EMPC with known future disturbances)

To compute the ideal solution, that we use as a benchmark for comparing our simplified method, we discretize the original full nonlinear optimal control problem using orthogonal collocation in a simultaneous approach (Biegler, 1984). In this approach, the differential equations are converted to algebraic ones by orthogonal collocation which should be satisfied only at the solution of the optimization problem (Biegler, 1984). The key characteristic here is that both states and manipulated variables profiles are approximated, with the same accuracy, by orthogonal polynomials, resulting in a large scale nonlinear programming problem (NLP). An interesting characteristic of this

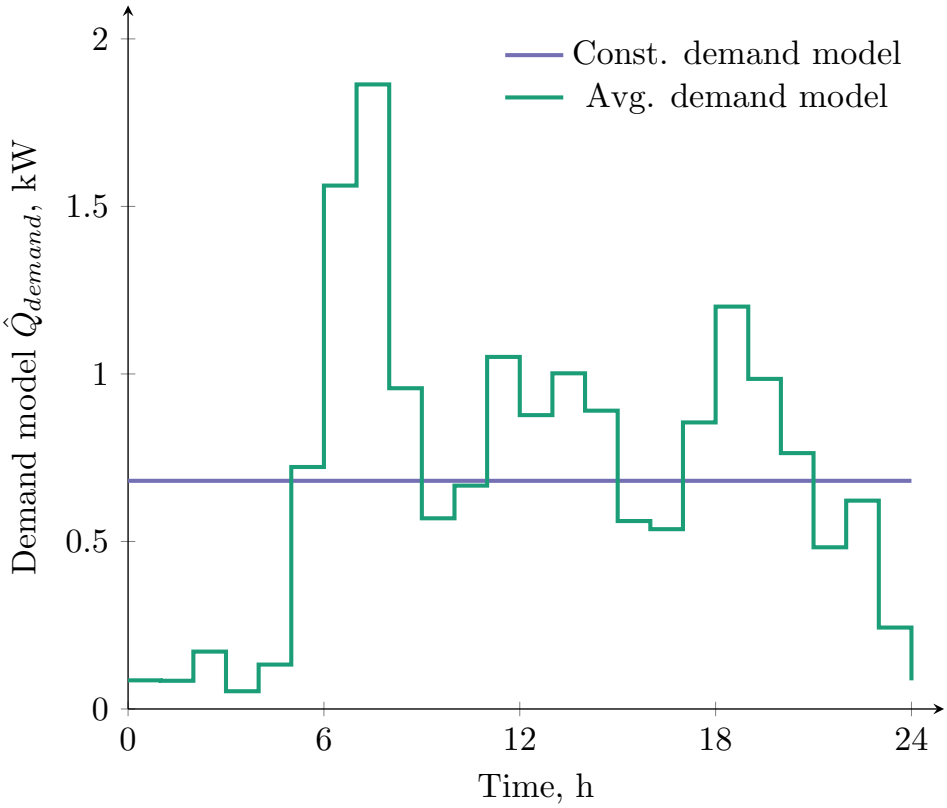

Figure 3.8: Simple demand models used in the MPC algorithm.

method is that it can efficiently handle problems with constraints on states and control inputs.

We formulate the problem in Matlab and solve it using the sparse NLP solver SNOPT (Gill et al., 2002). This solver employs a sparse SQP algorithm with quasi-Newton approximations to the Hessian. Gradient information is obtained using a symbolic differentiation approach. The interface between Matlab and SNOPT is handled by the optimization environment TOMLAB.

The optimization for every day is carried out independently, where we consider the initial time $t_0 = 4$h in the morning and a horizon $h = 24$ hours. The tank is always initially full ($E(t_0) = E_{max}$) and we impose the terminal constraint $E(t_f) = E_{max}$.

3.5.5 Simplified MPC

As in the ideal solution, we include the terminal constraint $E(t_f) = E_{max}$ into our optimization problem. This suggests a shrinking horizon approach where the optimization horizon h is periodically decreased according to

$$h_k = h_{k-1} - \Delta t \tag{3.23}$$

where Δt is the time between two consecutive optimizations. When $h_k = \Delta t$ we have to reset it to the initial horizon h_0. The initial horizon is chosen as $h_0 = 24$ h. The electricity price changes every hour so we discretize the optimization problem with sample time $\Delta t = 1$h. Note that Δt may differ from the time between consecutive optimizations Δt. In that case, we may need to vary the size of the first step of the discretized problem in order to synchronize with price variations. The LP problem in the MPC layer has at most $n = 2 \times 24 = 48$ decision variables (24 energy levels + 24 slack variables), resulting in very low computational requirements, making it suitable for implementation in low-cost embedded hardware.

3.5.6 Maximum storage policy (Base case)

For comparison we include simulations of a very simple policy where we try to maintain maximum storage in the tank at all times. This is achieved by fixing the tank temperature setpoint T_s and tank volume setpoint V_s at their maximum allowed value. This is the safest policy in terms of avoiding constraint violation caused by unforeseen high demand, but it does not try to compensate for price variations.

3.5.7 Simulation results

Figure 3.11 shows a comparison between the costs achieved by the various strategies when subjected to price and flows shown in Fig. 3.9. The figure includes the result for the simplified MPC approach with time between consecutive optimization $\Delta t = 30$min. The optimized profiles are able to produce considerable savings when compared to the base case.

The behaviour of the different methods can be analysed by looking at the tank volume and temperature in Fig. 3.13. We chose to show only the first 3 days to facilitate the visualization. Notice the temperature setpoint variation for the simple rule depending on the time of the day. The volume is kept at its maximum unless we needed to let it drop in order to maintain $T = T_{min}$. The base case attempts to maintain maximum temperature and

volume at all times. The simplified MPC and the ideal solution show similar temperature trends. However, they differ in terms of volume.

The information of temperature and volume can be summarized by the scaled energy levels E given by the different approaches, as shown in Fig. 3.14. Because of the perfect knowledge of the demand the ideal solution is able to take maximum advantage of price variations by letting the energy levels drop close to minimum. This is in contrast with the simplified MPC which enforces an additional buffer to ensure feasibility.

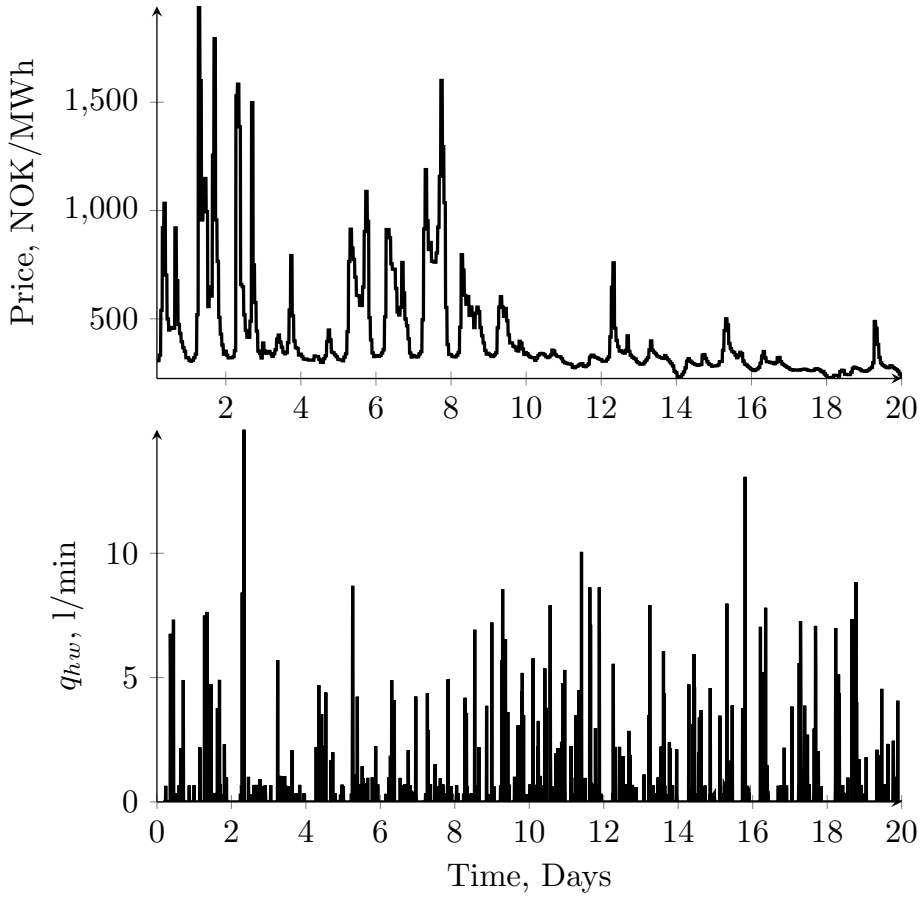

Figure 3.9: Electricity price and hot water consumption.

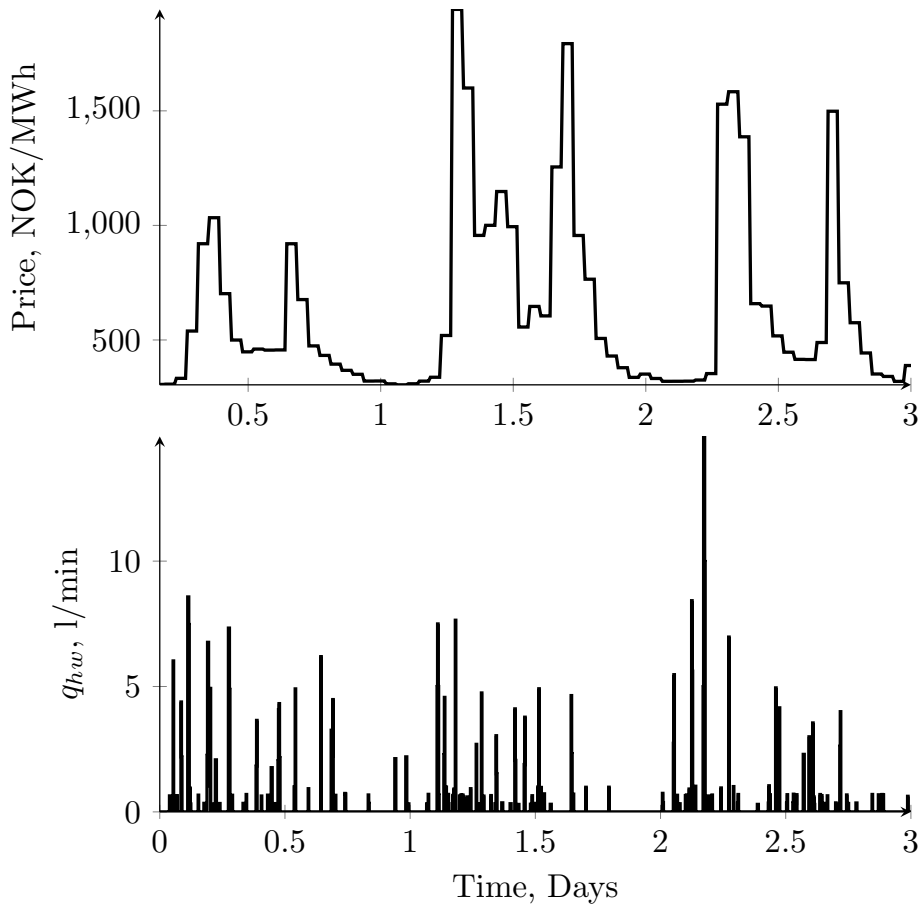

Figure 3.10: Electricity price and hot water consumption. Zoom in the first three days.

3.5.8 Effect of increasing optimization frequency

A very interesting observation is that the economic performance of the MPC approach can be noticeably improved by decreasing the sample time Δt. Figure 3.15 shows the results obtained with Δt =60, 30, 10 and 2 minutes, where we notice that the gap with respect to the ideal solution becomes small for short sample times. Even though the MPC controller has very limited knowledge of the actual demand profile, short sample times will result in faster feedback from the disturbance to the optimization algorithm, allowing it to improve the solution. It is worth pointing out, however, that the loss of optimality can never be eliminated due to the uncertainty in the demand.

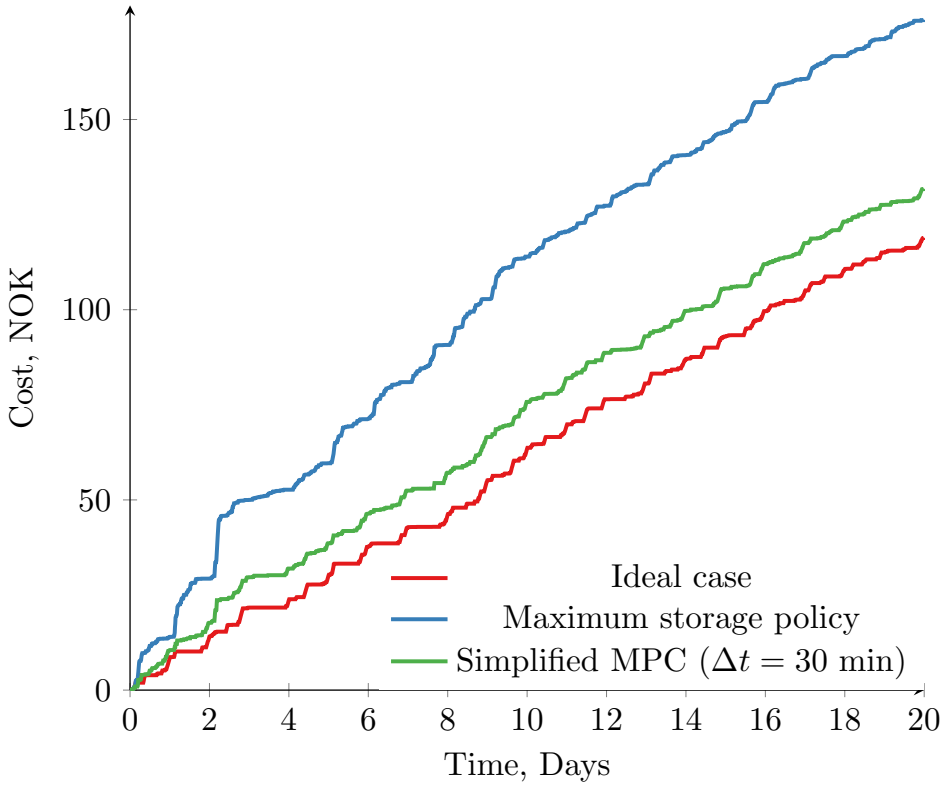

Figure 3.11: Accumlated cost for the different strategies.

3.5.9 Effect of the demand model

Figure 3.16 shows a comparison of the costs given by our approach using two different models to estimate future demand. The green solid line shows the cost when a constant flow model is used and the green dashed line is the cost for the hourly-average demand model (as shown in Fig. 3.8). In this case the benefit of having a more detailed model is around 2.3% after 20 days.

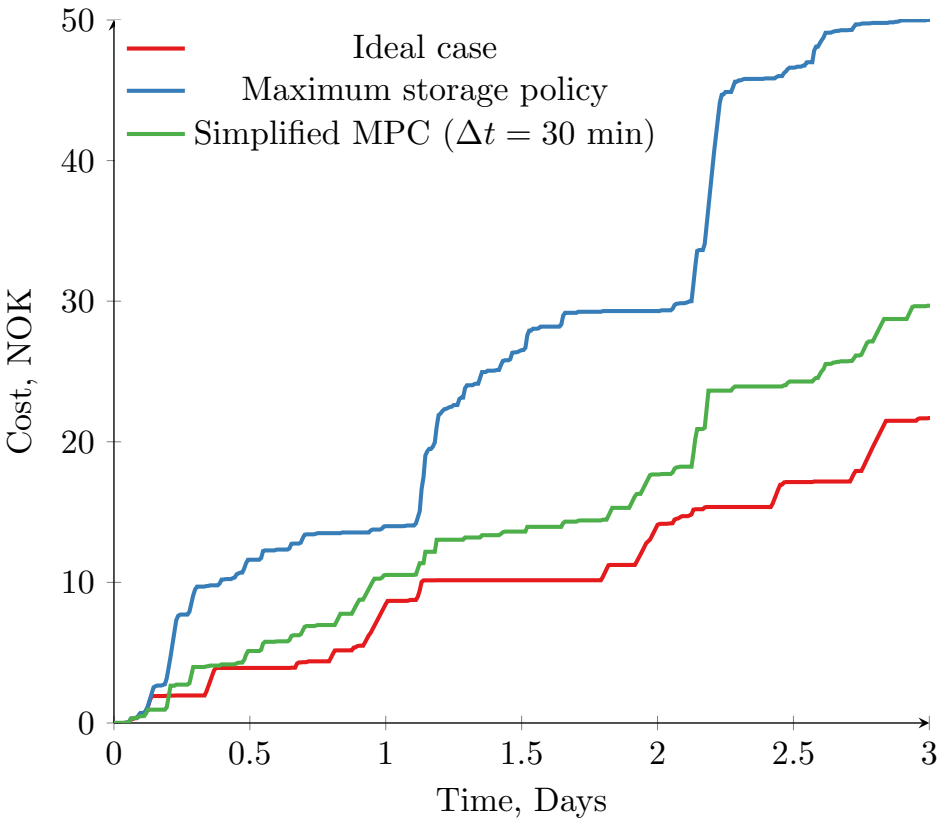

Figure 3.12: Accumlated cost for the different strategies. First three days.

3.6 Discussion

3.6.1 Remarks

In order to make our approach applicable in other problems it is necessary to distil the key elements and ideas which enable us to simplify our problem.

1. The first element is the introduction of the concept of energy storage E stock in the optimization problem. This concept is central to our approach, allowing the formulation of a linear program.

2. The original optimization problem has two decision variables: the heat input Q and the water refilling q_{in}. However, we are able to formulate the problem using E as the decision variable. This change of variables has important simplifying consequences. First, because of

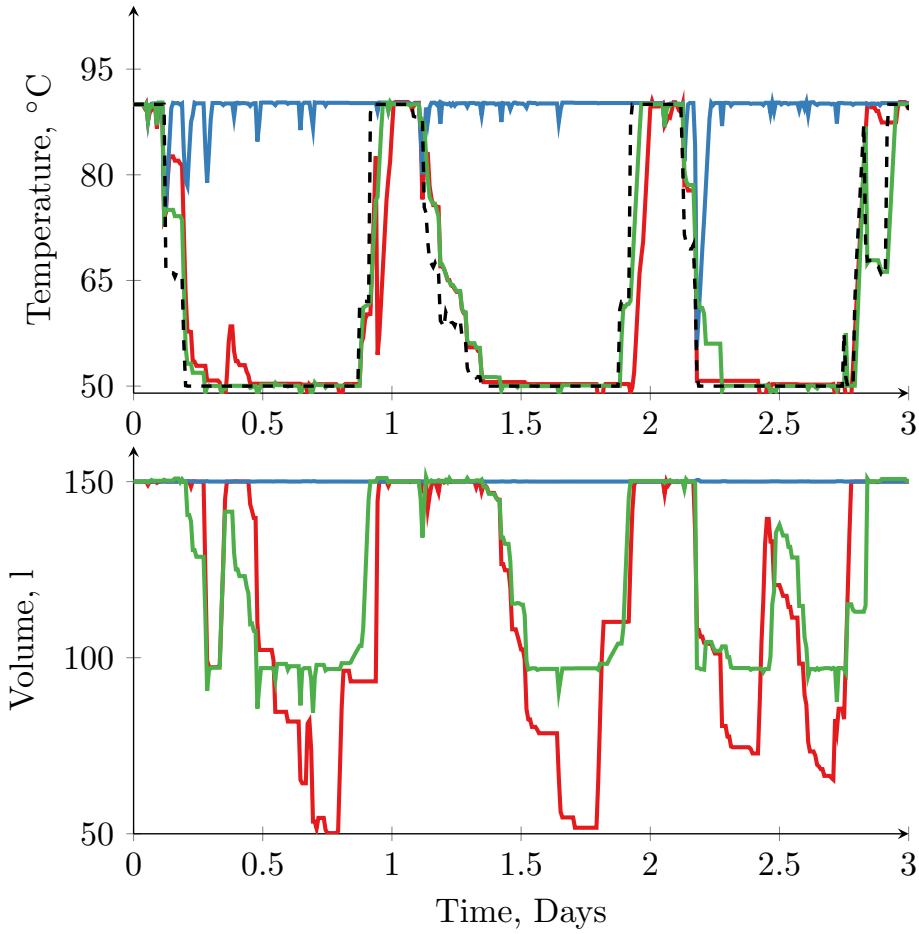

Figure 3.13: Tank volume and temperature. Red lines: ideal case. Blue lines: maximum storage policy. Green lines: our simplified MPC ($\Delta t = 30$ min).

our choice of reference temperature ($T_0 = T_{cw}$) used in the definition $E = \rho c_p V(T - T_{cw})$, the water refilling q_{in} has no effect on the current stock E and can be left out of the problem formulation, thus, reducing the number of decision variables. Second, eliminating Q as decision variable implies that we do not need to solve the problem at very high sampling frequency nor we need to discretize the problem very finely. This is because the energy storage E varies in a much slower time scale compared to the heat input Q. Another consequence is that detailed

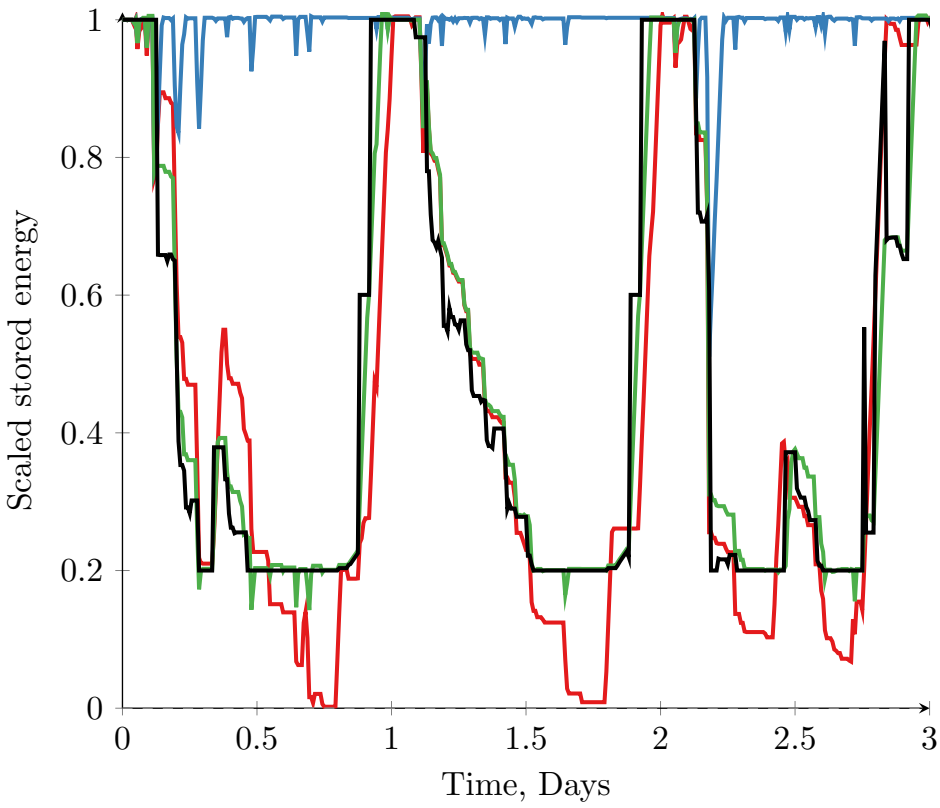

Figure 3.14: Scaled energy level $\bar{E}$ currently stored in the tank for the different strategies. Red line: ideal case. Blue line: maximum storage policy. Green line: our simplified MPC (Δt = 30 min).

information about the demand in the fast time scale is not needed.

Nonetheless, such a change of variables implies that a regulatory control layer is in place to control temperature and volume to their optimal setpoints. That is, the task of computing Q and q_{in} (and making sure constraints in T and V are satisfied)in the fast time scale is delegated to a feedback control layer underneath.

3. In the formulation of the optimization problem we neglect heat losses. However, when the optimal energy storage E_s is unconstrained, that is $E_{min} < E_s < E_{max}$, we have the freedom to choose V and T because of the non-uniqueness of $E = \rho c_p V(T - T_{cw})$. In this is case, we want the temperature T as low as possible to minimize heat losses. Thus,

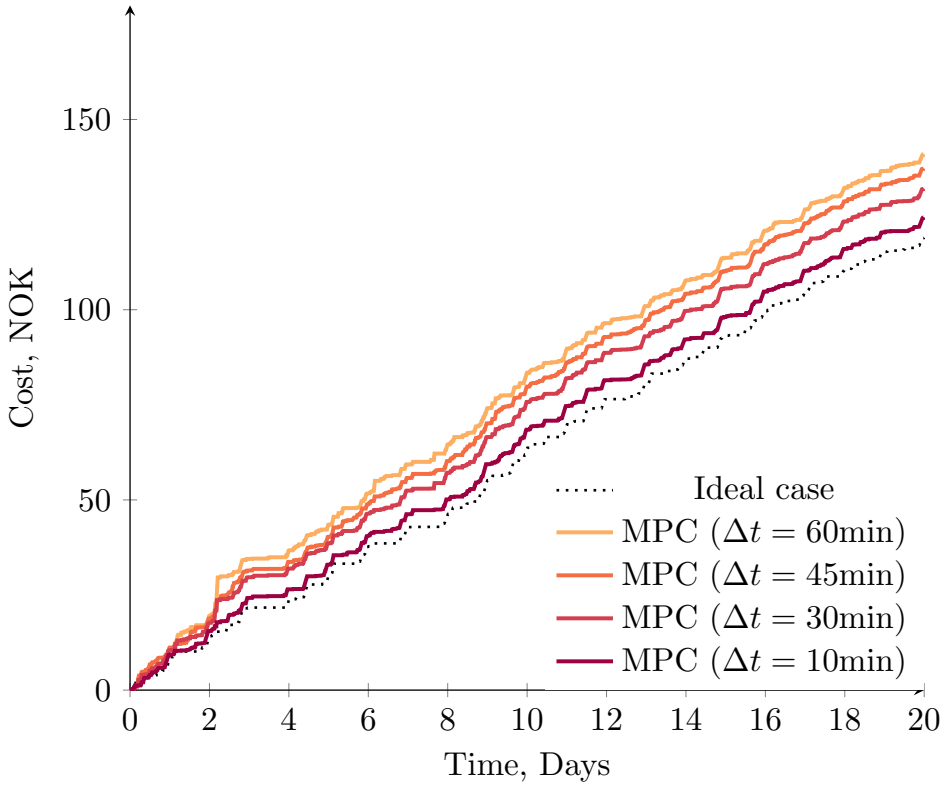

Figure 3.15: Accumlated cost achieved by our simplified MPC strategy using different sample times Δt.

in our approach we do not need to model heat losses or include it in the optimization problem but we are still able to achieve optimal solutions.

4. Our problem shows a periodic behaviour where the eletricity price tend to be lowest during night and the consumption the highest in early morning. This suggests that it we should add a constraint to force us to always have full tank ($E = E_{max}$) late in the night. This constraints decouples the optimization problem of two consecutive days, thus, reducing the size of the problem.

3.6.2 Comments on the problem formulation

The problem we are discussing in this paper is related to the optimization and control of inventories in production systems with unknown (stochastic)

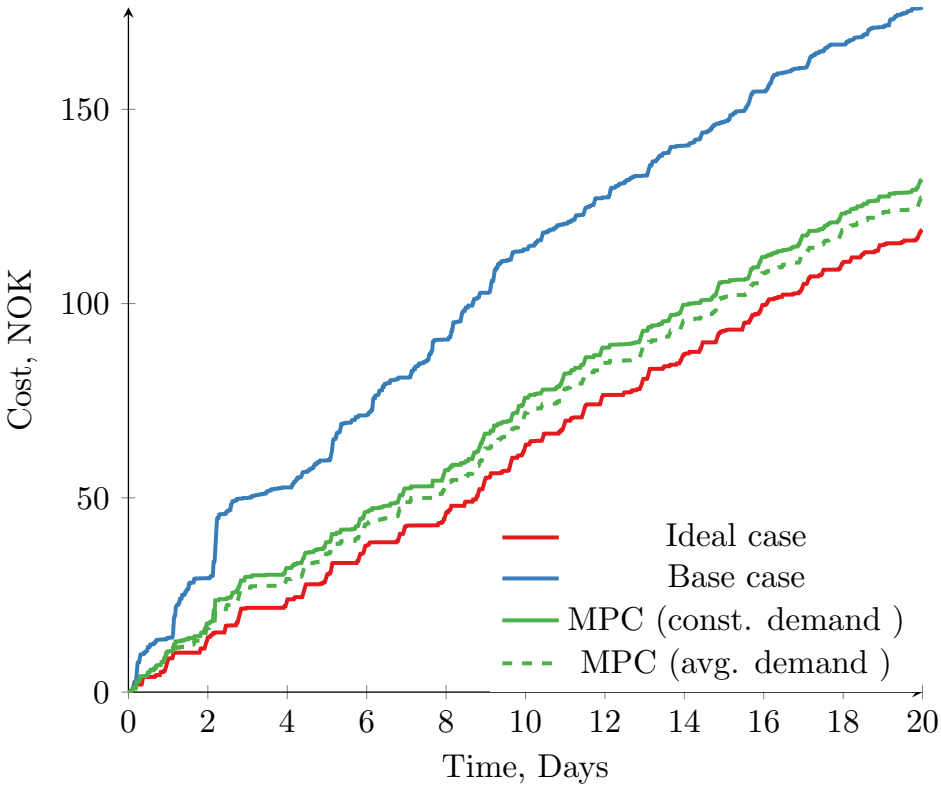

Figure 3.16: Accumlated cost achieved by our simplified MPC strategy using different sample times Δt.

demand where we usually observe:

- stochastic demands and supply;
- variable prices of the product and raw-material (the energy price in our problem);
- economic penalty for not attending the demand;
- deteriorating inventory with state-dependent rate of deterioration (when $Q_{loss} \neq 0$ in our problem)

Typically, due to the stochastic feature of this problem, the optimal policies can be found by means of the dynamic programming principle (Bryson and HO, 1975), where we seek for feedback polices that minimize the expected costs. Examples of research in this area are (Boukas et al., 1999; Baten and Kamil, 2011; Gallego and Hu, 2004).

Since the demand is stochastic, an alternative formulation is to use chance constraints (Li et al., 2008), where the goal is to minimize the cost J subject to input constraints $u \in U$ and subject to state constraints which are given as chance constraints, i.e.

$$P(x \in \mathcal{X}) \geq 1 - \alpha \tag{3.24}$$

where $\alpha \in [0, 1]$. This constraint requires that the condition $x \in \mathcal{X}$ is satisfied with probability $1 - \alpha$.

An alternative problem formulation is the risk-averse approach, where the goal is to minimize the risk of an undesirable outcome. For instance, in oil production optimization problems they seek to minimize the risk of negative profit. In this framework, a finite number of disturbance scenarios is defined and the optimal profit measure ψ_i for every case is computed. Then, based on the stochastic distribution of ψ an appropriate risk measure $R(\phi)$ is computed. The decision is then to choose those strategies that minimize the risk or that maintain the risk above an acceptable threshold. A detailed discussion on the risk measures can be found in Capolei et al. (2015).

3.7 Conclusion

In this paper we discussed the optimal operation of the water heater system. We proposed an implementation strategy to integrate dynamic optimization and control objectives using a two-layers scheme. The main benefit of our approach is that very good economic performance can be achieved at at very low computational costs and requiring minimum modelling efforts. We expect that the suggested framework can be used as a starting point to solve similar problems involving energy storage systems. Moreover, we hope that the development of these low-cost solutions will allow the widespread use of energy storage systems, which in term helps the integration of renewable energy sources into the grid.

Acknowledgements

This work was partially supported by the Danish Council for Strategic Research (contract no. 11-116843) within the *Programme Sustainable Energy and Environment*, under the EDGE (Efficient Distribution of Green Energy) research project.

Chapter 4

Dynamic online optimization of a house heating system in a fluctuating energy price scenario

We consider dynamic optimization of the energy consumption in a building with energy storage capabilities. The goal is to find optimal policies which minimize the cost of heating and respect operational constraints. A main complication in this problem is the time-varying nature of the main disturbances, which are the energy price and outdoor temperature. To find the optimal operable policies, we solve a moving horizon optimal control problem assuming known disturbances. Next, we proposed simple implementation based on feedback control, which gives near-optimal operation for a range of disturbances. The methods were successfully tested using simulation, which show that there is a great economical gain in using dynamic optimization for the case of variable energy price.

Published in the IFAC Proceedings series 2013. 463-468

4.1 Introduction

Due to increasing energy consumption and prices and greater concerns about greenhouse gases emissions, more efficient electric power production and us-

age is sought. Recently, great attention has been given to renewable generation sources like windturbine and photovoltaic parks. Although efficiency-wise attractive, these alternative energy sources suffer a major drawback due to their sharply varying energy production caused by wide-ranging weather conditions. This is an important limitation since the energy production should cover the demand at any given time.

One possible approach to overcome this, is demand side load management where the large fluctuations in the load are tackled by peak shaving and by shifting load to more beneficial periods (Molderink et al., 2009). Field tests in the USA have demonstrated that optimization of domestic energy consumption with variables prices can significantly reduce load peaks (Hammerstrom, 2007). This can be achieved by manipulating the energy price according to demand information and weather forecasts. The dynamic energy pricing for demand load management is in itself a non-trivial problem, and it is currently an active research area. The interested reader is invited to check the references Mardavij Roozbehani and Mitter (2010) and Goudarzi et al. (2011) for more information. This problem is outside the scope of this work.

In such a scenario, the adaptation of the energy consumption by the final consumer is essential to the success of the approach. Thus, in this article we focus on the local building heating system optimization where the goal is the minimization of energy costs.

The case studied here consists of a single room comprised of a floor heating device, a radiator and a ventilation system with adjustable flow. We consider bounds on the floor temperature, the room temperature (air) and the CO_2 levels. The floor heat capacity is assumed to be large enough so that we can store a considerable amount of energy in it, hence, giving us an extra degree of freedom for optimization. Other hardware configurations could also have been employed. For example, one could use a insulated tank filled with water.

The main complicating factor for this problem is the time-varying nature of the disturbances in the outdoor temperature and energy price. We assume that predictions of the temperature and price variation are available, but they are not necessarily correct. Thus, a dynamic real time optimization (DRTO) scheme is proposed to compensate this variations while minimizing the energy cost. In this scheme, a dynamic optimization problem is solved at each sample time with new states and disturbance measurements.

A drawback of the DRTO is the fact that the system operates in open-loop in between two consecutive optimizations. This may yield sub-optimal or even infeasible solutions in case of large disturbances. To deal with this

problem, we propose simple solutions solely based on feedback and offline analysis, where near-optimal control inputs are generated at low computational and maintenance costs. This extends the self-optimizing control idea (Skogestad, 2000) to dynamic optimization problems. We show that near-optimal solutions can be obtained by tracking *optimally invariant trajectories*, which we defined here as being the function of the measurements whose optimal profile does not change with disturbances.

The paper is organized as follows: Section 2 details the derivation of the dynamic. Section 3 shows the formulation of the dynamic optimization problem and describes the solution method used. In Section 4, the implementation of the optimal control solution is discussed and various comparative results presented. Section 5 gives the concluding remarks of the article.

4.2 Modeling

In this section, we develop a dynamic model based on energy and mass balances. The model describes a single $25m^2$ room comprised of a floor heating device, a radiator and a ventilation system with adjustable flow. It is assumed that all the heat lost by the floor is transferred to the air in the room whereas the heat in the air can be lost both through the walls and through the ventilation. The air entering is assumed to be at outdoor temperature and behaves as an ideal gas. The CO_2 accumulation due to breathing is modelled as a constant feed and the consumption of O_2 is neglected. To help visualizing the energy and mass flows in the system it is useful to use system topology graph as shown in Fig. 4.1. All state, manipulated and disturbance variables are described in Table 4.1. Other constant parameters are summarized in Table 4.2.

The energy balance for the floor is simply

$$\frac{dE_f}{dt} = Q_f - q_{f,r} \tag{4.1}$$

where the energy transfer to the room (air) $q_{f,r}$ is given by

$$q_{f,r} = UA_{f,r}(T_f - T_r). \tag{4.2}$$

Since the floor mass is constant we get

$$\frac{dT_f}{dt} = \frac{Q_f}{m_f c_{p,f}} - \frac{UA_{f,r}}{m_f c_{p,f}}(T_f - T_r) \tag{4.3}$$

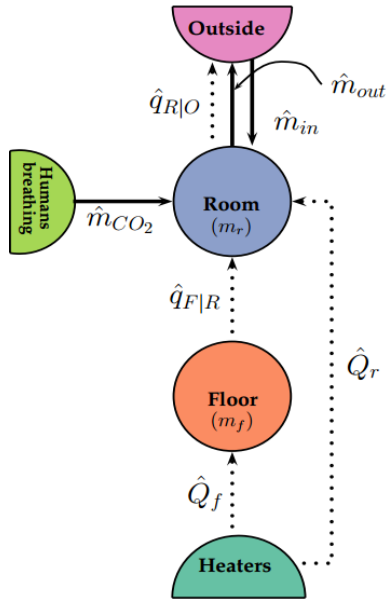

Figure 4.1: The system topology

Table 4.1: Variables description

State variables	Description	Unit
T_f	Floor temperature	K
T_r	Room temperature	K
m_r	Mass of air	kg
w	CO_2 mass fraction	-
Manipulated variables	**Description**	**Unit**
Q_f	Floor heat input	kW
Q_r	Room heat input	kW
$\hat{m}_{in}$	Air inflow	kg/s
Disturbance variables	**Description**	**Unit**
T_o	Outdoor temperature	K
p	Energy price	\$/kW

The energy balance for the room is

$$\frac{dE_r}{dt} = Q_r + q_{f,r} + q_{o,r} + q_{wall} - q_{r,o} \tag{4.4}$$

The mass of air in the room is not constant, therefore we get

$$\frac{dE_r}{dt} = c_{p,r}T_r\frac{dm_r}{dt} + c_{p,r}m_r\frac{dT_r}{dt} \tag{4.5}$$

Using the mass balance we have

$$\frac{dm_r}{dt} = \hat{m}_{in} - \hat{m}_{out} \tag{4.6}$$

where

$$\hat{m}_{out} = k(P_r - P_o) \tag{4.7}$$

is the out flow and $P_r = \frac{m_r R T_r}{M_r V_r}$ is the pressure inside the room. Combining Eq. 4.6 and (4.5) with (4.4) and using

$$\begin{aligned} q_{o,r} &= \hat{m}_{in}c_{p,r}T_o \\ q_{r,o} &= \hat{m}_{out}c_{p,r}T_r \\ q_{wall} &= UA_{r,o}(T_o - T_r) \end{aligned}$$

we obtain

$$\begin{aligned} \frac{dT_r}{dt} = \frac{Q_r}{m_r c_{p,r}} + \frac{\hat{m}_{in}}{m_r}(T_o - T_r) \\ + \frac{UA_{fr}}{m_r c_{p,r}}(T_f - T_r) + \frac{UA_{r,o}}{m_r c_{p,r}}(T_o - T_r) \end{aligned} \tag{4.8}$$

Finally, the component mass balance of CO_2 is given by

$$\frac{d(wm_r)}{dt} = \hat{m}_{in}w_{in} - \hat{m}_{out}w + B \tag{4.9}$$

using the product rule for differentiation we have

$$\frac{d(wm_r)}{dt} = m_r\frac{dw}{dt} + w\frac{dm_r}{dt} \tag{4.10}$$

and using the total mass balance in Eq.(4.6) yields

$$\frac{dw}{dt} = \frac{\hat{m}_{in}}{m_r}(w_{in} - w) + \frac{B}{m_r} \tag{4.11}$$

For sake of simplicity in the notation, we define the control inputs $u^T = [Q_f, Q_r, \hat{m}_{in}]$, the state vector $x^T = [T_f, T_r, m_r, w]$ and the disturbances $d^T = [T_o, p]$. Hence, we can pack the dynamics into the vector function f such that $\frac{dx}{dt} = f(x, u, d)$. In the next section we describe how to use this model to find optimal heating polices.

4.3 Dynamic optimization

This section presents the dynamic optimization problem and the approach used to solve it. It starts off by presenting the continuous time optimal control problem we would like to solve and evolves in a stepwise manner presenting modifications that helps the solution. Finally, we present the full discretization method based on orthogonal collocation as well as the formulation of the nonlinear program. The implementation is discussed in the subsequent section.

4.3.1 Problem definition

The optimization objective is to minimize the energy costs over an infinite horizon. A solution method is to use a moving horizon approach where we solve an optimal control problem within the fixed interval $[t_0, t_0 + h]$ where the horizon h is large enough to capture important trends in the system. At each time point t_0 a different optimization problem (4.12) is solved with different initial condition x_0 that is unknown in advance. We formulate our moving horizon problem in the Lagrangian form as:

$$\min_u \int_{t_0}^{t_0+h} p(t)(Q_f + Q_r)\, dt \tag{4.12}$$

subject to

$$\dot{x} = f(x, u, d), \quad x(t_0) = x_0 \tag{4.13}$$
$$T_r \geq T_{min} \tag{4.14}$$
$$T_f \leq T_{max} \tag{4.15}$$
$$w \leq w_{max} \tag{4.16}$$
$$Q_f \leq Q_{max} \tag{4.17}$$
$$Q_r \leq Q_{max} \tag{4.18}$$
$$Q_f, Q_r \geq 0 \tag{4.19}$$

The above control problem is singular, which may create troubles when direct numerical methods are used if accurate control profiles are sought. It can be shown that the Hessian matrix becomes very ill-conditioned as the time step size decreases (Biegler, 2010). To avoid convergence problems, we modify the cost function by adding a quadratic term:

$$\min_u \int_{t_0}^{t_0+h} p(t)[\beta(Q_f + Q_r)^2 + (Q_f + Q_r)]dt \tag{4.20}$$

where the weighting factor β is adjusted such that the linear term dominates the expression. In a constant price scenario the two formulations are equivalent since it would be optimal to simply minimize the input usage.

4.3.2 Disturbance modelling

The main disturbances are the outdoor temperature $T_o(t)$ and energy price $p(t)$. For simplicity, we assume that $p(t)$ is periodic and follows

$$p(t) = p_0 + A_p \text{sign}[\sin(\omega_p t + \phi_p)] \tag{4.21}$$

where parameters the A_p and ϕ_p are uncertain. More general dynamic pricing polices can also be treated in this framework in a straightforward manner. We assume the weather predictions are available numerically from weather models such that we can interpolate the predictions using polynomials. Therefore, we assume we have the predictions $\hat{T}_o(t) = P(t)$ where P is a polynomial fitted using the weather model data. For this case study we have used weather prediction data from Institutt (2012). It would not be realistic to embed a weather forecast model in the optimization loop due to its highly complex nature.

4.3.3 Softening constraints

During operation is possible that a disturbance brings the system outside the feasible region. The formulation based on hard constrains (4.14)-(4.19) would then fail to produce a reasonable solution since the initial state would already be infeasible. This problem can be overcome by softening the output constraints (4.14)-(4.16). It would not make sense to soften the input constrains as they represent real physical limitations.

Firstly, we rewrite the output constraints in a vector form such that we have $h_o(x, u) \geq 0$. Next, we introduce a vector of slack variables ε and define the following constraints in the optimization problem:

$$h_o(x, u) \geq 0 - \varepsilon \tag{4.22}$$

$$\varepsilon \geq 0 \tag{4.23}$$

Finally, the cost function is modified by adding penalties for the violation of the constraints

$$\min_u \int_{t_0}^{t_0+h} \{p(t)[\beta(Q_f + Q_r)^2 + (Q_f + Q_r)] + \mu \cdot \varepsilon\} dt \tag{4.24}$$

The linear penalty function was chosen because it is exact in the sense that minimizing (4.24) also minimizes the original cost function (4.20) provided that μ is large enough (Nocedal and Wright, 2006).

4.3.4 Simultaneous approach

The dynamic optimization stated so far is infinite dimensioned and in order to solve it numerically, a discretization method is needed. We have decided to discretize the problem using orthogonal collocation methods. In this approach, both the states and manipulated variables profiles are approximated by orthogonal polynomials and their coefficients become the decision variables. The polynomial approximation of the states is required to respect the model equations only at the solution of the optimization problem. This formulation yields a large-scale sparse nonlinear program (NLP) and is known as the simultaneous approach (Biegler, 2010).

For simplicity, we first transform the problem to the Mayer form by expanding the state vector with $\dot{J} = p(t)[\beta(Q_f + Q_r)^2 + (Q_f + Q_r)] + \mu \cdot \varepsilon$ such that we have $z^T = [x, J]$ and $\dot{z} = \hat{f}(z, u, d)$. The equivalent dynamic optimization problem is

$$\min_u J(t_0 + h) \tag{4.25}$$

subject to the constraints (4.17)-(4.19) and the model $\dot{z} = \hat{f}(z, u, d)$.

Proceeding to the discretization, we first divide the time interval into N time periods. Within each time period i the control inputs are represented by Lagrange interpolation

$$u(t) = \sum_{j=1}^{K} \bar{l}_j(\tau) u_{ij} \tag{4.26}$$

where

$$\bar{l}_j(\tau) = \prod_{k=1,\neq j}^{K} \frac{\tau - \tau_k}{\tau_j - \tau_k} \tag{4.27}$$

The collocation equations for the differential equations can be written as

$$\sum_{j=0}^{K} \dot{l}_j(\tau_k) z_{ij} - h_i \hat{f}(u_{ik}, z_{ik}, d_{ik}) = 0 \tag{4.28}$$

where $i \in [1, \ldots, N]$, $k \in [1, \ldots, K]$, $\dot{l}_l(\tau) = \frac{dl_j}{d\tau}$ and K is the degree of the polynomials. The length of the time intervals h_i are considered fixed and are not decision variables for the optimization problem. In fact, for this case we have chosen $N = 1$ which leads to a *pseudospectral method*. This class of methods can give very accurate solutions for dynamic optimization problems with smooth profiles (Biegler, 2010). Finally, the collocation points τ_k are

chosen as the roots of the Gauss-Legendre orthogonal polynomials. The resulting NLP is as follows:

$$\min J(t_0 + h) \tag{4.29}$$

$$\text{s.t.} \sum_{j=0}^{K} \dot{l}_j(\tau_k) z_j - h\hat{f}(u_k, z_k, d_k) = 0 \tag{4.30}$$

$$h_o(x_k, u_k, d_k) \geq -\varepsilon_k, \quad \varepsilon_k \geq 0 \tag{4.31}$$

$$k \in [1, \ldots, K] \tag{4.32}$$

The above problem is formulated in Matlab and solved using the sparse NLP solver SNOPT. This solver employs a sparse SQP algorithm with quasi-Newton approximations to the Hessian. Gradient information is obtained using automatic differentiation approach. The interface between Matlab and SNOPT is handled by the optimization environment TOMLAB.

4.4 Implementation approaches

We propose the implementation of a dynamic real time optimization where the optimal control problem is solved in a moving horizon fashion. At each time sample, t_0, a dynamic optimization problem is solved with a new initial state and disturbance measurements. We specified a horizon length $h = 24$h so that all the important dynamics are captured. However, only the first portion of the optimal profile corresponding to $t \in [t_0 + t_s]$ is implemented, where $t_s < h$ is the time between successive optimizations. In this paper we assume limited computation power so that we need to have $t_s = 2$ h. During this period the optimal inputs are extracted by using the Lagrange interpolation shown in (4.26).

In order to improve the accuracy of the solution and improve the convergence, the NLP is solved with successively larger number of collocation points, where the solution to the previous lower dimensioned problem is used as an initial guess for the next one. Here, we solve the NLP first with $K = 25$ and then using $K = 45$ collocation points. Another important point is the warm start of the NLP solver. This is done in two steps: first, the control inputs from previous solutions are shifted to to the next time window by assuming the inputs remain constant in the final time period. Then, the shifted inputs are used to simulate the model and the states are extracted. The shifted inputs and the simulated states are the initial guess to the next optimization problem. The overall algorithm is summarized as follows:

Algorithm 1 Simple moving horizon optimal control

Initialize: x_0, h, t_s, initial guess x_g and u_g
while $t \leq t_f$ **do**
  Solve the NLP (4.29)-(4.32)
  Implement solution for $t \in [t_0, t_0 + t_s]$
  Measure or estimate $x(t_0 + t_s)$
  Set $x_0 \leftarrow x(t_0 + t_s)$
  Shift previous solution $u_g \leftarrow u_{opt}(t)$ with $t \in [t_0 + t_s, t_0 + t_s + h]$
  Use u_g to simulate the model from x_0 and obtain x_g
  Set $t \leftarrow t_0 + t_s$
end while

4.4.1 Nominal optimal solution

Assuming perfect predictions, the solution for a whole day obtained with Algorithm 1 is shown. Figure 4.2 depicts the nominal price variations, the outdoor temperature variation and the accumulated energy cost. This temperature profile corresponds to the temperature measured in Trondheim, Norway on 03 January 2012 provided by the Norwegian Meteorological Institute which made the data freely available in Institutt (2012).

For the sake of comparison, we also implemented the most trivial solution to the problem where the room temperature is kept at minimum allowed value by varying the heat input Q_r using a PI controller. To get a fair comparison, the optimal air inflow was used. The second heat input,Q_f, was left unused. Note that keeping the room temperature at minimum allowed value is, in fact, the optimal policy if we would like to minimize the energy consumption instead of the economical cost.

A comparison between the optimal profiles and the simple strategy is given in Figures 4.3 and 4.4. Some interesting conclusions can be drawn from this results. First, notice that it is optimal to overheat the room and floor above the minimum constraint when the price is low. In this case, when the energy is cheap we will store enough heat in order to meet the temperature constraints until the next low price valley. We also confirmed (not shown here for brevity) that the air inflow is increased just enough to meet the CO_2 level constraint. This is trivial since over-ventilation would unnecessarily cool the room down and it would require extra energy to keep the temperature constraint.

The optimal energy cost for one day was \$12.45, whereas the simple temperature controller gave a cost of \$21.62, which is considerably higher than the optimal. The energy usage is 12.5 kWh; and 10.9 kWh, respectively. It

is clear that this difference in the cost is proportional to the ratio between high and low energy price. Notice that, in a constant price scenario, the optimal is to keep the temperatures at the minimum allowed value.

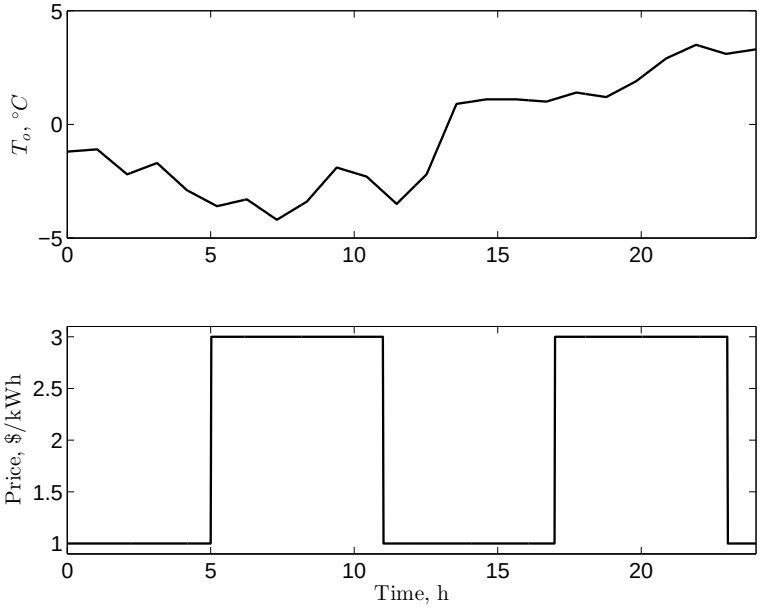

Figure 4.2: Disturbances - energy price and outdoor temperature.

4.4.2 Near-optimal solution by tracking optimally invariant trajectories

In this section, we propose a simple control implementation that gives near-optimal solutions without the need for re-optimization online. The main idea is to find a function of the measurements whose trajectory is optimally invariant to disturbances and then track the trajectory using standard feedback controllers. The structure is shown in Fig. 4.5 where $c_r(t)$ is the optimally invariant reference trajectory that we wish to track. In the sequel, we will derive a procedure to obtain such trajectories.

We define $y \in \mathcal{R}^{n_y}$ as the vector of known variables (measurements), which may include states, disturbances and control inputs. The disturbance model of price and outdoor temperature is parametrized by a vector of constants d_0. However, the *real* (unknown) parameters are denoted by d, and we may have deviations $\Delta d = d - d_0$. The nominal optimal measurement trajectory is referred to as $y_0(t, d_0)$.

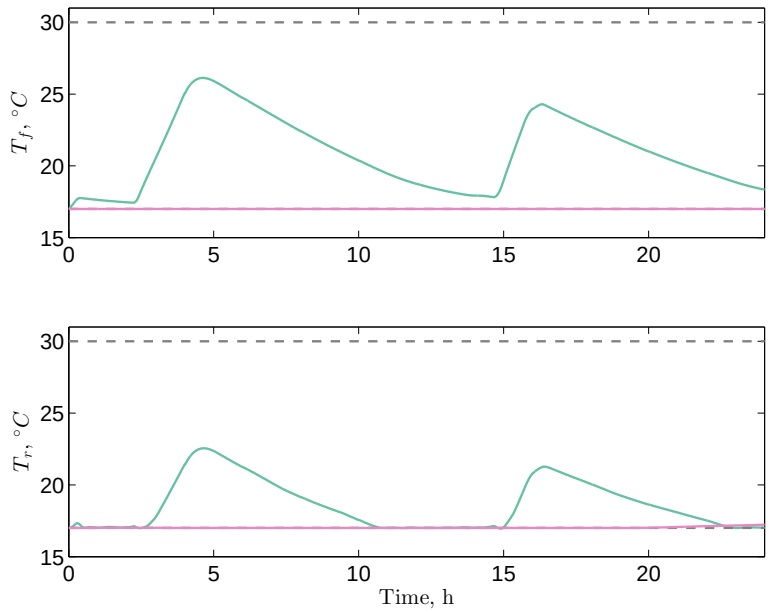

Figure 4.3: Temperatures - green lines: optimal solution; magenta lines: simple temperature controller with constant setpoint.

It can be shown that if the cost function J is twice continuously differentiable in a neighbourhood of the nominal solution and the linear independence constraint qualifications and the sufficient second-order conditions hold, then the optimal sensitivity matrix F is well defined:

$$F(t) = \frac{\partial y_{opt}(t,d)}{\partial d} \tag{4.33}$$

and, a first order, local approximation of the optimal solution in the neighbourhood can be obtained from

$$y_{opt}(t,d) \approx y_0(t,d_0) + F(t)\Delta d \tag{4.34}$$

Here, we are after a function of measurements $c(y(t),d)$ whose optimal value is independent of d, i.e., we want $c_{opt}(y(t),d) = c_0(y(t),d_0)$ for any d sufficiently small. A simple choice is a linear combination of the measurements:

$$c(t) \equiv H(t)y(t) \tag{4.35}$$

where $H(t)$ is a $n_u \times n_y$ matrix, and $c(t)$ is a $n_u \times 1$ vector. This way we can write

$$c_{opt}(t,d) = H(t)[y_0(t,d_0) + F(t)\Delta d] \tag{4.36}$$

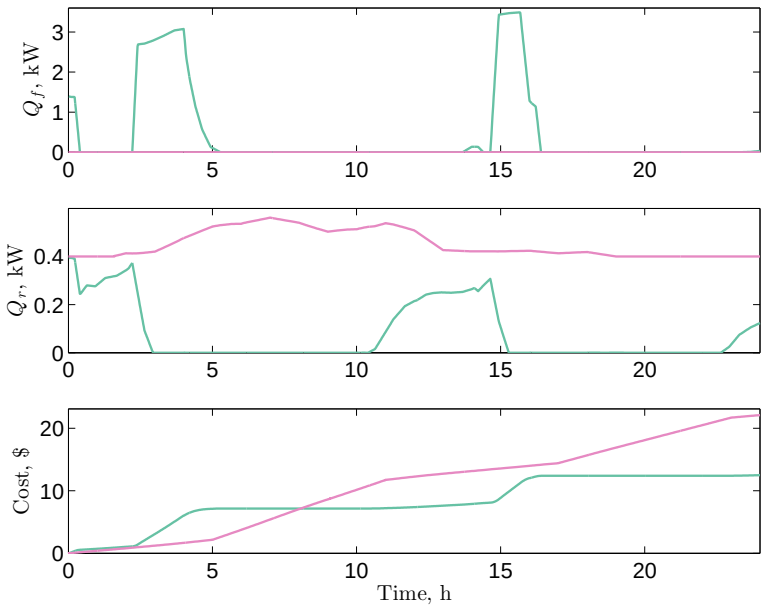

Figure 4.4: Inputs and energy cost - green lines: optimal solution; magenta lines: simple temperature controller with constant setpoint.

and we define the nominal combination of measurements:

$$c_0(t, d_0) = H(t)y_0(t, d_0) \tag{4.37}$$

By subtracting (4.37) from (4.36) we obtain:

$$c_{opt}(t, d) - c_0(t, d_0) = H(t)F(t)\Delta d \tag{4.38}$$

Therefore, the optimal combination $c_{opt}(t, d)$ equals the nominal $c_0(t, d_0)$ for any d if we select $H(t)$ such that $H(t)F(t) = 0$. This is always true if $H(t)$ lies in the left null space of $F(t)$. Using this approach we obtain a trajectory $c_{opt}(t, d)$ that is optimally invariant due to disturbance. We can transform the problem of implementing $u(t)$ in a 'open-loop' manner to a reference tracking problem with optimal setpoints $c_r(t, d) = c_{opt}(t, d)$ (see Fig. 4.5). By tracking c_r, a simple controller automatically generates inputs u that are optimal for any disturbance d sufficiently small and thus, the online optimization is avoided.

The whole procedure has offline and online steps which are summarized as follows:

Offline:

- Solve the dynamic optimization problem with d_0;
- Select appropriate measurements y;
- Compute the optimal sensitivities $F(t)$ and the combination $H(t)$;
- Compute the reference trajectories $c_r(t) = H(t)y_0(t)$.

Online:

- Track the reference c_r by a feedback controller.

Remark: It is only possible to choose H in the left null space of F if the number of independent measurements respect the condition $n_y \geq n_u + n_d$ where n_d and n_u are the number of disturbances and inputs, respectively. See Alstad and Skogestad (2007) for proof.

Here, we assume the air inflow q_{in} will remain at nominal trajectory such that two manipulated variables are available. Thus, since we are considering two disturbances we will need at least $n_y = 2 + 2 = 4$ measurements and we seek two trajectories $c_1(t)$ and $c_2(t)$ to track. Defining the measurement vector $y = [T_f, T_r, m_r, p]^T$ we compute the optimal sensitivities $F(t)$ for the whole horizon and obtain $H(t)$ and the reference trajectory $c_r(t)$. As controllers, we use two decentralized P controllers. Note that the only way to adapt to price changes is by measuring it explicitly as the model of the physical process does not depend on price explicitly.

This idea was tested by considering a disturbance in the phase shift (ϕ_p) of the energy price as well as a mismatch between prediction and actual outdoor temperatures. Figure 4.6 compares the predictions with the measured disturbance values. We compare the proposed method with the moving horizon strategy given in Algorithm 1 and with the true optimal solution assuming perfect knowledge of the disturbances. Figure 4.7 depict the input trajectories for the three different cases. The economical comparison is shown in bottom Fig. 4.7. The proposed simple method works surprisingly well for this case, given a relative loss of optimality of only 0.3175%. The relative loss given by the moving horizon strategy with imperfect disturbance model was 24.4%, which is considerably higher.

One of the reasons for the success of the method is the fact that, in this range of disturbances, the dynamics are close to linear and, therefore, the linear approximation of the NLP ends up near the true solution. A drawback of this approach is that it cannot explicitly handle constraints. Therefore, for a realistic implementation the proposed method should be combined with a periodic solution of the dynamic optimization where a new reference

solution is obtained, and new invariant trajectories $c(t)$ are computed. The idea is to recompute the optimal sensitivities $F(t)$ online after solving the current NLP and then apply the approach shown in Fig 4.5 in between two successive optimizations. This requires, however, fast online calculations of the sensitivities as those provided by the methods proposed by H. Pirnay and Biegler. (2011). Similar idea has been published in Würth et al. (2009) where the authors proposed to use sensitivity based neighbouring-extremal updates combined with real-time optimization. In this way, the frequency of optimizations can be greatly reduced.

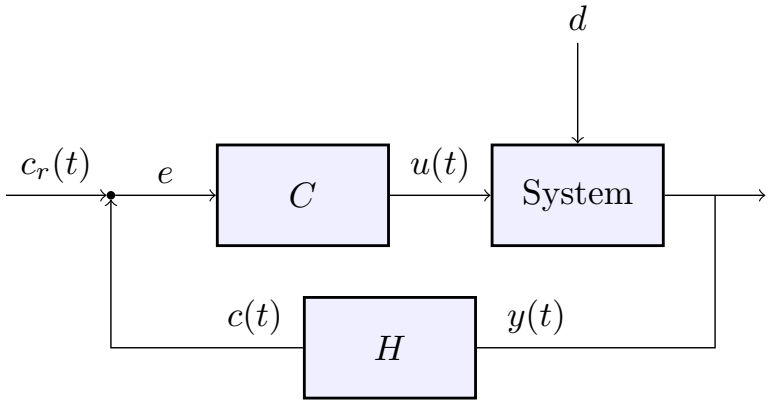

Figure 4.5: Proposed implementation based on simple feedback

4.5 Conclusion

In this paper various solutions to the optimal heating of a room problem have been proposed. We proposed a moving horizon dynamic optimization method, which uses predictions to compute the optimal heating polices and ensure feasibility. We showed that, in a scenario where the energy price is time varying, the economical benefit of using a real time dynamic optimization scheme is substantial. Finally, simple solutions based on feedback control and offline was derived and successfully tested. The simulation exampled showed that very little loss of optimality could be obtained for relatively small disturbances. The benefit of this method is the negligible online computational cost and the simplicity of the implementation. The ideas discussed here could also be applied to any other problem with energy storage capabilities where the energy price changes, such as the dynamic

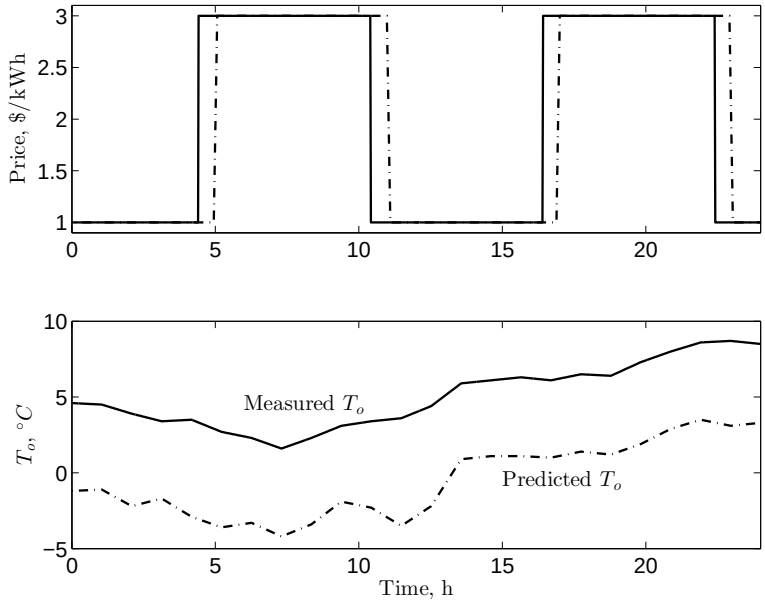

Figure 4.6: Disturbances - solid lines: measured; dash-dotted lines: predicted

optimization of supermarket refrigeration systems.

4.6 Model Parameters

Table 4.2: Parameters description

Parameter	Description	Value	Unit
$UA_{f,r}$	Heat transfer coefficient floor	0.1801	$kJ/(s \cdot K)$
$UA_{r,o}$	Heat transfer coefficient walls	0.0216	$kJ/(s \cdot K)$
m_f	Mass of the floor	3000	kg
$c_{p,f}$	Heat capacity of the floor	0.63	kg/kJ
$c_{p,r}$	Heat capacity of the air	1.005	kg/kJ
k	Valve constant	100	$kg/(bar \cdot s)$
w_{in}	CO_2 fraction in flow	$6.16 \cdot 10^{-4}$	-
B	CO_2 generated by breathing	$9.02 \cdot 10^{-6}$	kg/s

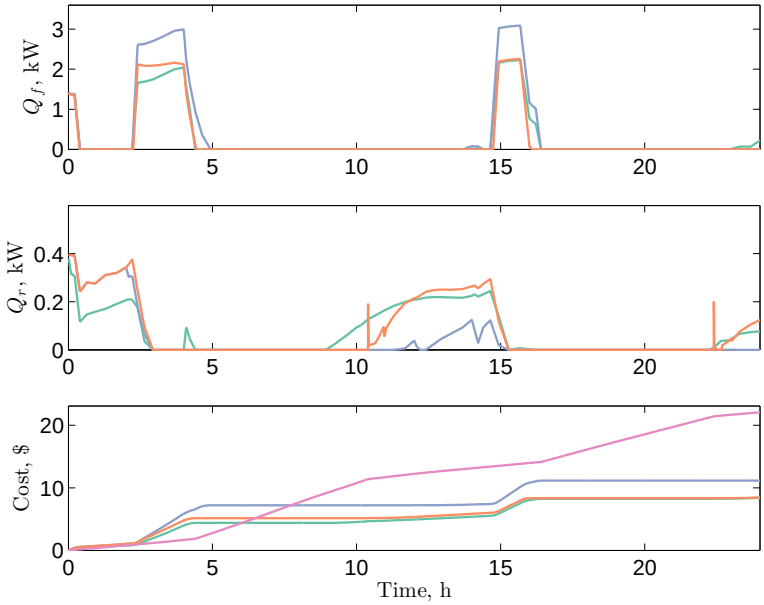

Figure 4.7: Inputs and economical comparison - blue lines: Algorithm 1 with imperfect predictions; orange lines: proposed implementation as shown in Fig. 4.5; green lines: optimal solution; magenta line: cost of a simple temperature tracking controller

Part II

Optimal operation of dynamic systems at their stability limit: application to anti-slug control

Chapter 5

An autonomous approach for driving systems towards their limit: an intelligent adaptive anti-slug control system for production maximization

Anti-slug control in multiphase risers involves stabilizing an open-loop unstable operating point. Existing anti-slug control systems are not robust and tend to become unstable after some time, because of inflow disturbances or plant dynamic changes, thus, requiring constant supervision and retuning. A second problem is the fact that the ideal setpoint is unknown and we could easily choose a suboptimal or infeasible operating point. In this paper we present a method to tackle these problems. Our complete control solution is composed of an autonomous supervisor that seeks to maximize production by manipulating a pressure set-point and a robust adaptive controller that is able to quickly identify and adapt to changes in the plant. The supervisor is able to automatically detect instability problems in the control loop and moves the system to a safer, stable operating point. Our proposed solution has been tested in a experimental rig and the results are very encouraging.

Presented at the 2nd IFAC Workshop on Automatic Control in Offshore Oil and Gas Production, 2015, Florianópolis, Brazil.

5.1 Introduction

The severe-slugging flow regime which is common at offshore oilfields is characterized by large oscillatory variations in pressure and flow rates. This multi-phase flow regime in pipelines and risers is undesirable and an effective solution is needed to suppress it (Godhavn et al., 2005). One way to prevent this behaviour is to reduce the opening of the top-side choke valve. However, this conventional solution reduces the production rate from the oil wells. The recommended solution to maintain a non-oscillatory flow regime together with the maximum possible production rate is active control of the topside choke valve (Havre et al., 2000). Measurements such as pressure, flow rate or fluid density are used as the controlled variables and the topside choke valve is the main manipulated variable.

From an economic point of view, we would like to have the lowest possible pressure (maximum valve opening) in the pipeline/riser system. This translates into low pressures at the bottom hole of the wells which maximizes the fluid inflow from the reservoir. However, as the pressure setpoint decreases the stabilization of the system becomes more difficult and, thus, the choice of the ideal setpoint is hard task. In fact, the ideal pressure setpoint is unknown and varies with the inflow conditions. Setting it too high reduces the production. Setting it too low may be infeasible (uncontrollable), leading to slug flow. Consequently, constant monitoring of the control system by the operators is needed.

Hence, we propose an autonomous supervisory system that safely drives the process in the direction of minimum pressure for production maximization. The main idea is to gradually decrease the pressure setpoint until just before the control performance is no longer acceptable due to slugging. The supervisor automatically assesses the performance and stability of the control loop and decides the direction in which we should change the pressure setpoint in order to ensure stable operation. For example, if we detect slow oscillations with growing amplitude in the output, the setpoint should be increased since it is safer and easier to stabilize.

Nonetheless, the standard linear controllers are typically designed for a given operating point and they may fail to give acceptable performance when the setpoint changes considerably. Another problem are the disturbances in the inflow, which greatly affect the dynamics of the plant.

For these reasons we implemented a robust adaptive anti-slug controller.

For our application we chose the robust-adaptive output feedback control design method proposed by Lavretsky (2012). This method falls into the model-reference adaptive control category (Lavretsky and Wise, 2013) and fits well in our approach. This controller is able to quickly identify and adapt to changes in the plant dynamics in order to recover the desired performance.

Our complete control solution is composed of the autonomous supervisor and the robust adaptive slug control. It turns out the combination of these two elements results in a great synergy: the periodic setpoint changes triggered by the supervisor gives enough excitement in the system for the adaptation to work well; a well functioning adaptive controller allows the supervisor to push the system closer to the limit for a wide range of operating conditions.

Its worth to point out that this approach is very general and can be applied in a variety of applications with similar characteristics: dynamics change when approaching the (possibly unknown) operating limit of the system.

This paper is organized as follows. Section 2 describes the pipeline-riser system. The general approach that we proposed is described in Section 3, where Details about the supervisor and the adaptive controller are found. The results are presented in Section 4. Finally, we summarize the main conclusions and remarks in Section 5.

5.2 Systems description

Fig. 5.1 shows a schematic presentation of the system. The inflow rates of gas and liquid to the system, $w_{g,in}$ and $w_{l,in}$, are assumed to be independent disturbances and the top-side choke valve opening ($0 < Z < 100\%$) is the manipulated variable. A fourth-order dynamic model for this system was presented by Jahanshahi and Skogestad (2011). The state variables of this model are as:

- m_{gp}: mass of gas in pipeline [kg]
- m_{lp}: mass of liquid in pipeline [kg]
- m_{gr}: mass of gas in riser [kg]
- m_{lr}: mass of liquid in riser [kg]

The four state equations of the model are

$$\dot{m}_{gp} = w_{g,in} - w_g \tag{5.1}$$

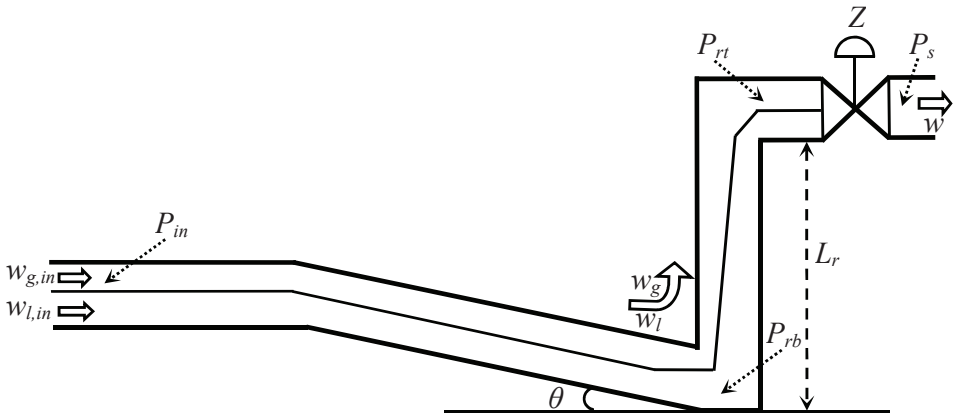

Figure 5.1: Schematic representation of system

$$\dot{m}_{lp} = w_{l,in} - w_l \tag{5.2}$$

$$\dot{m}_{gr} = w_g - \alpha w \tag{5.3}$$

$$\dot{m}_{lr} = w_l - (1-\alpha)w \tag{5.4}$$

The flow rates of gas and liquid from the pipeline to the riser, w_g and w_l, are determined by pressure drop across the riser-base where they are described by virtual valve equations. The outlet mixture flow rate, w, is determined by the opening percentage of the top-side choke valve, Z. The different flow rates and the gas mass fraction, α, in the equations (6.2)-(6.5) are given by additional model equations given by Jahanshahi and Skogestad (2011). In this paper we used the linearized version of this model for the control design methods. Alternatively, empirical low-order models could have been used (Jahanshahi and Skogestad, 2013a).

5.3 An autonomous approach for driving systems towards their limit

Here we propose an autonomous control system to drive a process towards its operational limit. Our solution is composed of two main elements:

- supervisory system that overlooks the control loop, assess stability and performance and makes a decision on which direction (increase or decrease) the setpoint should move. In our application, the strategy is to gradually reduce the pressure setpoint until a stability problem

is detected (e.g., slow oscillations start to build-up). At this point the supervisor should move the system to a safer operating point (increase setpoint).

- a robust adaptive controller that regulates the system to the setpoint specified by the supervisory controller. The controller must be able to identify changes in the plant dynamics and compensate for it to give acceptable closed-loop performance in a wide range of operating conditions.

We believe that the combination of frequent setpoint changes by the supervisor with and adaptive control scheme can be very fruitful because the periodic setpoint changes triggered by the supervisor gives enough excitement in the system for the adaptation to work well; a well functioning adaptive controller allows the supervisor to push the system closer to the limit compared to linear controllers.

5.3.1 Supervisory control

A key component in an autonomous supervisor is the ability to quickly detect problems in the control loop. In our application the main problem is the appearance of slugging flow which is characterized by growing (slow) oscillations in the pressures and flows with a certain frequency. Such oscillations are a signal that the controller is having problems to control the process at the given operating conditions and should move to a safer setpoint. Algorithm 2 exemplifies a basic supervisory scheme for the anti-slug control problem. P_{sp} is the pressure setpoint and ΔP_{sp} represents the size of the steps. The pressure can be measured at any point of the system (e.g. riser base or riser top). Note that the amplitude of the step when increasing or decreasing the setpoint may be different.

The basic idea is to periodically check for slow oscillations in the system and decrease the setpoint only if nothing is detected. On the other hand, we should quickly increase the setpoint if the amplitude of the oscillations are starting to grow. In this case, it could be desirable to reset the adaptation parameters to the previous good values using, for instance, a look-up table.

For a practical application, however, many other safeguards must be included. For example, if a major disturbance occurs, the controlled variable may drift away from the setpoint very rapidly and the oscillation detection system may fail to perceive in time. In order to quickly detect these major problems a second, independent check function must be implemented. In our case we periodically analyse the mean control error over a short time horizon.

A warning flag is raised if the mean error is increasing too quickly or if it crosses some large threshold. We must also include a routine to detect high frequency oscillations generally caused by having too high control gains for the given operating conditions. In this case we should decrease the setpoint instead. Other functions of the supervisor could include looking after the adaptive control (e.g. we may want to turn off the adaptation during the starting up period), fault detection, alarms, etc.

Algorithm 2 A simplified supervisory system algorithm

```
loop
    analyse measured data

    if slow oscillations detected then

        if amplitude is increasing then
            P_sp ← P_sp + ΔP_sp,1
            return to previous adaptation values
        else
            wait longer
        end if

    else
        P_sp ← P_sp − ΔP_sp,2
    end if
end loop
```

Oscillation detection system

A key component in an autonomous supervisor is the ability to quickly detect slow oscillations in the closed-loop system. This can be achieved by periodically applying a frequency analysis tool in the measured data (e.g. pressures) in a moving-horizon manner. Our chosen approach is to estimate the power spectral density using a fast Fourier transform and then check if the main frequency component of the signal lies in a neighbourhood of the slug frequency. If this is the case, a warning flag is raised. The same frequency analysis can be used to estimate the amplitude of the oscillation, allowing us to tell whether the oscillations are increasing or fading out.

Our practical experience has shown that this approach is quite robust and it only requires knowledge of the slug frequency for the specific application. No other tuning parameters are necessary.

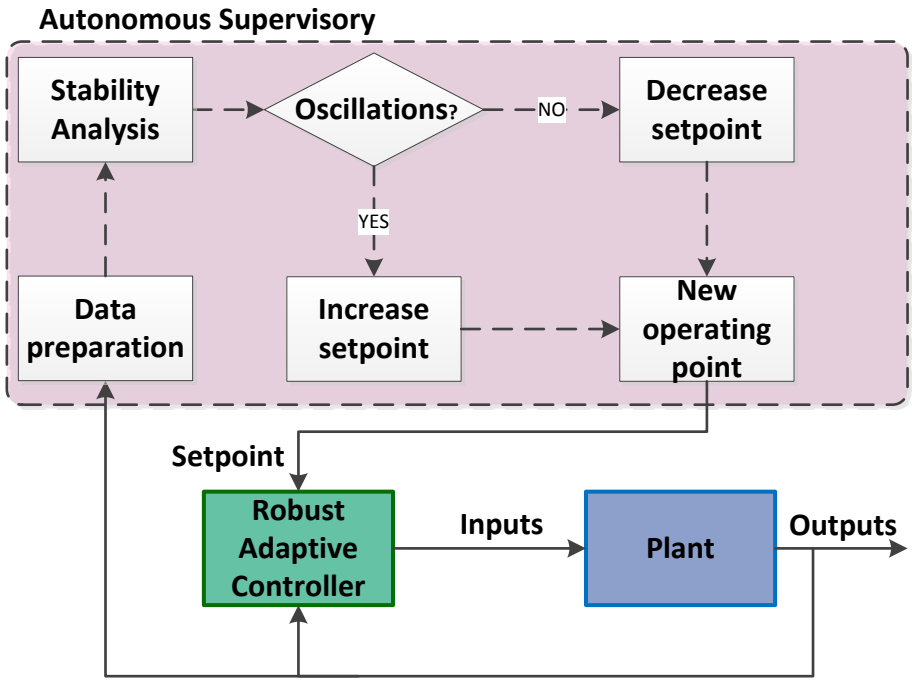

Figure 5.2: Simplified representation of the supervisory system

5.3.2 Robust Adaptive Control Design

We implemented the robust adaptive output feedback design method proposed by Lavretsky (2012). This method falls into the model-reference adaptive control category (Lavretsky and Wise, 2013). The main components of this controller are: an observer-like reference model which specifies the desired closed-lop response; a linear baseline controller that gives the desired performance and robustness at nominal conditions; the adaptation law which augments the input in order to recover the desired performance despite the disturbances and uncertainties (See Fig. 5.3). For completeness, we will outline in the following the design method that was used. We follow the notation of Lavretsky and Wise (2013).

We assume that system can be described in the following form

$$\begin{aligned} \dot{x} &= Ax + B\Lambda(u + \Theta^T\Phi(x)) + B_{sp}z_{sp} \\ y &= Cx, \qquad z = C_z x \end{aligned} \tag{5.5}$$

where $A \in R^{n\times n}$, $B \in R^{n\times m}$, $C \in R^{p\times n}$ and $C_z \in R^{m\times n}$ are known matrices. Note that the matrices may have been augmented to include the integral feedback connections. The vector $x \in R^n$ represents the system states, $y \in R^p$ are the available measurements, $u \in R^m$ are the inputs and $z \in R^m$ are the variables we wish to regulate to given setpoints z_{sp}. The uncertainties are described by an unknown diagonal matrix Λ, an unknown matrix of coefficients Θ and a known Lipschitz-continuous regressor $\Phi(x)$. We assume that the number of available measurements p is larger than the number of control inputs m. In this case, the system can be 'squared-up' using pseudo-control signals to yield minimum-phase plant dynamics.

Representation (5.5) fits well with our application. One of the main challenges is the very large process gain variation as we change the pressure setpoint. This can be represented by Λ. Furthermore, the poles and zeros of the linearized dynamics move considerably as the pressure reduces. This effect can be modelled by the term $\Theta^T\Phi(x)$ as long as we make a good choice for the regressor $\Phi(x)$.

The first step is to design a reference model with the desired closed-loop dynamics. In this case we compute an optimal state feedback K_{LQR} by employing the LQR method such that

$$A_{ref} = A - BK_{LQR} \tag{5.6}$$

as the desired dynamic characteristics. It has been shown (Lavretsky, 2012) that the transient dynamics of the adaptation scheme can be improved by

using an observer-like model reference. Thus, our reference model becomes

$$\begin{aligned} \dot{x}_{ref} &= A_{ref}x_{ref} + L_v(y - y_{ref}) + B_{sp}z_{sp} \\ z_{ref} &= C_z x_{ref} \end{aligned} \tag{5.7}$$

where $L_v \in R^{n\times m}$ is the prediction error feedback gain that is obtained by solving a certain algebraic Riccati equation (Lavretsky, 2012). The 'square-up' step of the plant dynamics should be performed prior to the design of L_v. More details can be found in Appendix B and Appendix C.

Our chosen implementation approach is to augment a baseline linear controller with the adaptor instead of using a fully adaptive control. The reasoning comes from the fact that in most realistic applications a stabilizing baseline controller might already be in place. This baseline controller would have been designed to give satisfactory performance under nominal conditions around an operating point. If the performance degrades due to changes of operating conditions, we will attempt to recover the desired performance by augmenting the baseline controller with an adaptive element. The total control input is the sum of the components

$$u = u_{bl} + u_{ad} \tag{5.8}$$

where u_{bl} denotes the baseline control input and u_{ad} is the adaptive augmentation control signal.

The adaptation increment u_{ad} is given by

$$u_{ad} = -\hat{K}_u u_{bl} - \hat{\Theta}^T \Phi(x_{ref}) \tag{5.9}$$

where $\hat{\Theta}$ is an estimation of Θ and $\hat{K}_u$ serves as an estimate of $(I_{m\times m} - \Lambda^{-1})$.

Given the adaptation rates Γ_Θ and Γ_u, the adaptive law with the Projector Modification (Pomet and Praly, 1992) can be written as

$$\frac{d\hat{\Theta}}{dt} = Proj(\hat{\Theta}, -\Gamma_\Theta \Phi(x_{ref}) e_y^T R_0^{-0.5} W S^T) \tag{5.10}$$

$$\frac{d\hat{K}_u}{dt} = Proj(\hat{K}_u, -\Gamma_u u_{bl} e_y^T R_0^{-0.5} W S^T) \tag{5.11}$$

where

$$e_y = y_{ref} - y \tag{5.12}$$

is the output tracking error and the matrices R_0, W and S are selected to ensure that the tracking error e_y becomes small in finite time.

The projector operator $Proj$ ensures that the adaptive parameters always lie inside a user-defined region and can never diverge. The robustness

of this adaptive law can be improved by including a dead-zone modification that stops adaptation when the error e_y is too small. Such modification ensures that the adaptation parameters will not drift because of measurement noise (Lavretsky and Wise, 2013).

Remark 1 *It is interesting to note that upon combining* (5.9) *and* (5.8) *we get*

$$u = (1 - \hat{K}_u)u_{bl} - \hat{\Theta}^T \phi(x_{ref}) \tag{5.13}$$

where we see that the adaptor is in essence modifying the baseline controller gain by a factor $(1 - \hat{K}_u)$*. The second term in the right-hand side of the equation tries to match and cancel the effect of the nonlinear uncertainties in* (5.5)*.*

Remark 2 *The observer-based model reference* (5.7) *works as a robust closed-loop Luenberger estimator when we select the baseline controller*

$$u_{bl} = -K_{LQR}x_{ref} \tag{5.14}$$

This leads to an output feedback controller equivalent to the loop transfer recovery using the Lavretsky method, which has been proven to have excellent robustness properties (Lavretsky and Wise, 2013). In our application, (5.14) *was our baseline controller of choice because of its robustness properties and its good performance observed in our experiments. Nonetheless, any other linear controller (e.g PI control) could have been selected for the baseline layer. In fact, our experiments have shown that the adaptive control scheme presented above is able to recover the desired performance even if a poorly tuned PI controller is used in the baseline (See Figures 5.11 and 5.12).*

Remark 3 *Another advantage of using the augmentation approach for the adaptive scheme (rather than fully adaptive control) is that the adaptation could be turned off when necessary without loosing control of the system. This can be particularly important in some situations such as start-up.*

5.4 Results

5.4.1 Experimental setup

The experiments were performed on a laboratory setup for anti-slug control at the Chemical Engineering Department of NTNU. Fig. 5.4 shows a schematic presentation of the laboratory setup. The pipeline and the riser

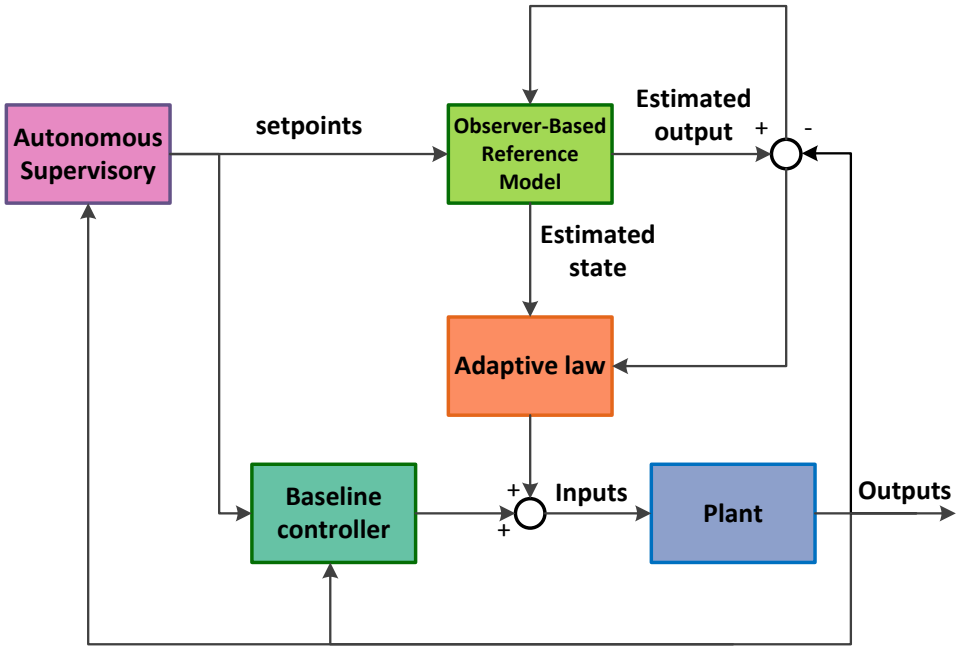

Figure 5.3: Simplified block diagram of the proposed adaptive control scheme

are made from flexible pipes with 2 cm inner diameter. The length of the pipeline is 4 m, and it is inclined with a 15° angle at the bottom of the riser. The height of the riser is 3 m. A buffer tank is used to simulate the effect of a long pipe with the same volume, such that the total resulting length of pipe would be about 70 m.

The topside choke valve is used as the input for control. The separator pressure after the topside choke valve is nominally constant at atmospheric pressure. The nominal feed into the pipeline is assumed to be at flow rates 4 l/min of water and 4.5 l/min of air. With these boundary conditions, the critical valve opening where the system switches from stable (non-slug) to oscillatory (slug) flow is at $Z^* = 15\%$ for the top-side valve. The bifurcation diagrams are shown in Fig. 5.5.

The desired steady-state (dashed middle line) in slugging conditions ($Z > 15\%$) is unstable, but it can be stabilized by using control. The slope of the steady-state line (in the middle) is the static gain of the system, $k = \partial y/\partial u = \partial P_{in}/\partial Z$. As the valve opening increase this slope decreases, and the gain finally approaches to zero. This makes control of the system

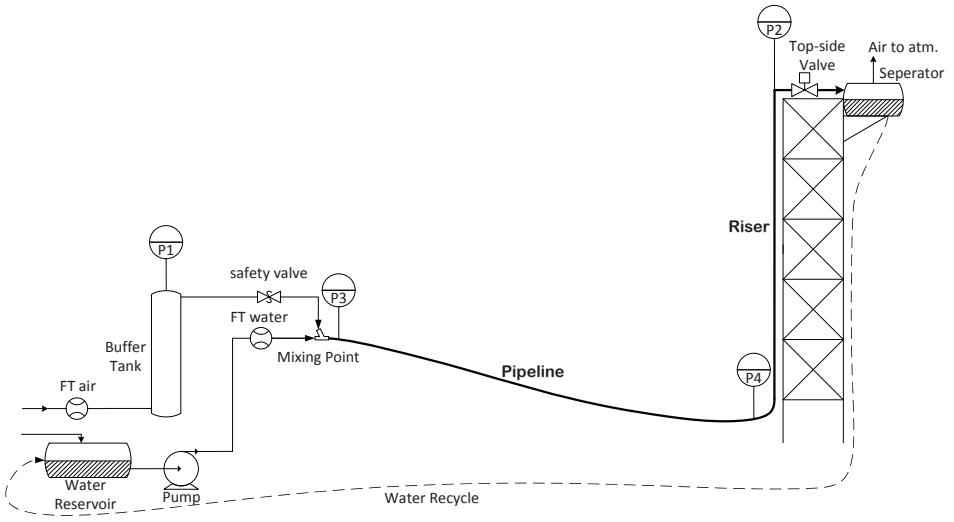

Figure 5.4: Experimental setup

with large valve openings very difficult.

5.4.2 Supervisory control

The main parameter for the implementation of the supervisory controller is the period of the slug oscillation. This variable depends mainly on the dimensions of the pipeline and riser, although the operating conditions (e.g. valve opening) do have some effect on it. For our purposes it is enough to have an estimation of the order of magnitude of the frequency of the oscillations. In our application we observed variations in the oscillation period ranging from 40 to 70 seconds. Thus, any oscillation in this frequency range will be reported by the oscillation detection algorithm. The core idea of our supervisor is Algorithm 2. The loop was executed every 20 seconds to avoid strong interactions with the stabilizing control layer. The length of the horizon for analyses in the oscillation detector was set to 90 seconds to ensure that a full slug cycle would be detected.

5.4.3 Adaptive Controller

We designed our controllers based on the linearized version of the model described on Section 2 for a valve opening $Z = 30\%$. In the control algorithm we consider measurements of both the inlet pressure of the pipeline (P_{in})

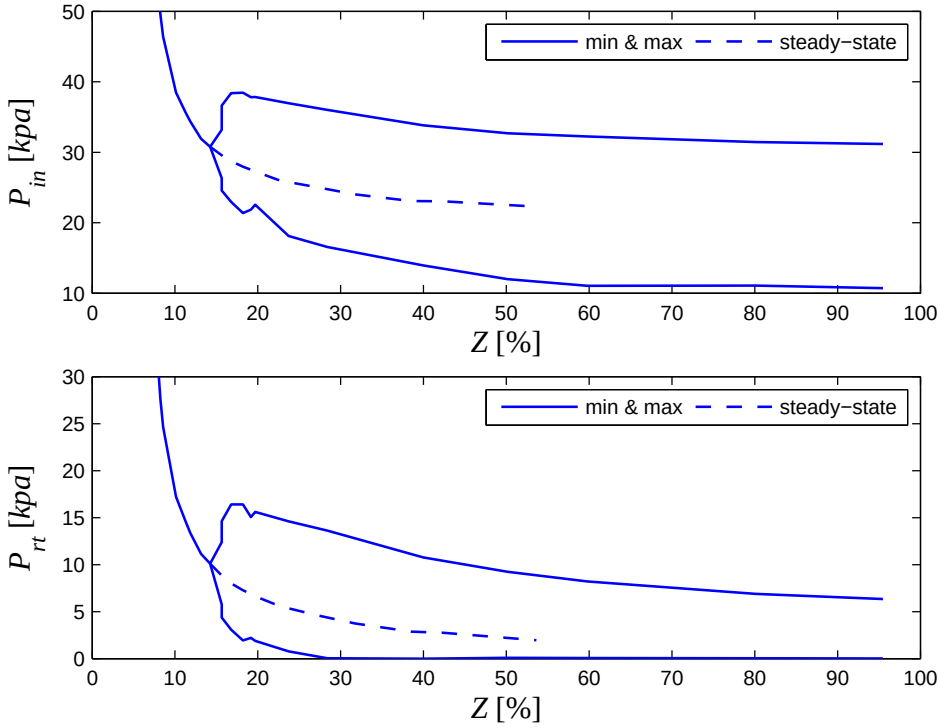

Figure 5.5: Bifurcation diagrams for experimental setup

and the pressure in the riser top (P_{rt}). The regulated output in experiments is $z = P_{in}$. The second measurement is used to ensure robustness properties of the LTR baseline and the adaptive controllers.

In our application we chose (5.14) as our baseline controller because of its excellent robustness properties and its good performance observed in our experiments. Prior to conducting the LQG/LTR controller design, we augmented the plant dynamics to include the integrated inlet pressure tracking error $e = P_{sp} - P_{in}$.

For the adaptive algorithm we chose as basis function Φ the linear relationship

$$\Phi(x_{ref}) = C_z x_{ref} \equiv \hat{P}_{in} \tag{5.15}$$

where $\hat{P}_{in}$ is an estimation of the inlet pressure. From our analysis this simple basis function is enough to describe the variation in the plant dynamics (zeros and poles) due to changes in the operating point (indicated by P_{in}). The gain uncertainty is described by the unknown scalar parame-

ter Λ. Therefore, our adaptation scheme is composed of two scalar adaptive parameters only. The Projector Operator ensures that these parameters are bounded and remain inside the interval $[-5,\ 5]$.

To improve the quality of our adaptation and to ensure the overall robustness of the system, we switched on the adaptation only after a setpoint change is made and for a limited amount of time (e.g. for 1 min). This prevents the system to wrongly adapt to the disturbances. When the supervisory layer detects a problem in the system and the setpoint is increased, the adaptation parameters are reset to the closest previously computed value for the given setpoint using a lookup table.

For comparison we have also implemented a PI controller in the baseline layer. Our experiments have shown that the adaptive control scheme presented in the previous section is able to recover the desired performance even if a poorly tuned PI controller is used in the baseline (See Figures 5.11 and 5.12).

5.4.4 Experimental results: nominal flow conditions

In this experiment the feed into the pipeline is set to be at constant flow rates, 4 l/min of water and 4.5 l/min of air. Figures 5.6 depict the results for a 48 minutes run of the complete system. The setpoint is indicated by the red solid line in the top plot. Note that the setpoint is only decreased when the supervisor is sure it is safe. The detection of growing oscillations is indicated by the red flag. In Fig. 5.6 these can be seen around the times 15.5, 27, 34 and 42 minutes. The supervisor is able to safely keep the system at stable conditions at fairly high valve openings. Figure 5.7 shows the adaptation parameter for the same experiment. The adaptation is switched on after 100 seconds to avoid the start-up dynamics. Its interesting to note that at first the parameter $\hat{K}_u$ increases (the gain $(1 - \hat{K}_u)$ decreases) indicating that initially the controller is a bit too aggressive for the given conditions. However, as the supervisor reduces the setpoint for P_{in} the parameter $\hat{K}_u$ decreases (the gain $(1 - \hat{K}_u)$ increases) considerably to maintain the desired performance. Note that we reset the adaptation parameters when a problem is detected (red flag).

5.4.5 Experimental results: large change of operating conditions

In this set of experiments we tested the more realistic and challenging conditions in which the gas to liquid ratio varies considerably throughout the experiment. Initially the feed into the pipeline is set to constant flow rates

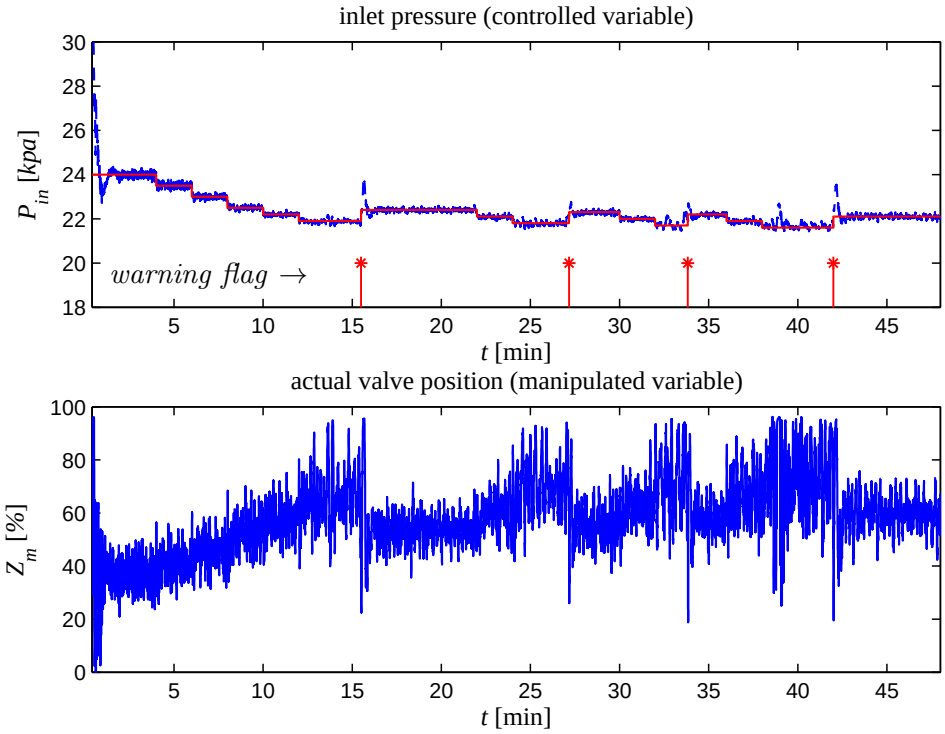

Figure 5.6: Experiment 1 : supervisory control and a well tuned LTR baseline controller: adaptation is ON

4 l/min of water and 4.5 l/min of air. Then, a sequence of steps in the air flow is applied: first we increase the air flow by 50% at $t = 5$ min followed by a 30% decrease at $t = 20$ min (see Fig. 5.8). Changes in the air flow and pressures naturally perturb the water flow. Note that these changes represent very serious disturbances that have big effect in the dynamics of the plant.

Figure 5.9 depicts the performance of the control system. The more serious disturbance here is when the air flow decreases ($t = 20$ min). The pressure rapidly diverges since it became very difficult to stabilize the system at these conditions. Nonetheless, the supervisory layer quickly detected the problem and immediately moved the system to a safer operating point. After stabilizing the process, the robust adaptive controller was able to adapt its parameters for the new dynamics (see Fig. 5.10), making it possible to reduce the pressure setpoint even under such harsh conditions. It is worth to point out that slugging flow did not occur at any moment and the good performance of the controller remained consistent, proving the great resilience

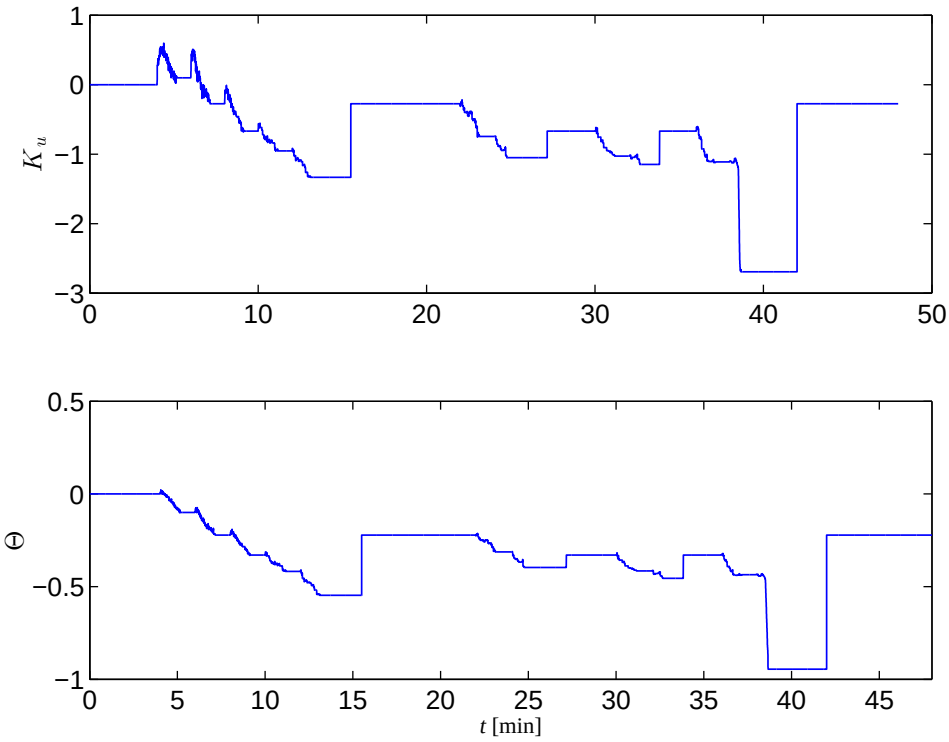

Figure 5.7: Experiment 1: adaptive parameters

of our proposed solution. Such a result would not have been possible to achieve without an autonomous supervisor and an adaptive controller.

5.4.6 Experimental results: using a poor baseline controller and nominal flow conditions

For comparison, it is interesting to investigate the effect of the baseline controller in the overall performance of the control system. The incentive for doing so is clear: in most realistic applications a stabilizing baseline controller might already be in place and perhaps we do not want to change it.

For this purpose we consider as the baseline a poorly tuned PI controller. Figure 5.11 shows the results of the autonomous supervisor with the PI controller without any adaptation. We observe an overall poor performance and the inability to operate with large valve openings.

The experiment was repeated with the same PI controller but now the adaptation was switched on. The same reference model used in experiments

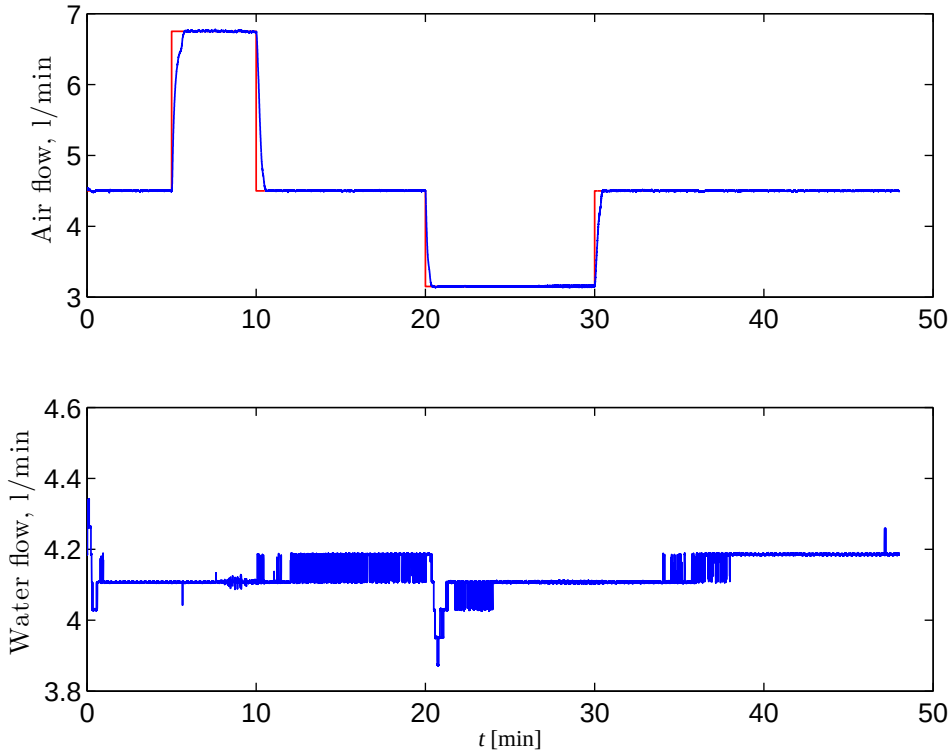

Figure 5.8: Experiment 2: major disturbance in the inlet flow rates

1 and 3 is employed here. Figure 5.12 depicts the results. Surprisingly, the closed-loop performance was greatly improved compared to Fig. 5.11 and we are able to operate at a larger valve opening. For a complete comparison, we ran the same experiment using our well tuned LTR controller (5.14) and the adaptation switched on. Figure 5.13 shows the result of this controller where we observe good tracking performance throughout the experiment.

Table 5.1 summarizes the results of the three experiments where we compare the tracking performance based on the integrated square error (ISE) and the 'economic' performance based on the mean valve opening and pressure. Note that the improvement from experiment 3 to 4 is substantial, where we observe an increase of 31% of the average valve opening. On the other hand, the improvement from experiment 4 to 5 is only minor. Nevertheless, our recommendation is to always use a good robust controller in the baseline. This will ensure safer operation during start-up (when the adaptation is likely to be turned off) or during reset of the control system.

It is important to point out that the adaptive controller we implemented

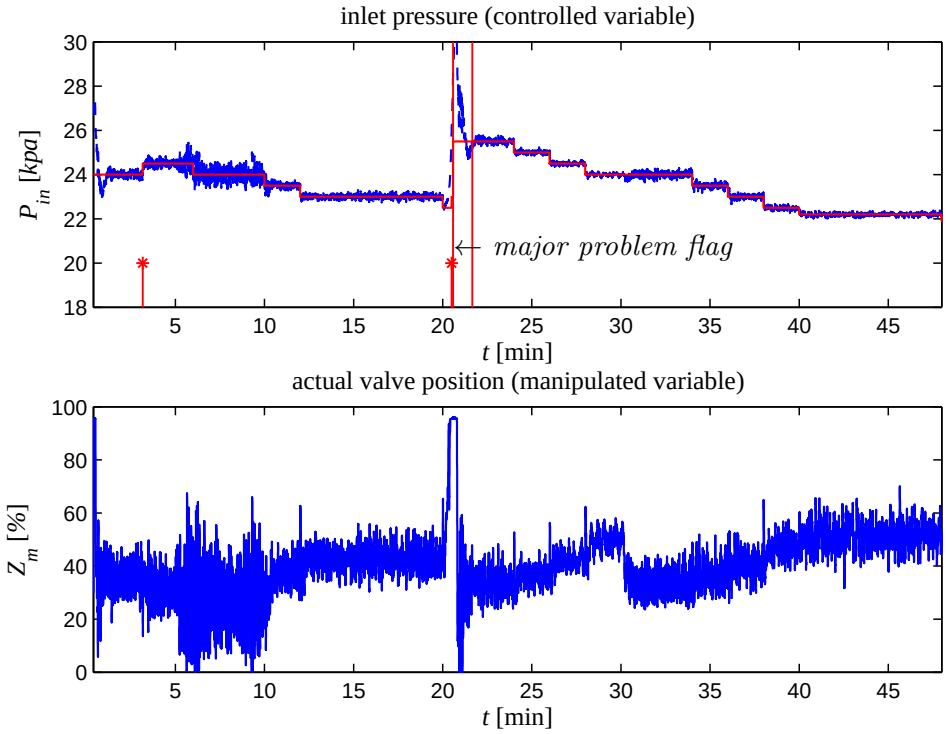

Figure 5.9: Experiment 2: major disturbance in the inlet flow rates. LTR baseline controller: adaptation is ON

relies on the measurement of both top and bottom riser pressure. It would be interesting to investigate the performance of this adaptive law for the case when only one of the measurements is available.

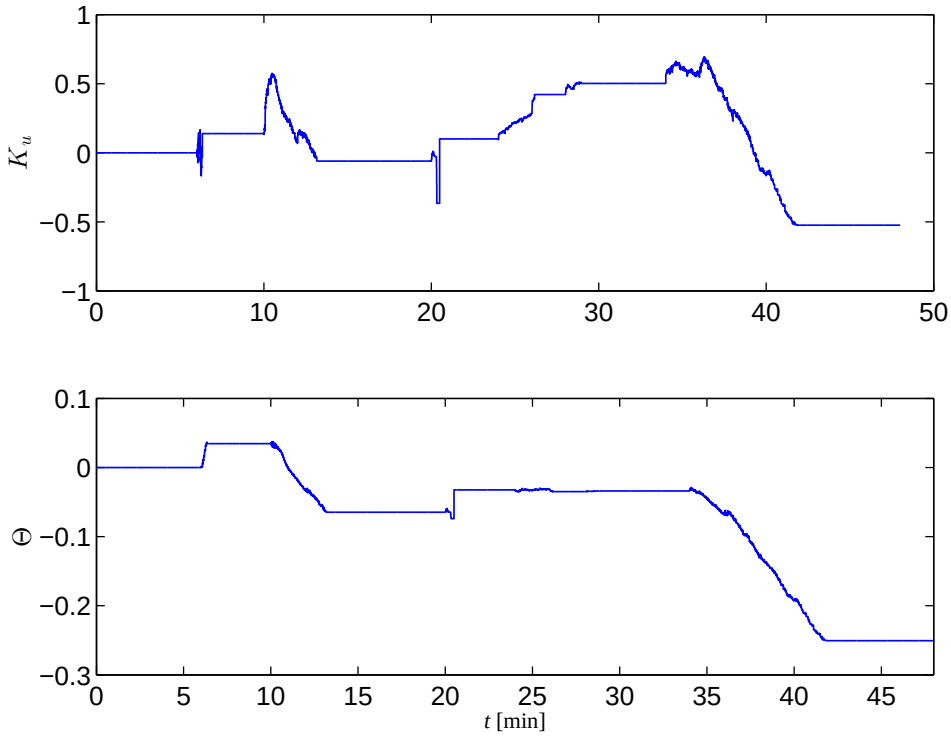

Figure 5.10: Experiment 2: adaptive parameters when using the LTR controller

Table 5.1: Comparison of different controllers with same experimantal conditions

Experiment	Controller	ISE	Mean Z[%]	Mean P_{in} [kpa]
3	Bad PI - adapt. OFF	6.2	38.45	23.58
4	Bad PI - adapt. ON	0.76	50.42	22.33
5	LTR - adapt. ON	0.64	53.23	22.29

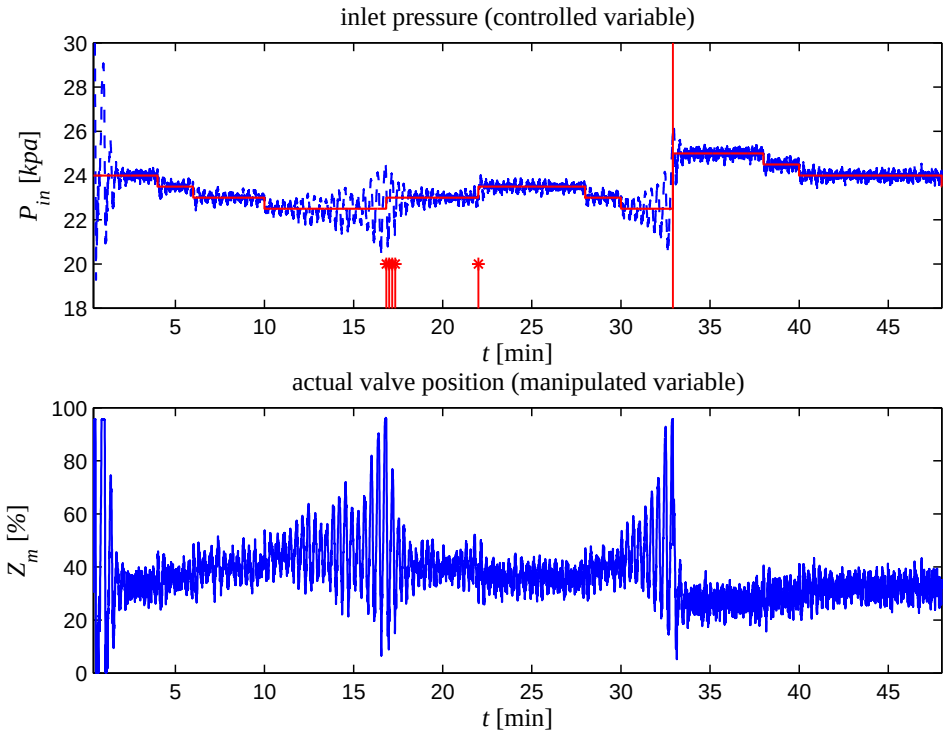

Figure 5.11: Experiment 3: supervisor control and a poorly tuned PI control as the baseline: adaptation is OFF

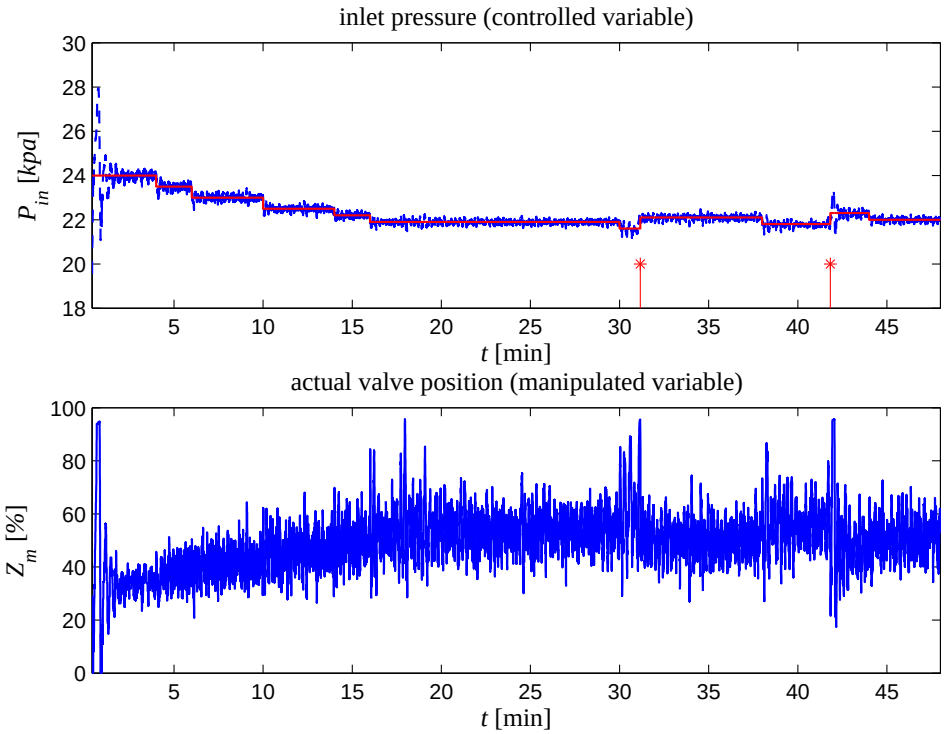

Figure 5.12: Experiment 4: supervisory control and a poorly tuned PI baseline controlerl: adaptation is ON

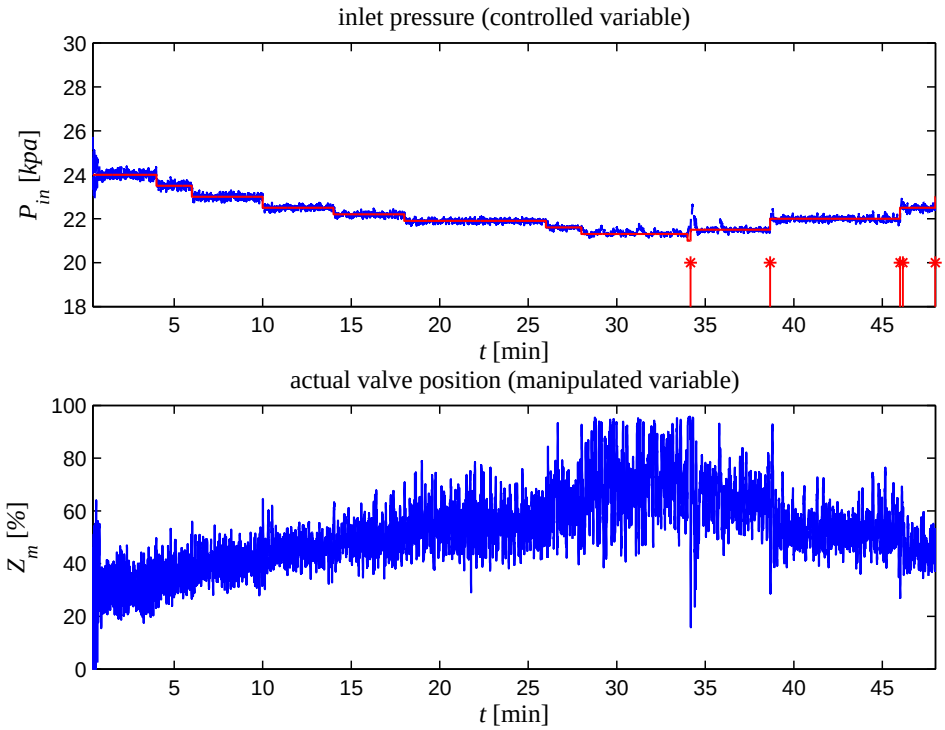

Figure 5.13: Experiment 5: supervisory control and a LTR baseline controller: adaptation is ON

5.5 Production increase analysis

The effect of the proposed control system in the oil production was tested with an OLGA simulation case taken from Jahanshahi (2013). OLGA is a commercial multiphase simulator widely used in the oil industry. The details are repeated here for completeness. The model describes a 4300m pipeline connected to a 300m vertical riser. The diameters of the pipeline and the riser are 0.12 m and 0.1 m respectively. The inlet is modelled as a pressure source.

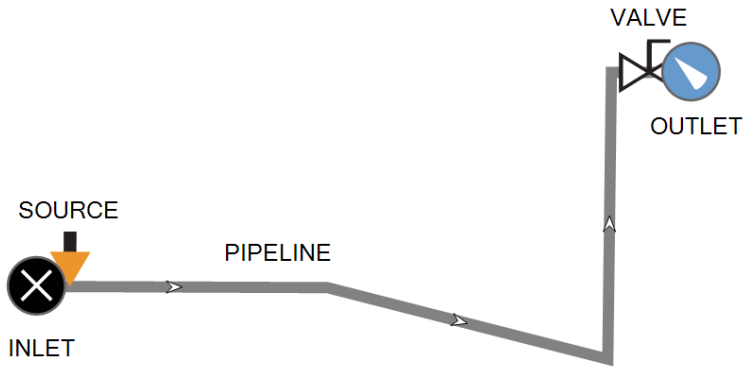

Figure 5.14: Simple representation of the OLGA pipeline-riser model

5.5.1 Supervisory and Adaptive Control design

Jahanshahi (2013) showed that the critical valve opening for this system is $Z^* = 5\%$ and the slug period is about 15.6 min. Above the critical valve opening the system is open-loop unstable. We chose as the initial operating point $Z^* = 10\%$ and repeated the control design procedure using a linearized version of the model described on Section 5.2. The model parameters have been adjusted for the OLGA case. The measured variables are the pressures at the riser bottom and riser top and the manipulated variable is the choke valve opening.

5.5.2 Performance evaluation and discussion

For comparison purposes we designed a robust controller using the $\mathcal{H}_\infty$ loop shaping design approach. Such controllers have been shown to give good trade-off between robustness and performance for this type of problems (Jahanshahi et al., 2014). The controller was designed for $Z^* = 10$ and tuned

to have the highest possible gain margin which still results in acceptable control input usage. The controllers were implemented in Matlab which was connected to Olga through an OPC server.

Starting from the initial operating point we would like to determine how large of a valve opening can we safely reach with the controllers. To ease comparison the autonomous supervisor was adjusted to stop decreasing the setpoint when it reached the minimum stable point. The minimum stable value was determined by in previous simulation runs. Figure 5.15 depicts the result of the closed-loop simulations for the $\mathcal{H}_\infty$ controller and the adaptive controller. The adaptation gains can be seen in 5.16. We have also included the simulation results for the commonly used strategy of operating the system in open-loop with a valve opening below the critical point to avoid slugs.

Table 5.2 summarize the results for the different cases. As expected, both closed-loop solutions perform significantly better than the open-loop approach. In addition, the achievable stable valve opening is considerably higher with the adaptive controller compared to the $\mathcal{H}_\infty$ controller. Nevertheless the resulting inlet pressure is not significantly lower and so the production rate increase is only minor in this case. This is not surprising because the steady state relationship between valve opening and pressure as seen in the bifurcation diagrams (see for instance Fig. 5.5) flattens out soon after the critical point. The main benefits of the proposed solution when compared to standard control solutions are however indirect. An autonomous adaptive control system that is able to stabilize the flow robustly in a wide range of conditions will increase the overall efficiency of the -production systems by reducing unplanned plant shut-downs due to pressure and liquid surges, by reducing gas flaring and by increasing the safety and reliability of the system. Other important benefits include reduction of the need for frequent retuning of the control loop performed by an expert and reduction of the work load of the operators. An interesting discussion of the economic gains and additional benefits of advanced anti-slug control systems can be found in Campos et al. (2015).

5.6 Conclusion

In this paper we proposed an autonomous control system that seeks to maximize oil production in off-shore oilfields. Our complete control solution is composed of an autonomous supervisor that manipulates the pressure setpoint and a robust adaptive controller that is able to quickly identify and adapt to changes in the plant. The supervisor was also able to automati-

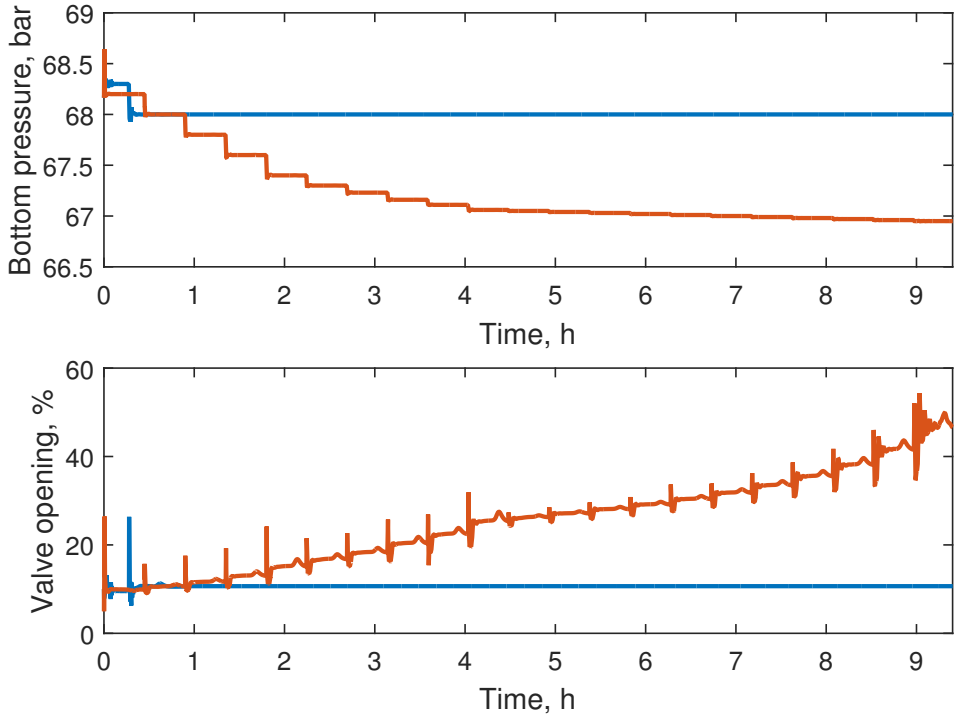

Figure 5.15: Performance of the controllers applied to the Olga model. Blue lines: H_∞ loop shaping controller; orange lines: adaptive LTR controller

cally detect instability problems in the control loop and moved the system to a safer operating point when necessary. The experimental results are very encouraging. The method demonstrated great resilience and good performance in a variety of operating conditions. Our solution will lessen the demand for manual supervision, will reduce the need for frequent retuning of the controller and will maximize the oil production.

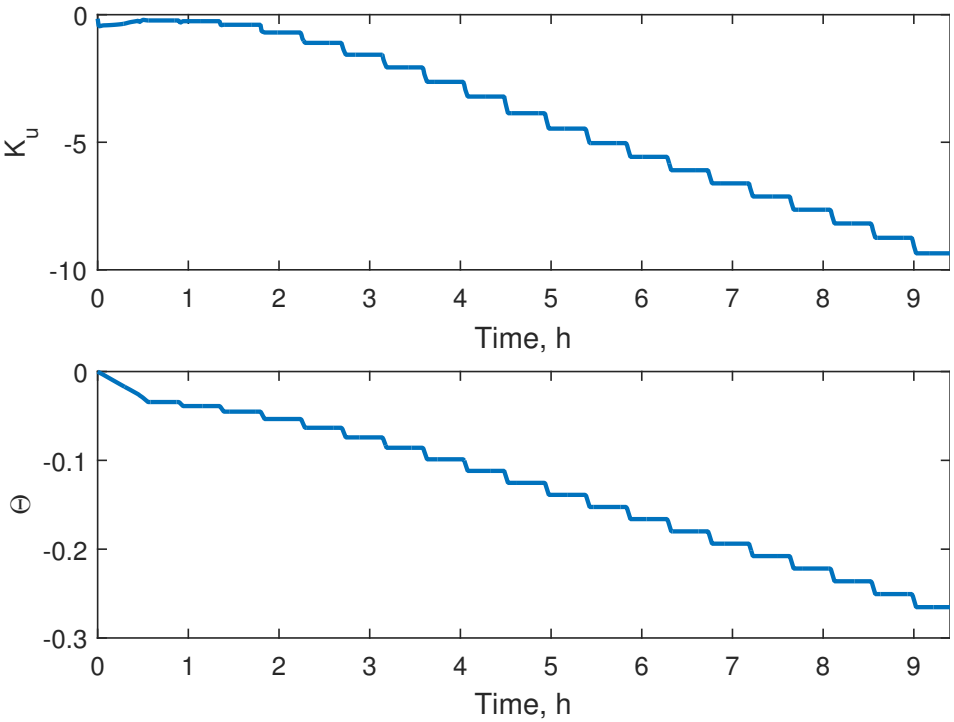

Figure 5.16: Adaptation gains for the Olga case

Table 5.2: Production analysis of different approaches

Controller	Max Z (%)	Min P(bar)	Max prod. (barrel/day)
Adaptive LTR	49	66.9	10200
$\mathcal{H}_\infty$	14	67.5	10150
Open-loop $Z = 4\%$	4	75.5	9505

Chapter 6

A comparison between Internal Model Control, optimal PIDF and robust controllers for unstable flow in risers

Anti-slug control of multiphase risers involves stabilizing an open-loop unstable operating point. PID control is the preferred choice in the industry, but appropriate tuning is required for robustness. In this paper, we define PIDF as a PID with a low-pass filter on its derivative action where the low-pass filter is crucial for the dynamics. We compared a new PIDF tuning based on Internal Model Control (IMC), together with two other tunings from the literature, with an optimal PIDF controller. The optimal PIDF tuning was found by minimizing a performance cost function while satisfying robustness requirements (input usage and complementary sensitivity peak). Next, we considered two types of robust $\mathcal{H}_\infty$ controller (mixed-sensitivity and loop-shaping). We compared the controllers based on their pareto-optimality, and we tested the controllers experimentally. We found that the new IMC-PIDF controllers is the closest to the optimal PIDF controller, but the robustness can be further improved by $\mathcal{H}_\infty$ loop-shaping.

Based on article presented in the 19th World Congress of the International Federation of Automatic Control, 2014, Cape Town, South Africa. The main contributions of the author to this article include the optimal control problem formulation and solution approach; IMC and robust control design and experimental result analysis.

6.1 Introduction

The severe-slugging flow regime which is common at offshore oilfields is characterized by large oscillatory variations in pressure and flow rates. This multi-phase flow regime in pipelines and risers is undesirable and an effective solution is needed to suppress it (Godhavn et al., 2005). One way to prevent this behaviour is to reduce the opening of the top-side choke valve. However, this conventional solution reduces the production rate from the oil wells. The recommended solution to maintain a non-oscillatory flow regime together with the maximum possible production rate is active control of the topside choke valve (Havre et al., 2000). Measurements such as pressure, flow rate or fluid density are used as the controlled variables and the topside choke valve is the main manipulated variable.

Existing anti-slug control systems are not robust and tend to become unstable after some time, because of inflow disturbances or plant changes. The main objective of our research is to find a robust solution for anti-slug control systems. The nonlinearity of the system is problematic for stabilization as the gain changes drastically between different operating conditions. In addition, another difficulty for stabilization is the effective time delay .

One solution is to use nonlinear model-based controllers to counteract the nonlinearity (e.g. Di Meglio et al., 2010). However, we have found that these solutions are not robust against time delays or plant/model mismatch (Jahanshahi and Skogestad, 2013b).

An alternative approach is to use PID controllers to stabilize the unstable flow. The PI and PID controllers are still the most widely used controllers in the industry and even from the academic point of view they are unbeatable in combined robustness and performance.

The purpose of this paper is to verify different tuning rules when applied to anti-slugging control and to give recommendations about the most appropriate rules to use. For this, we compare PID controllers with optimal controllers in simulations and experiments.

Jahanshahi and Skogestad (2013a) showed that a linear model with two unstable poles and one stable zero is sufficient for designing an anti-slug controller. They identified such a model from a closed-loop step test and

proposed a PIDF tuning based on Internal Model Control (IMC) for this system. This tuning rules were slightly modified by including the derivative action filter.

We here define a four-parameter PIDF controller as a PID controller with filtered derivative action (Åström and Hägglund, 2006).

$$K_{\text{PIDF}}(s) = K_p + \frac{K_i}{s} + \frac{K_d s}{T_f s + 1} \tag{6.1}$$

where K_p is the proportional gain, K_i is the integral action gain, K_d is the derivative action gain and T_f is the filter time constant. We differentiate this from a standard PID controller, because the low-pass filter is a crucial part of the controller for our application. That is, the filter time constant cannot be reduced without sacrificing performance.

One of the optimal controllers used for the comparison, is a PIDF where optimal tuning are found by minimizing a performance cost function while specifying robustness requirement (input usage and complementary sensitivity peak). Then, we consider use of two $\mathcal{H}_\infty$ robust controllers. $\mathcal{H}_\infty$ mixed-sensitivity design minimizes $\overline{\sigma}(S)$ for performance, $\overline{\sigma}(T)$ for robustness and low sensitivity to noise, and $\overline{\sigma}(KS)$ to penalize large inputs. In $\mathcal{H}_\infty$ loop-shaping design, we specify an initial plant loop shape, then the loop-shaping procedure increases robustness by maximizing the stability margin (Skogestad and Postlethwaite, 2005b). The PIDF controller found by Jahanshahi and Skogestad (2013a) is used to make the initially shaped plant for the loop-shaping design.

For sake of completeness, we have also included in our study the simple PID tuning rules for unstable processes proposed by Rao and Chidambaram (2006) and Lee et al. (2006).

This paper is organized as follows. Section 2 describes the pipeline-riser system. The new PIDF tuning is presented in Section 3, and the optimal PIDF tuning is introduced in Section 4. Mixed-sensitivity and loop-shaping designs are presented in Section 5 and Section 6, respectively. The results are presented in Section 7. Finally, we summarize the main conclusions and remarks in Section 8.

6.2 Systems description

Fig. 6.1 shows a schematic presentation of the system. The inflow rates of gas and liquid to the system, $w_{g,in}$ and $w_{l,in}$, are assumed to be independent disturbances and the top-side choke valve opening ($0 < Z < 100\%$) is the manipulated variable. A fourth-order dynamic model for this system was

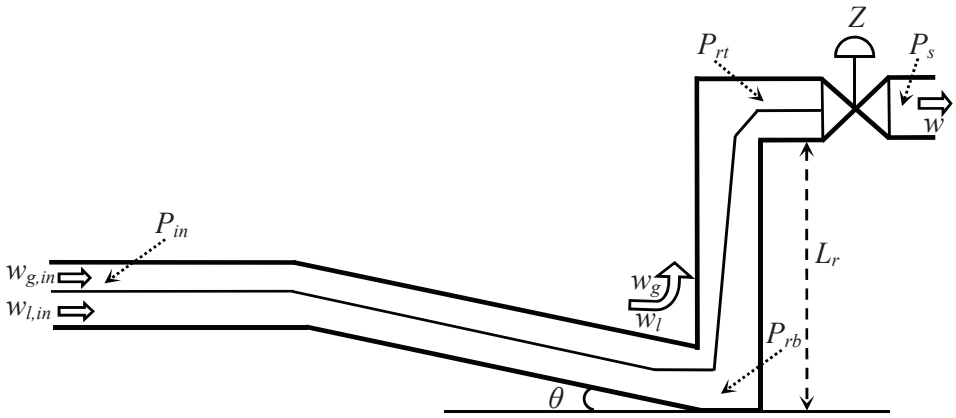

Figure 6.1: Schematic presentation of system

presented by Jahanshahi and Skogestad (2011). The state variables of this model are as:

- m_{gp}: mass of gas in pipeline [kg]
- m_{lp}: mass of liquid in pipeline [kg]
- m_{gr}: mass of gas in riser [kg]
- m_{lr}: mass of liquid in riser [kg]

The four state equations of the model are

$$\dot{m}_{gp} = w_{g,in} - w_g \tag{6.2}$$

$$\dot{m}_{lp} = w_{l,in} - w_l \tag{6.3}$$

$$\dot{m}_{gr} = w_g - \alpha w \tag{6.4}$$

$$\dot{m}_{lr} = w_l - (1-\alpha) w \tag{6.5}$$

The flow rates of gas and liquid from the pipeline to the riser, w_g and w_l, are determined by pressure drop across the riser-base where they are described by virtual valve equations. The outlet mixture flow rate, w, is determined by the opening percentage of the top-side choke valve, Z. The different flow rates and the gas mass fraction, α, in the equations (6.2)-(6.5) are given by additional model equations given by Jahanshahi and Skogestad (2011).

However, Jahanshahi and Skogestad (2013a) showed that a second-order model with two unstable poles and one stable zero is enough for the control design purposes, and such a model can be identified by a closed-loop step test.

6.3 PIDF tuning based on IMC Design

6.3.1 IMC design for unstable systems

The Internal Model Control (IMC) design procedure is summarized by Morari and Zafiriou (1989). The block diagram of the IMC structure is shown in Fig. 6.2. Here, $G(s)$ is the nominal model which in general has some mismatch with the real plant $G_p(s)$. $\tilde{Q}(s)$ is the inverse of the minimum phase part of $G(s)$ and $f(s)$ is a low-pass filter for robustness of the closed-loop system.

The IMC configuration in Fig. 6.2 cannot be used directly for unstable systems; instead we use the conventional feedback structure with the stabilizing controller

$$C(s) = \frac{\tilde{Q}(s)f(s)}{1 - G(s)\tilde{Q}(s)f(s)}. \tag{6.6}$$

For internal stability, $\tilde{Q}f$ and $(1 - G\tilde{Q}f)$ have to be stable. We use the identified model with two unstable poles and one stable zero (Jahanshahi and Skogestad, 2013a) as the plant model:

$$G(s) = \frac{\hat{b}_1 s + \hat{b}_0}{s^2 - \hat{a}_1 s + \hat{a}_0} = \frac{k'(s + \varphi)}{(s - \pi_1)(s - \pi_2)} \tag{6.7}$$

and we get

$$\tilde{Q}(s) = \frac{(1/k')(s - \pi_1)(s - \pi_2)}{s + \varphi} \tag{6.8}$$

We design the filter $f(s)$ as explained by Morari and Zafiriou (1989), which gives the following third order filter

$$f(s) = \frac{\alpha_2 s^2 + \alpha_1 s + \alpha_0}{(\lambda s + 1)^3}, \tag{6.9}$$

where λ is an adjustable closed-loop time-constant. We choose $\alpha_0 = 1$ to get integral action and the coefficients α_1 and α_2 are calculated by solving the following system of linear equations:

$$\begin{pmatrix} {\pi_1}^2 & \pi_1 & 1 \\ {\pi_2}^2 & \pi_2 & 1 \end{pmatrix} \begin{pmatrix} \alpha_2 \\ \alpha_1 \\ \alpha_0 \end{pmatrix} = \begin{pmatrix} (\lambda\pi_1 + 1)^3 \\ (\lambda\pi_2 + 1)^3 \end{pmatrix} \tag{6.10}$$

Finally, from (6.6) the feedback version of the IMC controller becomes (Jahanshahi and Skogestad, 2013a)

$$C(s) = \frac{[\frac{1}{k'\lambda^3}](\alpha_2 s^2 + \alpha_1 s + 1)}{s(s + \varphi)}. \tag{6.11}$$

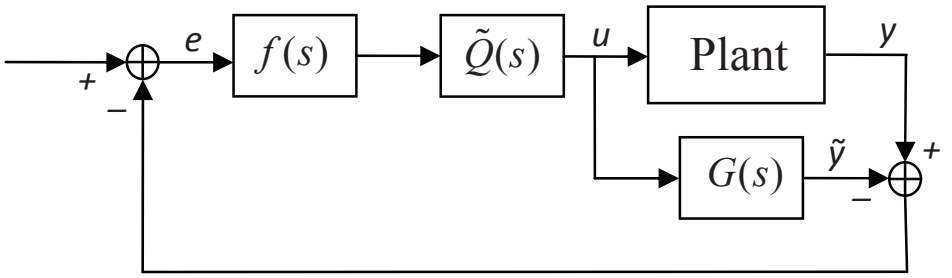

Figure 6.2: Block diagram of Internal Model Control system

6.3.2 PIDF implementation of IMC controller

The IMC controller in (6.11) is a second order transfer function which can be written in form of a PID controller with a low-pass filter.

$$K_{\text{PIDF}}(s) = K_p + \frac{K_i}{s} + \frac{K_d s}{T_f s + 1} \tag{6.12}$$

where

$$T_f = 1/\varphi \tag{6.13}$$

$$K_i = \frac{T_f}{k'\lambda^3} \tag{6.14}$$

$$K_p = K_i\alpha_1 - K_i T_f \tag{6.15}$$

$$K_d = K_i\alpha_2 - K_p T_f \tag{6.16}$$

For the controller work in practice, we require that $K_p < 0$ and $K_d < 0$; and we must choose λ such that these two conditions are satisfied.

6.4 Optimal PIDF control

For comparison purpose, we will define an optimal PIDF controller. However, optimality is generally difficult to define as we need to balance various factors such as output performance, robustness, input usage and noise sensitivity. We follow Grimholt and Skogestad (2012) and define the output performance as a weighted sum of the integrated square error (ISE) for disturbance at the plant input and output. However, a controller with good

performance (low J) may not be robust. Thus, Grimholt and Skogestad (2012) proposed to optimize J for a given robustness (M_s value). This gives a set of pareto-optimal controllers. However, we found that for our application it was necessary to add a third dimension to constraint the input usage (M_{ks}). This results in a pareto optimal surface.

6.4.1 Evaluation of performance, robustness and input usage

Performance:

Output performance is related to the difference between the measurement $y(t)$ and the setpoint y_s, and can be quantified in several different ways. In this paper we chose to quantify the performance in terms of a single scalar, namely the integrated squared error:

$$\text{ISE} = \int_0^\infty (y(t) - y_s(t))^2 \, dt \tag{6.17}$$

To balance the servo/regulatory trade-off we choose a weighted average of ISE for a step input load disturbance d_i and ISE for a step output load disturbance d_o:

$$J(K) = 0.5 \left[\frac{\text{ISE}_{do}(K)}{\text{ISE}^\circ_{do}} + \frac{\text{ISE}_{di}(K)}{\text{ISE}^\circ_{di}} \right] \tag{6.18}$$

where K is a PIDF-controller. The weighting factors ISE°_{di} and ISE°_{do} are for reference PIDF-controllers, which for the given process is ISE-optimal for a step load change on input and output, respectively. More details about this formulation can be found in Grimholt and Skogestad (2012).

Robustness:

Robustness can be quantified in several ways. Most commonly used is the sensitivity peak (M_s), complementarity sensitivity peak (M_t), gain margin (GM), phase margin (PM), and allowable time delay error ($\frac{\Delta\theta}{\theta}$). In this paper we have chosen to quantify robustness as

$$M = \max(M_s, M_t) \tag{6.19}$$

where $M_s = \|S\|_\infty = \max_\omega |S|$ and $M_t = \|T\|_\infty = \max_\omega |T|$ for all frequencies and

$$S = \frac{1}{1 + GK}, \qquad T = \frac{GK}{1 + GK} \tag{6.20}$$

$\|\cdot\|_\infty$ is the $\mathcal{H}_\infty$-norm, which gives the peak value in the frequency domain. A small M tells that large relative perturbations in the process transfer functions are permitted (Åström and Hägglund, 2006). Since our system is unstable, we will normally have $M = M_t$. For stable processes, however, we would generally have $M = M_s$.

Input usage:

A major concern in our application is to limit the input usage. This can be achieved by limiting the magnitude peak $M_{ks} = \|KS\|_\infty = \max_\omega |KS|$, where

$$KS = \frac{K}{1 + GK} \tag{6.21}$$

6.4.2 Optimization problem:

The pareto optimal PIDF controller (K) was found by solving the following optimization problem

$$\min_K \quad J(K) = 0.5 \left[\frac{\text{ISE}_{do}(K)}{\text{ISE}^\circ_{do}} + \frac{\text{ISE}_{di}(K)}{\text{ISE}^\circ_{di}} \right]$$

$$\text{s.t.} \quad M = m; \qquad M_{ks} = m_{ks} \tag{6.22}$$

for various combinations of m (the desired M value) and m_{ks} (the specified bound in the magnitude of the input signal).

Computing the optimal controller:

We propose solving the above optimization problem using gradient based nonlinear programming (NLP) techniques due to their fast convergence properties. However, the reliability of such methods depends on the quality of the gradients used by the NLP solvers. For this purpose, we use forward sensitivity calculation to obtain the exact gradients ($\nabla_K J$) of the objective function with respect to the parameters of the controller. The forward sensitivity method principle resides on first calculating $E = \frac{dx}{dt}$, where x are the closed-loop states of the system, and then relating this to J through chain-rule. Following the derivation by Biegler (2010), E can be obtained by solving the system

$$\frac{dE}{dt} = \frac{\partial f}{\partial x} E(t) + \frac{\partial f^T}{\partial K}, \quad B(0) = 0 \tag{6.23}$$

where $f \equiv \frac{dx}{dt} = A(K)x + B(K)u$ represents the state-space model of the closed-loop system. The gradient is then computed by

$$\nabla_K J = \frac{\partial J}{\partial x} E(t_f) + \frac{\partial J}{\partial K} \tag{6.24}$$

Note that the required partial derivatives may be computed using automatic differentiation or symbolic differentiation tools. The analytical calculation of the constraint gradients is more involved and should be further investigated. Here, the constraint gradients are approximated by central differences. It is worth to point out that, due to the nonconvexity of the optimization problem, we are bound to converge to a local minimum. One possibility to overcome this problem is to initialize the NLP solver with several different initial guesses and then choose the best overall solution. Alternatively, one may use a global optimization approach.

6.5 $\mathcal{H}_\infty$ mixed-sensitivity design

We consider an $\mathcal{H}_\infty$ problem where we want to bound $\overline{\sigma}(S)$ for performance, $\overline{\sigma}(T)$ for robustness and low sensitivity to noise, and $\overline{\sigma}(KS)$ to penalize large inputs. These requirements may be combined into a stacked $\mathcal{H}_\infty$ problem (Skogestad and Postlethwaite, 2005b).

$$\min_K \|N(K)\|_\infty, \quad N \triangleq \begin{bmatrix} W_u KS \\ W_T T \\ W_P S \end{bmatrix} \tag{6.25}$$

where W_u, W_T and W_P determine the desired shapes of KS, T and S, respectively. Typically, W_P^{-1} is chosen to be small at low frequencies to achieve good disturbance attenuation (i.e., performance), and W_T^{-1} is chosen to be small outside the control bandwidth, which helps to ensure good stability margin (i.e., robustness). W_u is often chosen as a constant. The solution to this optimization problem gives a stabilizing controller K that satisfies (Doyle et al., 1989; Glover and Doyle, 1988):

$$\begin{aligned} \overline{\sigma}(KS(j\omega)) &\leq \gamma \underline{\sigma}(W_u^{-1}(j\omega)) \\ \overline{\sigma}(T(j\omega)) &\leq \gamma \underline{\sigma}(W_T^{-1}(j\omega)) \\ \overline{\sigma}(S(j\omega)) &\leq \gamma \underline{\sigma}(W_P^{-1}(j\omega)) \end{aligned} \tag{6.26}$$

y_2 is the particular output for feedback control in the generalized plant in Fig. 6.3. The value of γ in equation (6.26) should be as small as possible for good controllability. However, it depends on the design specifications W_u, W_T and W_P.

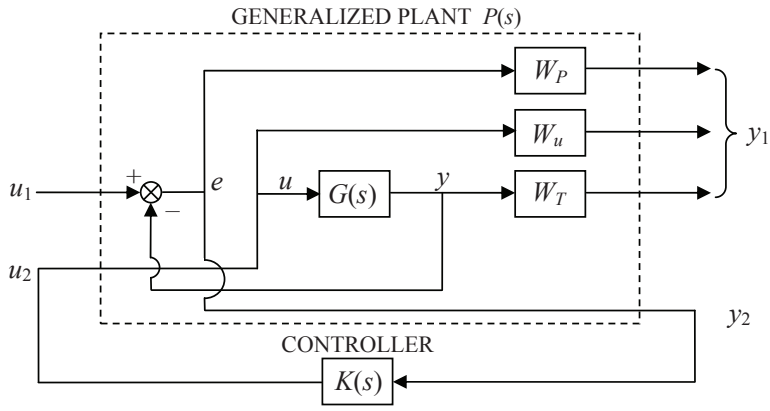

Figure 6.3: Closed-loop system for mixed sensitivity control design

6.6 $\mathcal{H}_\infty$ loop-shaping design

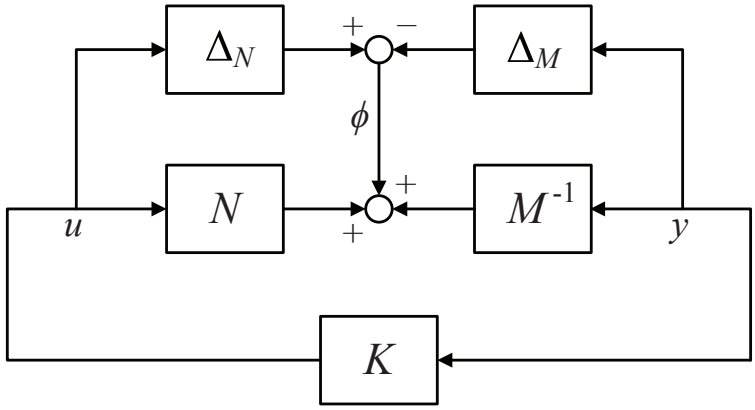

Figure 6.4: $\mathcal{H}_\infty$ robust stabilization problem

We consider the stabilization of the plant G which has a normalized left coprime factorization

$$G = M^{-1}N \tag{6.27}$$

A perturbed plant model G_p can then be written as

$$G_p = (M + \Delta_M)^{-1}(N + \Delta_N) \tag{6.28}$$

where Δ_M and Δ_N are stable unknown transfer functions which represent the uncertainty in the nominal plant model G. The objective of robust stabilization is to stabilize not only the nominal model G, but a family of perturbed plants defined by

$$G_p = \left\{(M + \Delta_M)^{-1}(N + \Delta_N) : \|[\Delta_N \;\; \Delta_M]\|_\infty < \epsilon\right\} \tag{6.29}$$

where $\epsilon > 0$ is then the stability margin (Skogestad and Postlethwaite, 2005b). To maximize this stability margin is the problem of robust stabilization of normalized coprime factor plant description as introduced and solved by Glover and McFarlane (1989).

For the perturbed feedback system of Fig. 6.4, the stability property is robust if and only if the nominal feedback system is stable and

$$\gamma_K \triangleq \left\| \begin{bmatrix} K \\ I \end{bmatrix} (I - GK)^{-1} M^{-1} \right\|_\infty \leq \frac{1}{\epsilon} \tag{6.30}$$

Notice that γ_K is the $\mathcal{H}_\infty$ norm from ϕ (see Fig. 6.4) to $\begin{bmatrix} u \\ y \end{bmatrix}$ and $(I - GK)^{-1}$ is the sensitivity function for this positive feedback arrangement. A small γ_K is corresponding to a large stability margin.

6.7 Results

All the results (simulation and experimental) in this paper are based on the following model.

$$G(s) = \frac{-0.0098(s + 0.25)}{s^2 - 0.04s + 0.025} \tag{6.31}$$

This model was identified by Jahanshahi and Skogestad (2013a) from an experimental closed-loop step test around an operating point with the valve opening of $Z = 30\%$.

6.7.1 Pareto-Optimality Comparison

The optimization problem (6.4.2) was solved for a range of desired M_{ks} and M_t values using the linear model (6.31) (Here we assumed $M = M_t$ for all cases since we have an unstable system). This results of the optimizations form a Pareto front surface, which can be seen in Fig. 6.5. For simplicity, we did not include T_f as a degree of freedom in the optimization; instead, we fixed $T_f = 4$. This choice makes the filter counteract the effect of the zero of the plant, which is close to optimal this case. The NLP was solved

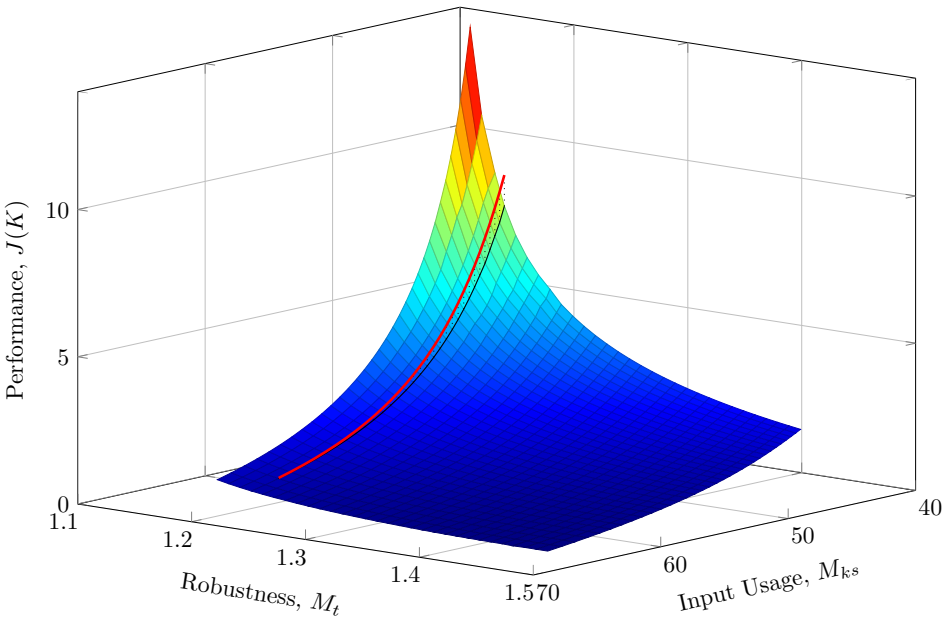

Figure 6.5: Pareto optimal PIDF surface and IMC PIDF controller (red line).

using SNOPT (Gill et al., 2005). Some points have been validated using brute force extensive search.

Figure 6.5 clearly depicts the trade-off between robustness, performance and input usage. The red line in Fig. 6.5 is the result from the IMC PIDF for different values of closed-loop time constant λ. By decreasing λ we get a faster controller with larger input usage M_{ks}, but M_t remains approximately constant. Note that the performance of the IMC PIDF is close to the pareto optimal surface for a large range of M_{ks}.

Figure 6.6 shows a cross-section of the PIDF Pareto surface with $M_{ks} = 50$, where the other controllers are also shown. All the controllers are tuned to give $M_{ks} = 50$. Compared to Chidambaram-PIDF and Lee-PIDF, IMC-PIDF gives a better trade-off between robustness and performance. $\mathcal{H}_\infty$ loop-shaping controller gives a better combined performance and robustness. However, it is a higher order controller. Surprisingly, $\mathcal{H}_\infty$ mixed sensitivity gave a inferior performance compared to PIDF. Perhaps, a better performance could be achieved by a finer tuning of the weighting transfer functions W_P, W_T and W_u.

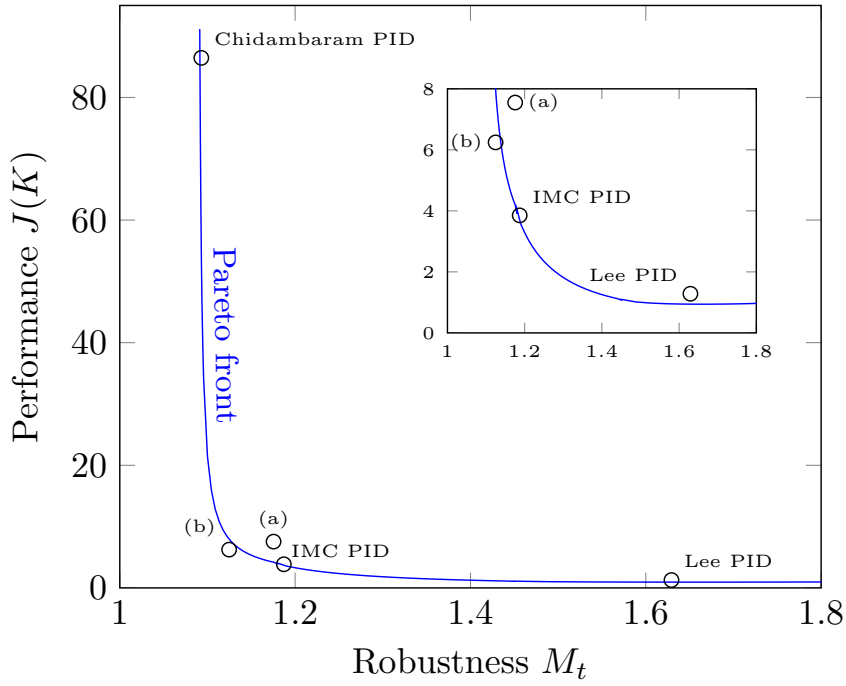

Figure 6.6: Pareto front for $M_{ks} = 50$ for PIDF with $T_f = 4$. Point (a) represents the $\mathcal{H}_\infty$ mixed-sensitivity controller; point (b) represents the $\mathcal{H}_\infty$ loop-shaping controller.

6.7.2 Experimental setup

The experiments were performed on a laboratory setup for anti-slug control at the Chemical Engineering Department of NTNU. Fig. 6.7 shows a schematic presentation of the laboratory setup. The pipeline and the riser are made from flexible pipes with 2 cm inner diameter. The length of the pipeline is 4 m, and it is inclined with a 15° angle. The height of the riser is 3 m. A buffer tank is used to simulate the effect of a long pipe with the same volume, such that the total resulting length of pipe would be about 70 m.

The topside choke valve is used as the input for control. The separator pressure after the topside choke valve is nominally constant at atmospheric pressure. The feed into the pipeline is assumed to be at constant flow rates, 4 l/min of water and 4.5 l/min of air. With these boundary conditions, the critical valve opening where the system switches from stable (non-slug) to oscillatory (slug) flow is at $Z^* = 15\%$ for the top-side valve. The bifurcation

diagrams are shown in Fig. 6.8.

The desired steady-state (dashed middle line) in slugging conditions ($Z > 15\%$) is unstable, but it can be stabilized by using control. The slope of the steady-state line (in the middle) is the static gain of the system, $k = \partial y/\partial u = \partial P_{in}/\partial Z$. As the valve opening increase this slope decreases, and the gain finally approaches to zero. This makes control of the system with large valve openings very difficult.

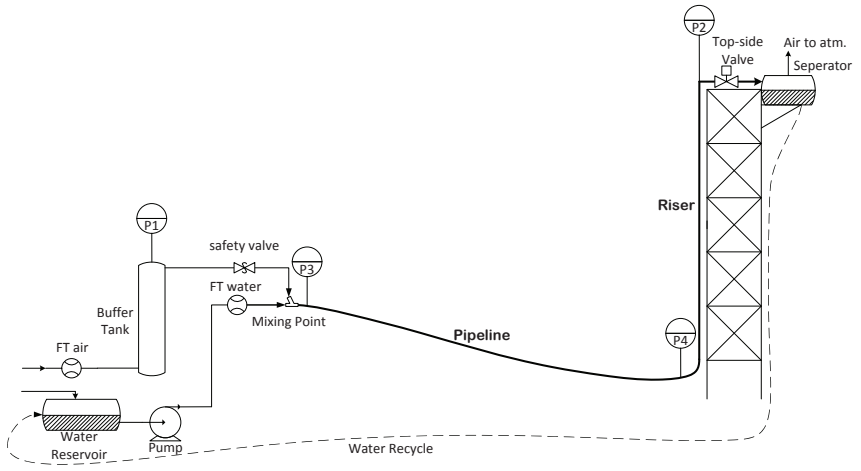

Figure 6.7: Experimental setup

6.7.3 Experimental results

The controlled output in experiments is the inlet pressure of the pipeline (P_{in}) and we use the same set of descending pressure set-points in all experiments. As mentioned in above controlling the system with large valve openings (low pressure set-points) is difficult. We decrease the controller set-point to see if the controller can stabilize the system with lower set-point. The controllers are tuned (designed) for a valve opening of $Z = 30\%$, and controllers with good gain margin can stabilize the system with larger valve openings (lower set-points). To have an impartial comparison for robustness of the controllers, we tune the controllers with the same values of input usage ($M_{ks} = 50$). One interesting relationship for the KS peak of the PIDF controller in (6.12) can be written as follows.

$$M_{ks} = -(K_d/T_f + K_p) \tag{6.32}$$

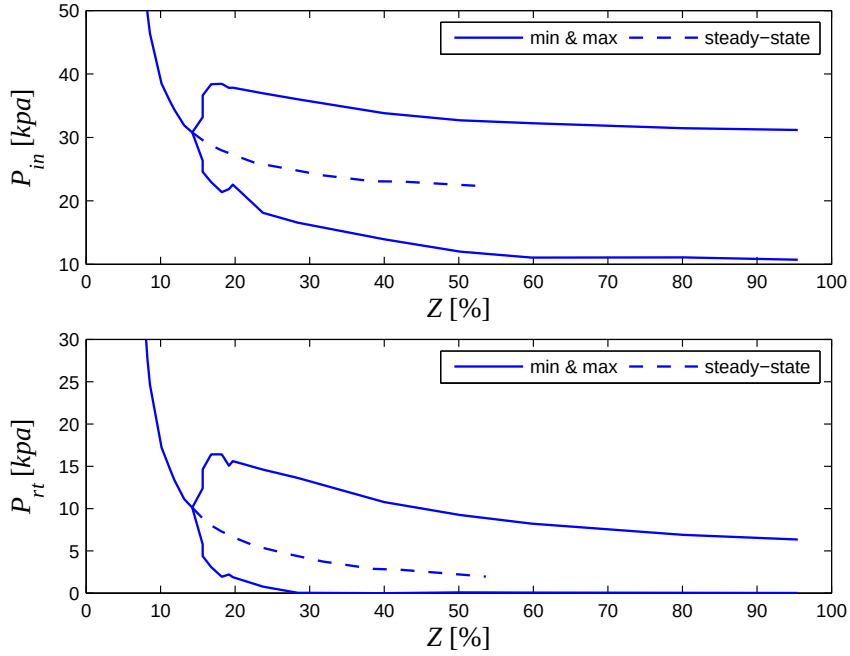

Figure 6.8: Bifurcation diagrams for experimental setup

Optimal PIDF:

Fig. 6.9 and Fig. 6.10 show experimental result of two optimal PIDF controllers, optimal PIDF (1) and optimal PIDF (2). The controller tunings are given in Table. 6.1. The optimal PIDF (2) was optimized for a smaller values of M_t which resulted in a better gain margin and less oscillations is observed in Fig. 6.10 (better robustness). However, the optimal PIDF (2) yields higher values for ISE (Table. 6.1).

IMC PIDF :

We used the identified model in (6.31) for an IMC design. We chose the filter time constant $\lambda = 6.666\ s$ to get $M_{ks} = 50$. The resulting IMC controller becomes

$$C(s) = \frac{-50(s^2 + 0.0867s + 0.0069)}{s(s + 0.25)}. \tag{6.33}$$

Note that the integral time for this controller is $\tau_I = {}^{K_p}/_{K_i} = 8.58$ s and the derivative time is $\tau_D = {}^{K_d}/_{K_p} = 12.89$ s. Since we have $\tau_I < 4\tau_D$,

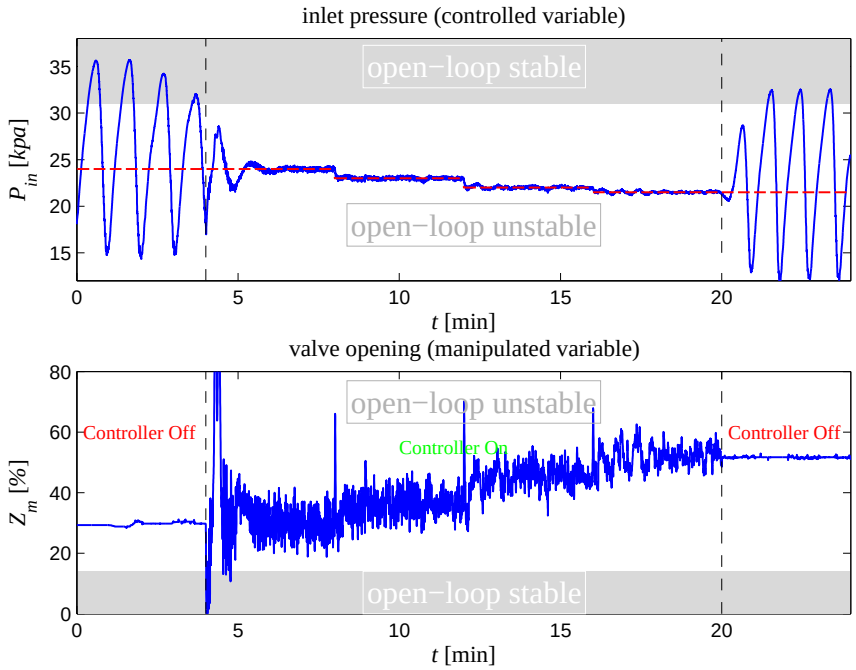

Figure 6.9: Experimental result of optimal PIDF (1) with $K_p = -3.089$, $K_i = -1.62$, $K_d = -186.73$, $T_f = 4$

the zeros are complex and the controller cannot be implemented in cascade (series) form. The PIDF tuning resulted from this controller is given in Table. 6.1, and Fig. 6.11 shows performance of the IMC-PIDF controller in the experiment.

Chidambaram PIDF :

The Chidambaram tuning (Rao and Chidambaram, 2006) is for systems with one zero, two unstable zeros and time delay. However, we do not have time delay our system, and we expect the tuning rules with $\theta = 0$ are still valid. The problem with this controller is that it does not have a low-pass filter on the derivative action; this results in a large KS peak and the controller becomes very aggressive. To solve this problem, we added the same low-pass filter as the one used in the IMC-PIDF controller. With this modification the Chidambaram tuning gives good results; the experimental result of this controller is shown in Fig. 6.12. We used $\tau_c = 20.17$ s to get $M_{ks} = 50$; the resulting tuning is given in Table. 6.1.

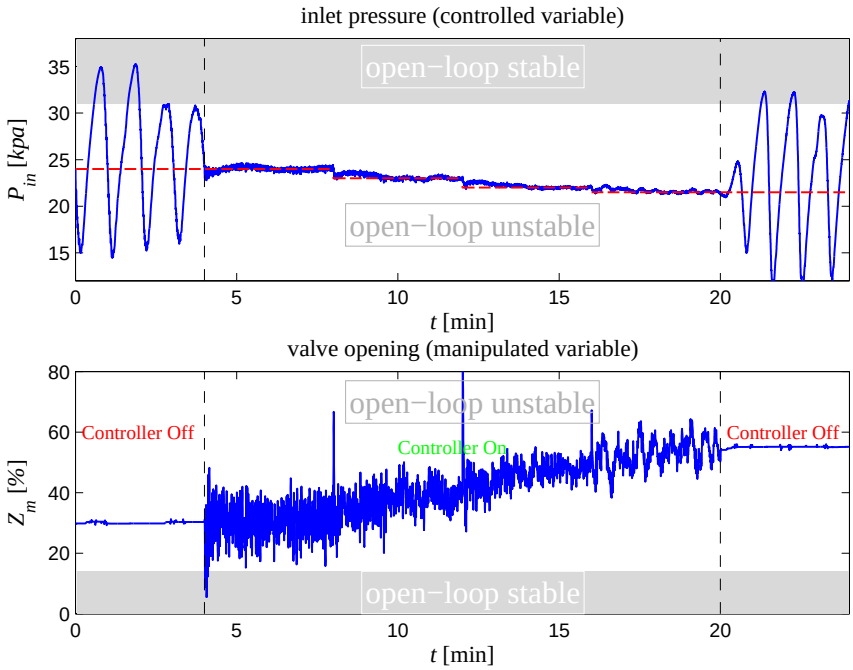

Figure 6.10: Experimental result of optimal PIDF (2) with $K_p = 0.15$, $K_i = -0.198$, $K_d = -198.10$, $T_f = 4$

Lee PIDF :

The Lee tuning (Lee et al., 2006) is based on analytic IMC-PIDF for first-order unstable systems with time delay. We had to approximate the model in (6.31) to a first-order model. We neglected the constant terms in the numerator and the denominator which are small values. This is same as what the model reduction toolbox of Matlab (*modred* routine with 'Truncate' option) does which preserves the high-frequency information. The reduced-order model is given in (6.34), and we used $\lambda = 5.35$ s to get $M_{ks} = 50$; the experimental result is shown in Fig. 6.13.

$$G_{red} = \frac{-0.245}{25s - 1} \tag{6.34}$$

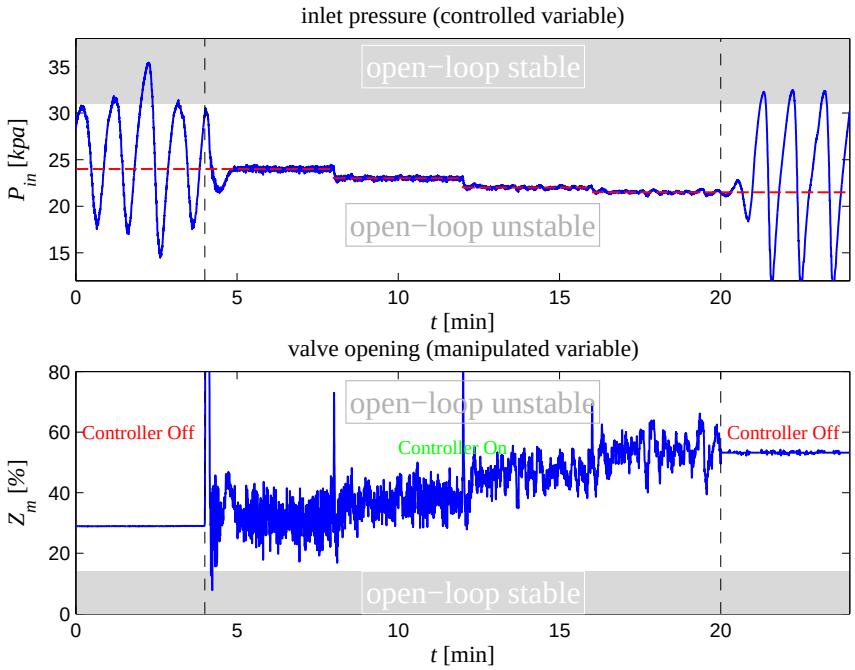

Figure 6.11: Experimental result of IMC PIDF with $K_p = -11.84$, $K_i = -1.38$, $K_d = -152.65$, $T_f = 4$

$\mathcal{H}_\infty$ loop-shaping:

We used the IMC-PIDF controller to obtain the initially shaped plant for the $\mathcal{H}_\infty$ loop-shaping design. The following fifth-order controller was resulted.

$$C(s) = \frac{-188.49(s^2 + 0.02s + 0.005)(s^2 + 0.087s + 0.0069)}{s(s + 0.25)(s + 3.76)(s^2 + 0.082s + 0.0067)} \tag{6.35}$$

The experimental result of the controller in (6.35) is shown in Fig. 6.14.

$\mathcal{H}_\infty$ mixed-sensitivity:

We design the $\mathcal{H}_\infty$ mixed-sensitivity controller with the following design specifications:

$$W_P(s) = \frac{s/M_s + \omega_B}{s + \omega_B A}, \tag{6.36}$$

$$W_T(s) = \frac{s/(10\omega_B) + 1}{0.01s + 1}, \tag{6.37}$$

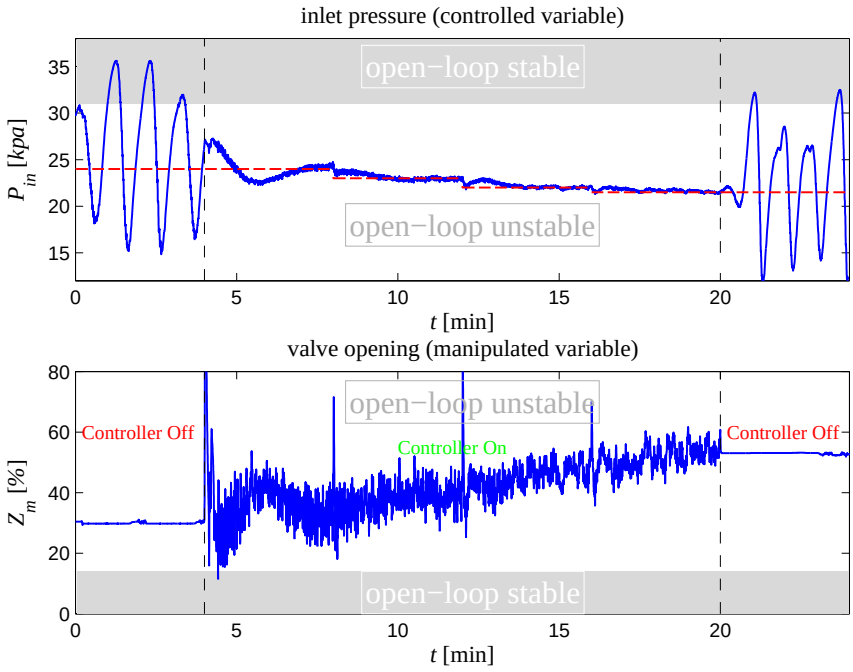

Figure 6.12: Experimental result of Chidam. PIDF with $K_p = 1.69$, $K_i = -0.15$, $K_d = -206.91$, $T_f = 4$

$$W_u = 0.0135, \tag{6.38}$$

where $M_s = 1$, $\omega_B = 0.14$ rad/s and $A = 0.01$. We chose these design specifications so that we achieve $M_{ks} = 50$ and good robustness properties. We get the following fourth-order stabilizing controller.

$$C(s) = \frac{-9.08\times10^6(s+100)(s^2+0.0137s+0.011)}{(s+1.8\times10^5)(s+112.5)(s+0.231)(s+0.0014)} \tag{6.39}$$

We achieved $\gamma = 1.21$ with this controller; the experimental performance is shown in Fig. 6.15.

6.8 Conclusion

In this paper we developed and compared feedback controllers for unstable multiphase flow in risers. The study included three sets of simple PIDF tuning rules, optimal PIDF and two $\mathcal{H}_\infty$ controllers. The comparison was based on Pareto optimality and experimental tests carried out in a prototype flow

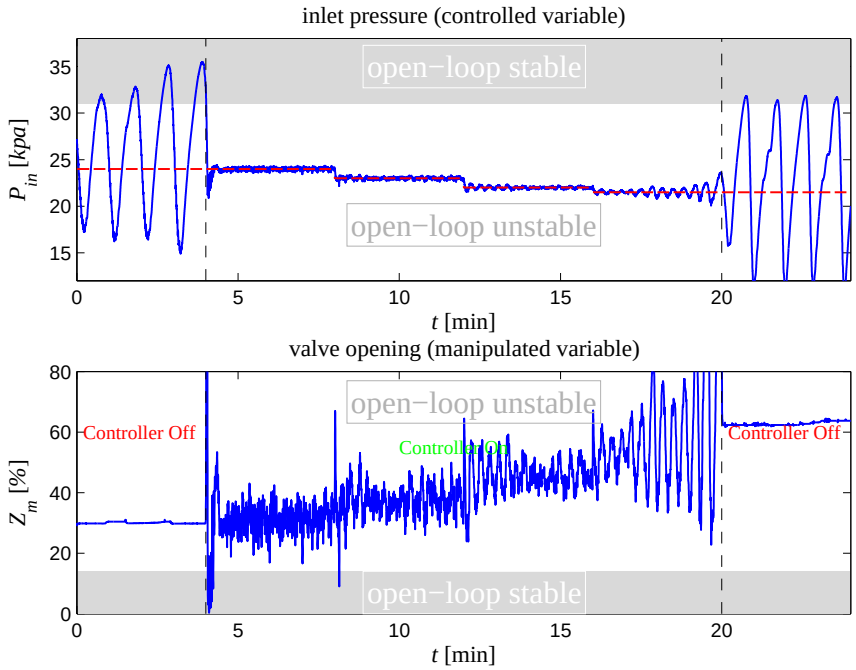

Figure 6.13: Experimental result of Lee PIDF with $K_p = -41.05$, $K_i = -3.42$, $K_d = -0.082$, $T_f = 4$

Table 6.1: Comparison of different controllers in experiments

Controller	ISE	$\|S\|_\infty$	$\|T\|_\infty$	$\|KS\|_\infty$	GM	DM
Optimal PIDF (1)	160.79	1.00	1.15	50	0.12	2.67
Optimal PIDF (2)	647.175	1.00	1.09	50	0.086	2.80
IMC PIDF	171.45	1.00	1.19	50	0.11	2.49
Chidambaram PIDF	864.75	1.13	1.09	50	0.084	2.81
Lee PIDF	726.88	1.20	1.62	50	0.17	1.70
$\mathcal{H}_\infty$ Loop Shaping	184.98	1.10	1.12	50	0.10	2.48
$\mathcal{H}_\infty$ Mixed Sensitivity	330.25	1.00	1.18	50	0.15	3.00

system. We showed that for this case the IMC-PIDF controllers are very close to the PIDF Pareto optimal surface for a large range of the tuning parameter. Better results can be achieved by the $\mathcal{H}_\infty$ loop-shaping approach, where we employ the IMC-PIDF controller to obtain the initially shaped

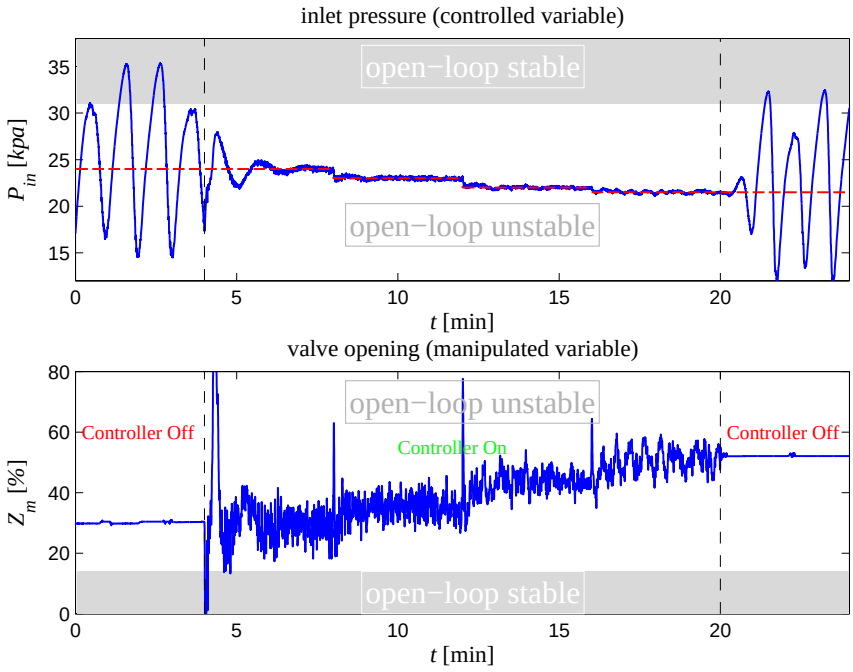

Figure 6.14: Experimental result of loop-shaping $\mathcal{H}_\infty$

plant. However, this method results in higher order controllers which may not be desired by the practitioner. The $\mathcal{H}_\infty$ mixed-sensitivity design is more involved as it requires tuning of many weights simultaneously. However, we could not achieve better results than that of a PIDF controller for this case and further investigation is needed.

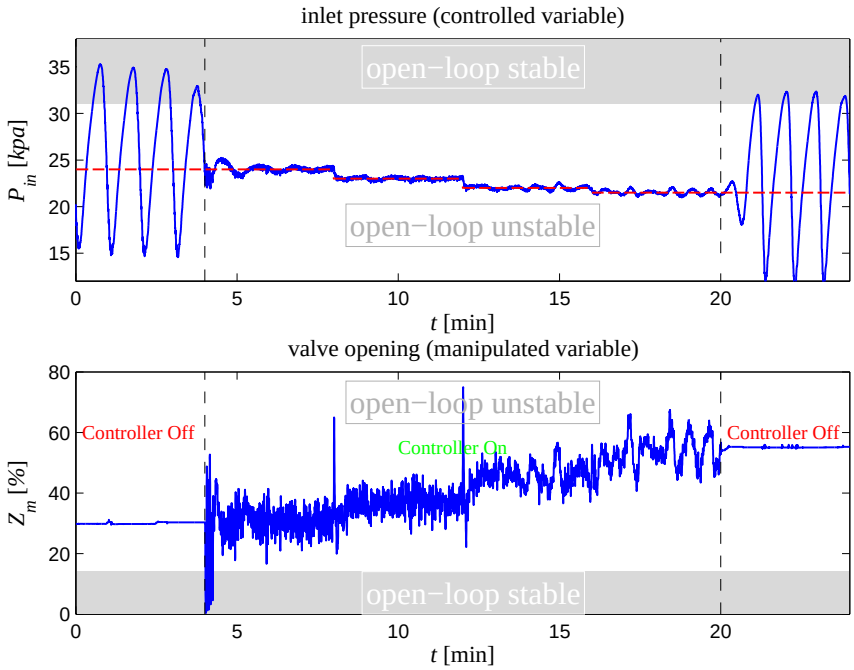

Figure 6.15: Experimental result of mixed-sensitivity $\mathcal{H}_\infty$

Part III

Near-optimal operation of uncertain batch systems

Chapter 7

Neighbouring-Extremal Control for Steady-State Optimization Using Noisy Measurements

Optimal operation of chemical plants is usually accomplished by finding the optimal steady state using the nominal set of disturbances and model parameters. The optimization is in most cases model based and therefore subject to uncertainties. This may lead to sub optimal control actions with significant economical losses. One idea to tackle this problem is to use the available measurements to adapt the inputs during operation in a feedback control scheme. This can be achieved by a neighbouring extremal controller that updates the inputs based on the deviation of the measured outputs from their nominal value. In this paper we generalize the neighbouring extremal control design that has been presented in the literature to explicitly handle measurement noise and implementation errors. The benefits of our method are illustrated in a case study where we show that the sensitivity of the controller performance to measurement noise is considerably reduced.

Presented at the International Symposium on Advanced Control of Chemical Processes, 2015, Whistler, British Columbia, Canada.

7.1 Introduction

We consider the context of steady state process optimization and robust implementation of optimal policies. Our goal is to develop simple polices that guarantee near-optimal operation under all conditions using feedback. Here, 'under all conditions' means for the defined disturbances, plant changes and implementation errors.

One approach is the so called Neighbouring-Extremal (NE) control proposed by Gros et al. (2009a), where first-order approximations of the optimal inputs are computed based on the deviations of the measured outputs due to disturbances or parametric uncertainties. This method can be implemented in a simple static output feedback control scheme, which results in near-optimal operation at a negligible online computation costs. Figure 7.1 illustrates the implementation approach. The main idea with the NE controller is to update the nominal control inputs based on the deviation of the measurements to their nominal value. However, in practice the economic performance of the NE controller can be severely impaired due to the presence of measurement noise and implementation errors. In this paper we generalize the NE design method to explicitly handle noise and implementation errors. The new design is based on a two-step approach. First, we compute a static estimator which optimally estimates the disturbances using noisy measurements. Then, based on the linearized necessary conditions of optimality the optimal input updates are obtained. Finally, we show that the method can be implemented as a simple static output feedback controller. The strength of the new NE controller for process optimization is illustrated on a continuous chemical reactor.

The paper is organized as follows. Section 2 presents the mathematical preliminaries and the problem formulation; Section 3 shows how to extend the NE approach to consider noisy measurements; Section 4 brings a simulation example to illustrate the method; In Section 5 you will find the discussion and conclusions of the paper.

7.2 Problem formulation

7.2.1 Static optimization problem

We consider the following unconstrained static optimization problem

$$\min_{u} J(x, u, d) \tag{7.1}$$

$$\text{s.t. } F(x, u, d) = 0 \tag{7.2}$$

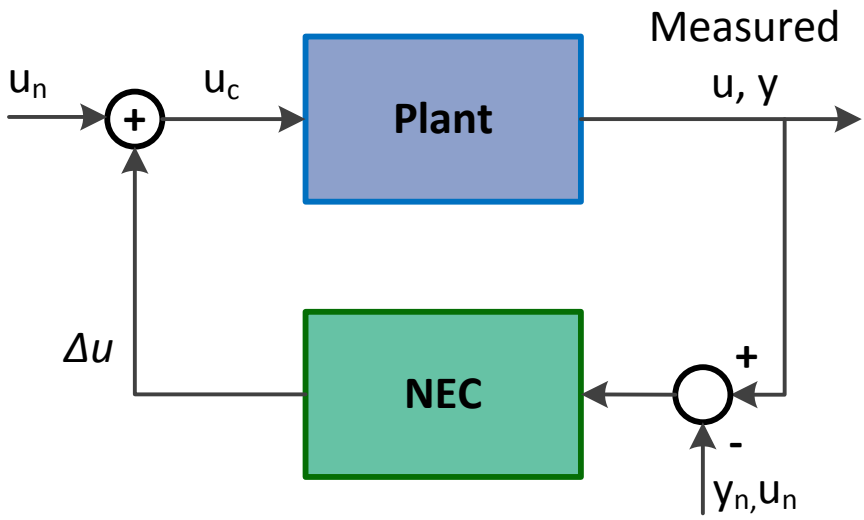

Figure 7.1: Schematic of the neigbouring extremal control scheme. The nominal inputs and outputs are represented by u_n and y_n, respectively.

where $u \in \mathbb{R}^{n_u}$ are the degrees of freedom, $x \in \mathbb{R}^{n_x}$ are the states and $d \in \mathbb{R}^{n_d}$ are the disturbances. Here the objective is $J : \mathbb{R}^{n_x+n_u+n_d} \mapsto \mathbb{R}$, and $F : \mathbb{R}^{n_x+n_u+n_d} \mapsto \mathbb{R}^{n_x}$ denotes the model equations. The output equations at steady-state read

$$y = R(x, u, d) \tag{7.3}$$

with the mapping $R : \mathbb{R}^{n_x+n_u+n_d} \mapsto \mathbb{R}^{n_y}$.

7.2.2 Optimality conditions

Let us define the Lagrangian function $L(x, u, d, \lambda) = J(x, u, d)+\lambda^T F(x, u, d)$ where λ are the multipliers. Under a suitable second-order condition and constraint qualification such as LICQ, the necessary conditions of optimality of problem (7.1)-(7.2) are

$$L_u = J_u + \lambda^T F_u = 0 \tag{7.4}$$
$$L_x = J_x + \lambda^T F_x = 0 \tag{7.5}$$
$$L_\lambda = F^T = 0 \tag{7.6}$$

where the notation $(\cdot)_X = \frac{\partial(\cdot)}{\partial X}$.

We can combine (7.4)-(7.5) to have:

$$L_u = J_u - J_x F_x^{-1} F_u = \frac{dJ}{du} = 0 \tag{7.7}$$

where this total derivative is the (reduced) gradient of the cost function with respect to u and will be denoted by the n_u dimensional vector $g \equiv \frac{dJ}{du}$. Here we assume that F_x is invertible.

7.2.3 First-order variation of the NCO

We consider small variations in the disturbance $\Delta d = d - d_{nom}$ around the nominal value d_{nom}. The linearized optimality conditions can be written as (François et al., 2014):

$$\Delta L_u \approx L_{ux}\Delta x + L_{uu}\Delta u + F_u^T \Delta\lambda + L_{ud}\Delta d = 0 \tag{7.8}$$

$$\Delta L_x \approx L_{xx}\Delta x + L_{xu}\Delta u + F_x^T \Delta\lambda + L_{xd}\Delta d = 0 \tag{7.9}$$

$$\Delta L_\lambda \approx F_x^T \Delta x + F_u^T \Delta u + F_d^T \Delta d = 0 \tag{7.10}$$

where the notation Δ indicates the deviation of the variable with respect to the nominal value.

We may use equations (7.8) and (7.9) to express the Δx and $\Delta\lambda$ in terms of Δu and Δd

$$\Delta x = -F_x^{-1} F_u \Delta u - F_x^{-1} F_d \Delta d \tag{7.11}$$

$$\Delta\lambda = -F_x^{-T} L_{xx}\Delta x - F_x^{-T} L_{xu}\Delta u - F_x^{-T} L_{xd}\Delta d \tag{7.12}$$

Here the notation $(\cdot)^{-T} = (\cdot)^{-1^T}$. Combining (7.11) and (7.12) with (7.8) we get

$$\Delta L_u = J_{uu}\Delta u + J_{ud}\Delta d \tag{7.13}$$

where

$$J_{uu} \equiv L_{uu} - L_{ux}F_x^{-1}F_u - F_u^T F_x^{-T} L_{xu} + F_u^T F_x^{-T} L_{xx} F_x^{-1} F_u \tag{7.14}$$

$$J_{ud} \equiv L_{ud} - L_{ux}F_x^{-1}F_d - F_u^T F_x^{-T} L_{xd} + F_u^T F_x^{-T} L_{xx} F_x^{-1} F_d \tag{7.15}$$

where $J_{uu} = \frac{d^2 J}{du^2}$ is the $n_u \times n_u$ reduced Hessian matrix and $J_{ud} = \frac{d^2 J}{du\, dd}$ is a $n_u \times n_d$ matrix.

The term ΔL_u is the first order approximation of the reduced gradient for the perturbed system, and we want to enforce it to zero. Therefore, the variation Δu that is necessary to optimally offset the effect of Δd is

$$\Delta u_{opt} = -J_{uu}^{-1} J_{ud} \Delta d \tag{7.16}$$

If the variations Δd are known, it is straightforward to compute the input corrections to keep the gradient equal to zero despite the disturbances. However, Δd is generally unknown and the challenge is to infer it from the noisy measurements.

7.2.4 Linear model

The linearized output equations is given by

$$\Delta y = R_x \Delta x + R_u \Delta u + R_d \Delta d \tag{7.17}$$

Upon linearising the model equation (7.2) and solving for the state deviations we get

$$\Delta x = -F_x^{-1} F_u \Delta u - F_x^{-1} F_d \Delta d \tag{7.18}$$

This results in

$$\Delta y = G \Delta u + G_d \Delta d \tag{7.19}$$

where

$$G = R_u - R_x F_x^{-1} F_u \tag{7.20}$$

$$G_d = R_d - R_x F_x^{-1} F_d \tag{7.21}$$

7.2.5 Measurement noise and input disturbance

We assume that our measurements are corrupted with noise ($y_m = y + \eta_y$) and that the computed inputs (by the optimization/controller) u_m differ from the actual plant inputs u due to input disturbances η_u. In deviation variables we have

$$\Delta y_m = \Delta y + \eta_y \tag{7.22}$$

$$\Delta u_m = \Delta u - \eta_u \tag{7.23}$$

where η_y and η_u are zero-mean Gaussian measurement noise. For simplicity, we will use the following notation

$$\eta = \begin{bmatrix} \eta_y \\ -\eta_u \end{bmatrix} \tag{7.24}$$

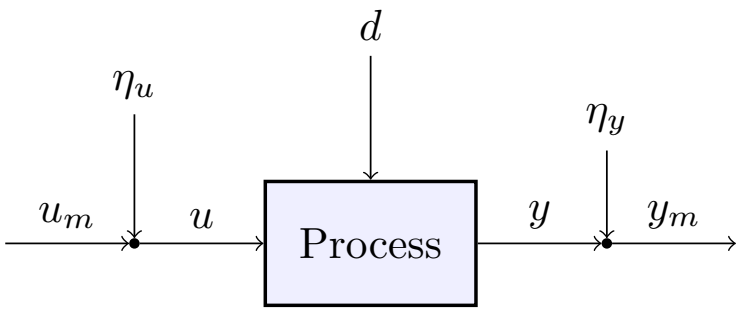

Figure 7.2: Plant setup with disturbances and noise

7.3 Dealing with measurement noise

7.3.1 Optimal static estimator open-loop

We would like to find an estimator in the form

$$\Delta\hat{d} = \underbrace{[H_1 \; H_2]}_{H} \begin{bmatrix} \Delta y_m \\ \Delta u_m \end{bmatrix} \tag{7.25}$$

that optimally approximate the disturbance Δd in the case of noisy measurements. By optimal it is meant here that we want to minimize the prediction error

$$e = \Delta d - \Delta\hat{d} \tag{7.26}$$

Let us consider the augmented linear model

$$w = \begin{bmatrix} \Delta y \\ \Delta u \end{bmatrix} = \underbrace{\begin{bmatrix} G \\ I \end{bmatrix}}_{G_u^w} \Delta u + \underbrace{\begin{bmatrix} G_d \\ 0 \end{bmatrix}}_{G_d^w} \Delta d \tag{7.27}$$

It can be shown that the prediction error is given by

$$e(H) = [-HG_u^w \quad (I - HG_d^w) \quad -H_1 \quad -H_1 G] \begin{bmatrix} \Delta u \\ \Delta d \\ \eta_y \\ \eta_u \end{bmatrix} \tag{7.28}$$

Next, the magnitudes of the disturbances, measurement errors and inputs are quantified by the scaling diagonal matrices W_d, W_{du}, W_n and W_u re-

spectively so that we can write

$$\Delta u = W_u u' \tag{7.29}$$
$$\Delta d = W_d d' \tag{7.30}$$
$$\eta_y = W_n \eta_y' \tag{7.31}$$
$$\eta_u = W_{du} \eta_u' \tag{7.32}$$

where the elements u', d', η_y' and η_u' are assumed to be normally distributed with zero mean and unit standard deviation. The diagonal scaling matrices contain the standard deviations of the elements in Δu, Δd, η_y and η_u. The prediction error can be expressed by

$$e(H) = \overbrace{\begin{bmatrix} -HG_u^w W_u & (I - HG_d^w)W_d & -H_1 W_n & -H_1 G W_{du} \end{bmatrix}}^{M(H)} \begin{bmatrix} u' \\ d' \\ \eta_y' \\ \eta_u' \end{bmatrix} \tag{7.33}$$

It can be shown that the expected value of the 2-norm of the prediction error is

$$E(\|e\|_2) = \|M(H)\|_F^2 \tag{7.34}$$

See Ghadrdan et al. (2013) for a similar proof. The matrix M can be rewritten as

$$M = Y - HX \tag{7.35}$$

where

$$Y = \begin{bmatrix} 0 & W_d & 0 \end{bmatrix} \tag{7.36}$$
$$X = \begin{bmatrix} G_u^w W_u & G_d^w W_d & \tilde{W}_n & G_u^w W_{du} \end{bmatrix} \tag{7.37}$$

and

$$\tilde{W}_n = \begin{bmatrix} W_n \\ 0 \end{bmatrix} \tag{7.38}$$

Minimizing the estimation error variance ($\|e\|_2$) is equivalent to minimizing $\|M(H)\|_F^2$. The optimization problem can be written as

$$\min_H \|Y - HX\|_F \tag{7.39}$$

which we recognize as a least-squares problems with explicit solution

$$H = YX^\dagger \tag{7.40}$$

Note that this is NOT the same as simply finding the least squares solution for d from measurement equation (7.19), as has been propozed by Gros et al. (2009a).

7.3.2 Neighbouring extremal control considering measurement noise and input disturbances

The next step is to combine the optimal disturbance estimator (7.25) with the optimal input update (7.16) to obtain the iterative control rule

$$\Delta u_{k+1} = K_u \Delta u_{m.k} + K_y \Delta y_{m,k} \tag{7.41}$$

where

$$\begin{aligned} K_y &= -J_{uu}^{-1} J_{ud} H_1 \\ K_u &= -J_{uu}^{-1} J_{ud} H_2 \end{aligned} \tag{7.42}$$

Figure 7.1 depicts a simplified block diagram of the proposed implementation approach. Note that the neighbouring extremal controller updates the control input based on the deviation of the measurements to their nominal value. In the next section we will illustrate the application of the method for the optimization of a chemical reactor.

7.4 Simulation example

Consider the steady state optimization of an isothermal continuously stirred reactor (CSTR) in which the reactions $A + B \rightarrow C$ and $2B \rightarrow D$ are taking place, see Fig. 7.3. The example is borrowed from Gros et al. (2009a). The operational goal is to determine the feed rates q_A and q_B of the components A and B into the reactor to maximize the production of the component C at steady state. This optimization problem can be formulated as

$$\max_u J(u) = \frac{c_C^2 (q_A + q_B)^2}{q_A \, c_{Ain}} - 0.5(q_A^2 + q_B^2) \tag{7.43}$$

subject to

$$\begin{aligned} 0 &= -k_1 c_A c_B + \frac{q_A}{V} c_{Ain} - \frac{q_A + q_B}{V} c_A \\ 0 &= -k_1 c_A c_B - 2k_2 c_B^2 + \frac{q_B}{V} c_{Bin} - \frac{q_A + q_B}{V} c_B \\ 0 &= k_1 c_A c_B - \frac{q_A + q_B}{V} c_C \end{aligned} \tag{7.44}$$

Where $u = [q_A, q_B]^T$, c_X describes the molar concentration of component X, V is the volume of liquid in the reactor, k_1 and k_2 are the rate constants

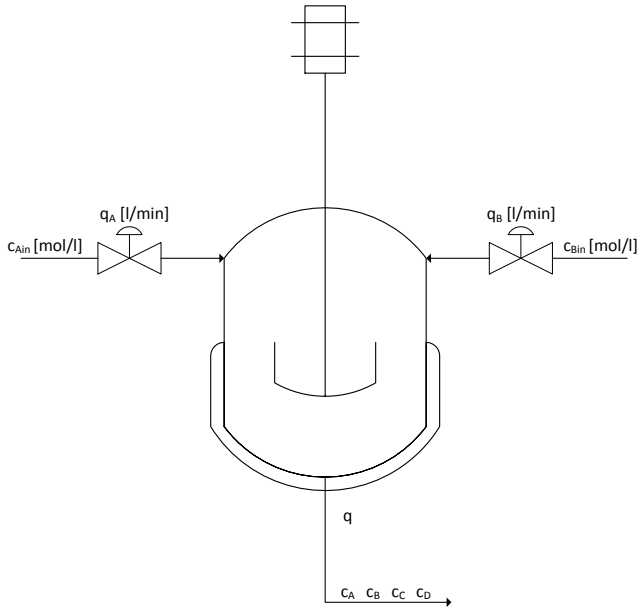

Figure 7.3: Schematic diagram of a CSTR

of the chemical reactions, c_{Ain} and c_{Bin} are the concentrations of the feed streams. The nominal model parameters are given in table 7.1. The main disturbances are the rate constants k_1 and k_2. Solving the optimization problem under nominal conditions gives

$$u_n = \begin{bmatrix} q_A \\ q_B \end{bmatrix} = \begin{bmatrix} 0.56 \\ 0.77 \end{bmatrix}, \quad y_n = \begin{bmatrix} c_A \\ c_B \\ c_C \end{bmatrix} = \begin{bmatrix} 0.058 \\ 0.05 \\ 0.78 \end{bmatrix} \tag{7.45}$$

which are referred to as nominal optimal conditions.

7.4.1 Design of the new neighbouring extremal control

The task now is to design neighbouring extremal controllers to update the nominal inputs to keep the process operating near optimal conditions despite the uncertainties. The main disturbance d are the rate constants ($d = [k_1, k_2]^T$). Our measurement vector is defined as $y = [c_A, c_B, c_C]^T$. The second order derivatives at the nominal point are

$$J_{uu} = \begin{bmatrix} 18.17 & -12.12 \\ -12.12 & 9.71 \end{bmatrix}, \quad J_{ud} = \begin{bmatrix} -0.17 & -28.6 \\ -0.06 & 22.9 \end{bmatrix} \tag{7.46}$$

Table 7.1: Nominal model parameters and operating conditions

Parameter	*Value*	*Unit*
k_1	0.65	l/(mol h)
k_2	0.014	l/(mol h)
c_{Ain}	2	mol/l
c_{Bin}	1.5	mol/l
V	500	l

The only information missing for the computation of the controller (7.42) is the matrix $H = [H_1, H_2]$. For this we need to compute the matrices G and G_d of the linearized model (7.27). Using symbolic differentiation and inserting the nominal optimal inputs we get

$$G = \begin{bmatrix} 0.54 & -0.36 \\ -0.45 & 0.36 \\ 0.34 & -0.28 \end{bmatrix}, \qquad G_d = \begin{bmatrix} -0.06 & 0.71 \\ -0.03 & -0.73 \\ 0.06 & -0.71 \end{bmatrix} \tag{7.47}$$

Next, we assume the parameters k_1 and k_2 may lie in the range $\pm 50\%$ with 95% probability. This gives the scaling matrices $W_d = \mathrm{diag}(0.1625, 0.0035)$ and $W_u = \mathrm{diag}(0.0017, 0.0025)$. We also assume an expected measurement noise of 10% standard deviation, resulting in $W_n = \mathrm{diag}(0.0003, 0.0003, 0.0039)$ and $W_{du} = \mathrm{diag}(0.0028, 0.0038)$. Gathering all these pieces we are now able to solve (7.40) to obtain

$$H = \begin{bmatrix} -11.69 & -11.95 & 0.29 & 0.84 & 0.24 \\ 0.07 & -0.71 & -0.25 & -0.27 & 0.21 \end{bmatrix} \tag{7.48}$$

which results in the following controller gains

$$K_y = \begin{bmatrix} -1.34 & -0.66 & 0.26 \\ -1.76 & -0.49 & 0.46 \end{bmatrix}, \qquad K_u = \begin{bmatrix} -0.35 & 0.17 \\ -0.57 & 0.32 \end{bmatrix} \tag{7.49}$$

7.4.2 Neighbouring extremal controller design ignoring noise

For comparison we will follow the neighbouring extremal approach of Gros et al. (2009a) where the estimation of the disturbance Δd comes from the direct invention of the linearized model (7.19). This results in the following gains

$$K_y^{Gros} = \begin{bmatrix} -0.87 & -0.42 & 0.86 \\ -1.21 & -0.07 & 1.21 \end{bmatrix}, \quad K_u^{Gros} = \begin{bmatrix} -0.015 & 0.08 \\ 0.22 & -0.06 \end{bmatrix} \tag{7.50}$$

Table 7.2: Disturbance cases

Case	*Disturbance*	*Optimal inputs*
case 1	$k_1 = k_{1,nom} + 20\%$ $k_2 = k_{2,nom} + 20\%$	$q_A = 0.57$ $q_B = 0.78$
case 2	$k_1 = k_{1,nom} - 20\%$ $k_2 = k_{2,nom} - 20\%$	$q_A = 0.54$ $q_B = 0.75$
case 3	$k_1 = k_{1,nom} + 20\%$ $k_2 = k_{2,nom} - 20\%$	$q_A = 0.57$ $q_B = 0.79$
case 4	$k_1 = k_{1,nom} - 20\%$ $k_2 = k_{2,nom} + 20\%$	$q_A = 0.53$ $q_B = 0.74$

7.4.3 Results

In this section we will compare the controllers for several disturbances realizations and for different measurement noise levels. For completeness, we also included the results for a trivial open-loop policy, in which the control inputs are kept constant at their nominal values.

Table 7.2 summarizes the different disturbance cases that were tested. We compared the controllers using four levels of measurement noise: 0%, 5%, 10% and 20% standard deviation Gaussian noise. We ran every case 1000 times and computed the average performance. Figure 7.5 shows the results for cases 1 to 4. Both strategies are significantly better than the open-loop policy in the noise-free case (top left plot in Fig. 7.5).

Not surprisingly, the neighbouring extremal controller (7.50), which was designed neglecting the noise, results in better performance in the noise-free experiment. Nonetheless, the economic benefits of (7.50) decrease significantly as the noise level increases. The proposed approach remain consistently better than open-loop policy in all cases.

Figure 7.4 exemplifies the performance obtained for different noise levels. In all cases we show c_A and c_B measurements, the control inputs and the objective function to be maximized. Measurement of c_C was omitted from the plot to ease the visualization. The red solid line is the NE controller (7.50) designed assuming perfect measurements; the green solid line is the proposed method; the dashed **black** line represent the open-loop solutions using nominal inputs; the blue lines represent the optimal solution. The objective function was normalized with respect to the optimal value.

7.5 Discussion and Conclusion

It is worth pointing out that the NE control updates can be beneficial up to some noise level, in which there would be no gain compared to the open-loop strategy. This threshold, however, depends on the size of the disturbance Δd, but it can be analytically computed as shown in Gros et al. (2009a). The intuition is that we need to be able to detect the effect of the process disturbance in the noisy measurements y_m. For a fixed level of noise, the relative efficiency (with respect to the open-loop policy) of the NE approaches improves with an increase in the magnitude of Δd.

Both NE control methods are based on linearization of the problem around some operation point. For this reason we restricted our simulations to a local neighbourhood of the nominal case. Due to the inherent nonlinearity of real processes, little can be said about the performance NE controllers for excessively large parameter variations. Nonetheless, in our proposed method we are able to define the range of expected disturbances and find the best option for the given range.

Our design approach is based on two steps: first we find the optimal static estimator and then we combine it with the optimal sensitivities to obtain the NE gains K_u and K_y. An interesting question that arises is whether we can compute the optimal gains in one step, that is, can we directly find gains K_u and K_y that minimizes the average loss? It is not perfectly clear that the solution to this problem is equivalent to the solution obtained with the two step approach. More in depth analysis of these questions will be presented in a future paper.

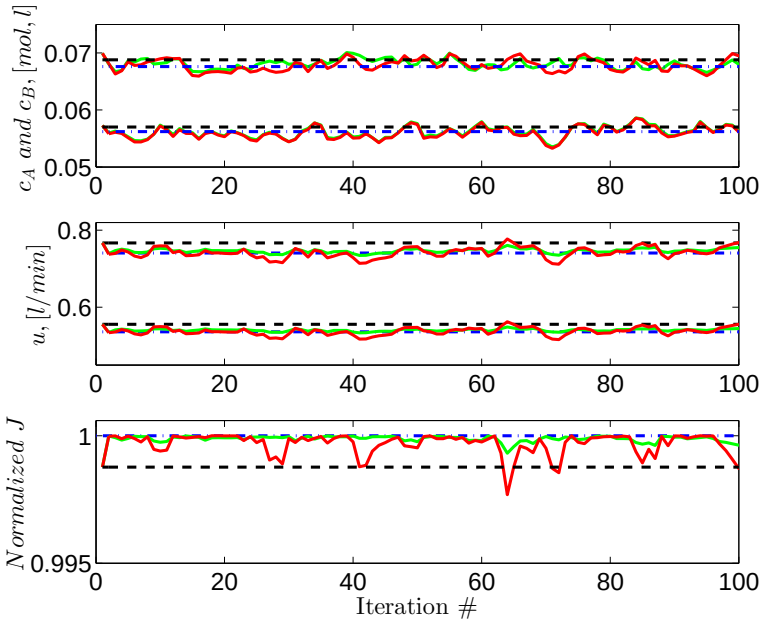

(a) Case 4 with 10% standard deviation Gaussian noise

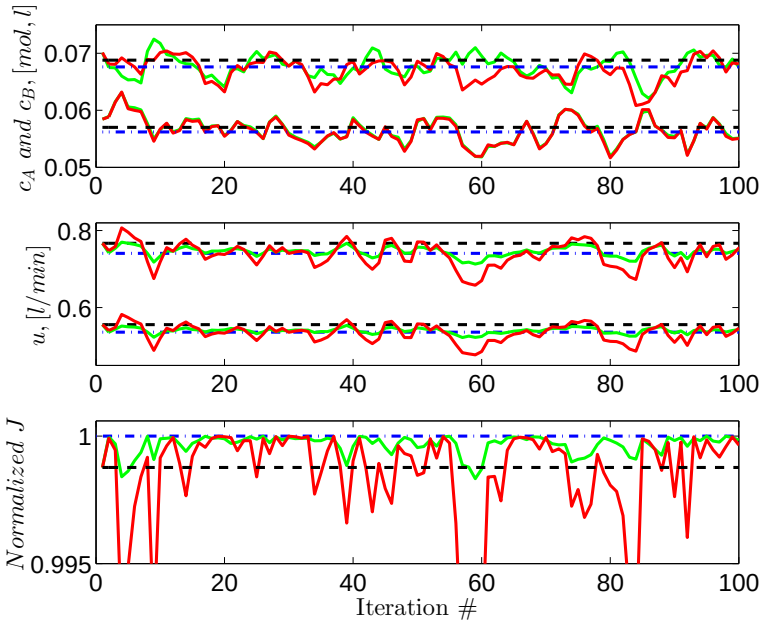

(b) Case 4 with 20% standard deviation Gaussian noise

Figure 7.4: Comparison of the different approaches for two different measurement noise levels. The red lines are given by the NE controller (7.50) that was designed without taking noise in consideration. The green lines are the result of the proposed NE controller (7.49). Note that the new method is considerably less sensitive to noise.

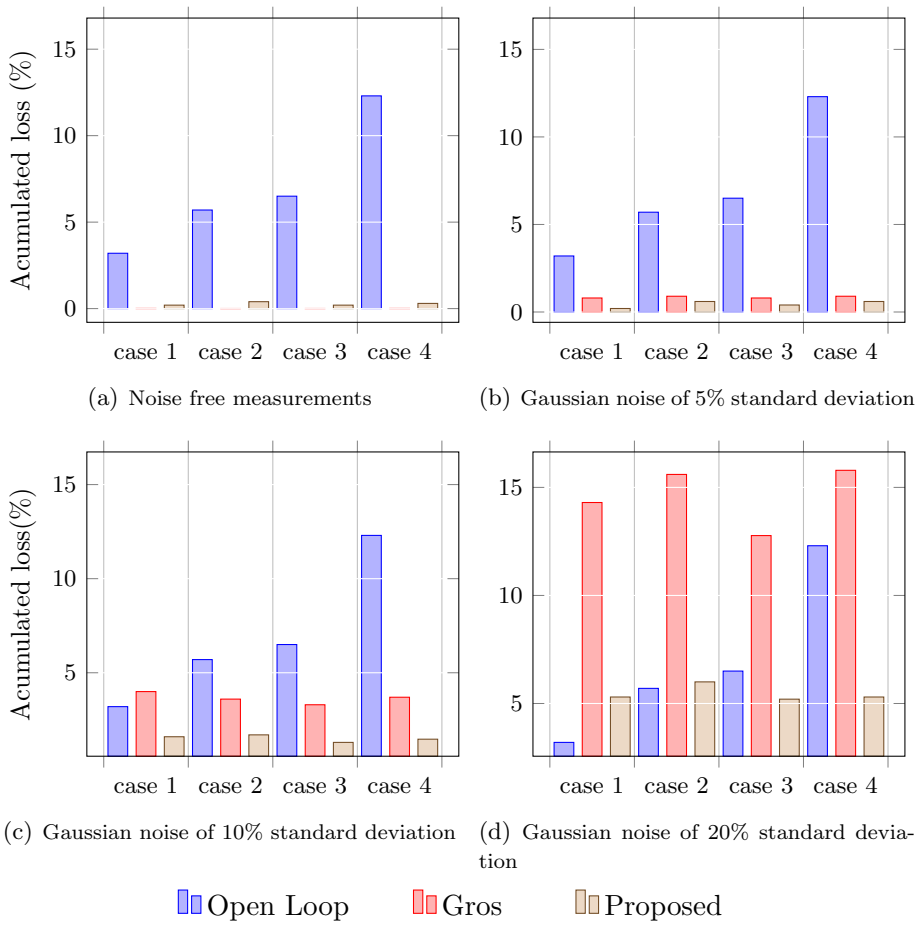

(a) Noise free measurements

(b) Gaussian noise of 5% standard deviation

(c) Gaussian noise of 10% standard deviation

(d) Gaussian noise of 20% standard deviation

Figure 7.5: Comparison of control strategies with different disturbances affecting the system. The results represent an average over 1000 runs considering different levels of measurement noise.

Chapter 8

Null-space method for optimal operation of transient processes

We consider batch process optimization and robust implementation of optimal control policies. The dynamic optimization of such processes is in most cases model based, and therefore subject to uncertainties. This may lead to sub-optimal control trajectories with significant economical losses. In this paper we extended the concept of self-optimizing control for the optimal operation of transient processes. The main idea is to find a function of the measurements whose trajectory is optimally invariant to disturbances, and then track the trajectory using standard feedback controllers. Doing so results in near-optimal economic operation in spite of varying disturbances without the need for re-optimization. We show that the invariant trajectories can be computed as linear combinations of the measurement vector, where the combination matrix is easily obtained from optimal sensitivities. We illustrate the application of the proposed method in a semi-batch reactor case study.

Chapter based on paper presented at DYCOPS-CAB 2016

8.1 Introduction

Optimal economic operation of chemical processes may be in general formulated as a dynamic optimization problem. This includes problems that

are transient in nature, where the dynamic behaviour must be considered, such as batch operations, grade changes and start-up and shut-down of continuous plants. The optimal solutions should not be implemented in an open-loop manner in most cases because of uncertain and unknown disturbances, which may lead to large economic losses or even infeasibility.

Two paradigms exist for implementation of near optimal control: an on-line approach, where the optimization problem is solved in real-time at every sample time when new information is available. An example of this approach is the economic model predictive control (EMPC)(Ellis et al., 2014).

An example of the offline optimization paradigm is self-optimizing control, which combines an off-line analysis with an on-line implementation using feedback control to track the optimal properties of the solution. For processes whose economics are defined by the steady-state behaviour the concept of self-optimizing control was introduced by Skogestad (2000).

Self-optimizing control focuses on selecting a set of controlled variables c that, when kept at constant setpoints, indirectly result in near-optimal economic operation in spite of disturbances without the need for re-optimization. Diverse systematic methods are available to find the right variables to control for steady-state problems. Skogestad and Postlethwaite (2005a) proposed the Maximum Gain Rule to select individual measurements. Alstad and Skogestad (2007) presented the Null Space method to select optimal linear combinations of measurements to be controlled. The Null Space method is very simple and yet gives zero economical loss if enough measurements are available and measurement noise is negligible.

In this paper we extended the steady state Null Space method to optimal control of batch processes. The main idea is to find a function of the measurements $c_r(t)$ whose trajectory is optimally invariant to disturbances and then track the trajectory using standard feedback controllers. By doing so, the input trajectories are optimally updated in case disturbances occur.

In this paper, we show that the invariant trajectories can be computed as linear combinations of the measurement vector. The optimal combination matrix can be easily computed off-line using optimal sensitivity information, which is easy to calculate. Our proposed control structure is shown in Fig. 8.1 where $c_r(t)$ is the optimally invariant reference trajectory that we track. As illustrated in a fed-batch case study, the proposed method is very simple and intuitive and yet is able to give near-optimal results.

There are alternative approaches for self-optimizing control of batch processes currently available in the literature (see for instance (Grema et al., 2015; Jaschke et al., 2011; Wuhua Hu, 2012)). However, the method pre-

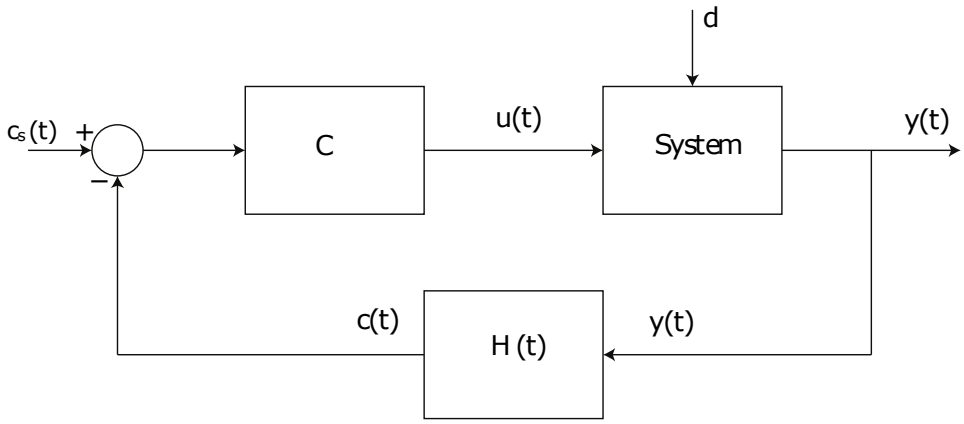

Figure 8.1: Proposed implementation based on simple feedback

sented in this paper stands out for its simplicity and ease of implementation.

The paper is divided as follows: Section 2 outlines the proposed method; Section 3 gives the results for the semi-batch reactor case study; Sections 4 and 5 show a discussion and the conclusion for the paper, respectively.

8.2 Null-scape method for transient processes

Consider the following dynamic optimization problem:

$$\min_{u} J(x(t_f), d) \tag{8.1}$$

subject to:

$$\dot{x} = f(x, u, d) \tag{8.2}$$
$$y = g(x) \tag{8.3}$$
$$p(x, u) \leq 0 \tag{8.4}$$

where t_f is the final time, $x \in \mathcal{R}^{n_x}$ are the state variables and $u \in \mathcal{R}^{n_u}$ are the control inputs. In addition, we define $y \in \mathcal{R}^{n_y}$ as the vector of known variables (measurements), which may include states, disturbances and control inputs. The optimization problem depends explicitly on the uncertain parameters by $d \in \mathcal{R}^{n_d}$. State and input constraints are summarized by $p(x, u)$. In this paper we make the assumption that the active constraint set does not change with the disturbances and time.

Assume the nominal optimal input sequence $u_0(t)$ and nominal optimal measurements $y_0(t)$ for a given disturbance d_0 is known a priori. The goal

is to obtain all the neighbouring solutions for deviations $\Delta d = d - d_0$ in the problem parameters without the need for re-optimization. It can be shown that if the cost function J is twice continuously differentiable in a neighbourhood of the nominal solution and the linear independence constraint qualifications and the sufficient second-order conditions hold, then the optimal sensitivity matrix F is well defined:

$$F(t) = \frac{\partial y_{opt}(t,d)}{\partial d} \tag{8.5}$$

and, a first order, local approximation of the optimal solution in terms of outputs y in the neighbourhood can be obtained from

$$y_{opt}(t,d) \approx y_0(t,d_0) + F(t)\Delta d \tag{8.6}$$

To find the invariant measurement combination, $c(y(t),d)$ whose optimal value is independent of Δd, i.e., we want $c_{opt}(y(t),d) = c_0(y(t),d_0)$ for any Δd sufficiently small. A simple choice is a linear combination of the measurements:

$$c(t) \equiv H(t)y(t) \tag{8.7}$$

where $H(t)$ is a $n_u \times n_y$ matrix, and $c(t)$ is a $n_u \times 1$ vector. This way we can write

$$c_{opt}(t,d) = H(t)[y_0(t,d_0) + F(t)\Delta d] \tag{8.8}$$

and we define the nominal combination of measurements:

$$c_0(t,d_0) = H(t)y_0(t,d_0) \tag{8.9}$$

By subtracting (8.9) from (8.8) we obtain:

$$c_{opt}(t,d) - c_0(t,d_0) = H(t)F(t)\Delta d \tag{8.10}$$

To have optimality with the given control policy, we must require that $c_{opt}(t) = c_0(t)$ or

$$c_{opt}(t,d) - c_0(t,d_0) = 0 \tag{8.11}$$

or

$$H(t)(y_{opt}(t) - y_0(t)) = 0 \tag{8.12}$$

or

$$H(t)F(t)\Delta d = 0 \tag{8.13}$$

Since this must hold for any value of Δd, we must select $H(t)$ such that for any t we have $H(t)F(t) = 0$. This is always true if $H(t)$ lies in the left null space of $F(t)$. The main result is summarized in the following theorem.

Theorem 1 (Nullspace method for dynamic systems) *Consider a disturbance vector Δd consisting of perturbations in the initial value of certain system parameters, and let $F(t)$ denote the optimal sensitivity matrix of the measured outputs y with respect to these disturbances, that is, $\frac{\partial y_{opt}}{\partial d}(d) = F(t)\Delta d$. Then for a small disturbance (within a range where $F(t)$ is independent of the magnitude of Δd) the controlled system, with the control policy $c(t) = c_0(t)$, behaves optimally if we select $H(t)$ such that it lies in the nullspace of $F^T(t)$, that is*

$$H(t)F(t) = 0, \quad \forall t \tag{8.14}$$

A non-trivial optimal solution $H(t)$ of rank n_u can always be found if we have sufficient number of independent measurements $y(t)$. This requires that $n_y \geq n_u + n_d$.

In this approach there is an indirect assumption of 'perfect control' since we assume that we can adjust $u(t)$ such that $c(t)$ is kept at its setpoint $c_0(t)$ for all t. This may seem limiting but this is often not the case. First, we know that there does exists a feasible $u(t)$, because this is how we obtain $c_0(t)$ and $\frac{\partial y_{opt}}{\partial d}(d) = F(t)\Delta d$. Second, there may be fundamental limitations, such as time delay, which limits perfect control, but this will not be important for the economics if the time scale required for optimal dynamic operation is much longer than the achievable closed-loop time constant for control.

Using this approach we obtain a trajectory $c_{opt}(t, d)$ that is optimally invariant due to disturbance. We can transform the problem of implementing $u(t)$ in a 'open-loop' manner to a reference tracking problem with optimal setpoints $c_r(t, d) = c_{opt}(t, d)$ (see Fig. 8.1). By tracking c_r, a simple controller automatically generates inputs u that are optimal for any disturbance d sufficiently small and thus, the online optimization is avoided.

The whole procedure has offline and online steps which are summarized as follows:

Offline:

- Solve the dynamic optimization problem with d_0;
- Select appropriate measurements y;
- Compute the optimal sensitivities $F(t)$ and the combination $H(t)$;
- Compute the reference trajectories $c_r(t) = H(t)y_0(t)$.

Online:

- Track the reference c_r by a feedback controller.

The first step of the offline analysis is often the most time-consuming step of the procedure because a large nonlinear optimization problem needs to be solved in order to obtain u_0 and $y_0(t)$. In the second step, the measurements should be selected to ensure good controllability, which is achieved by having high input-output gains.

An important assumption in our approach is the time-scale separation between the (slower) dynamic evolution of the overall trajectory and the (faster) optimal input update given by the feedback control. That is, the local convergence to the setpoint ($c(t) = c_s(t)$) is much faster than the evolution of $c_s(t)$ and may be considered instantaneous from the slower scale point of view.

Remark 4 *The proposed approach is closely related to the neighbouring-extremal (NE) control introduced in the seventies (see Bryson and HO (1975) for details). In NE control, and optimum state feedback law is applied to compute fast corrections of the control trajectory for small deviations. However, the controller is obtained from a boundary value problem whose solution is not straightforward. Furthermore, differently from our approach, in NE control all the states are required to be measured or estimated.*

Remark 5 *The optimal sensitivity has been used recently to compute online fast optimal control updates in the context of nonlinear model predictive control (as for example in Zavala and Biegler (2009)) and real time dynamic optimization as in Würth et al. (2009). However, in both cases the proposed methods required measurement or estimation of the disturbance/model uncertainty Δd. Here we only require enough independent measurements y and the solution is given by an simple output feedback controller.*

8.3 Simulation example: Fed-batch reactor

Consider the fed batch reactor optimization problem studied in Srinivasan et al. (2003), Jaschke et al. (2011) and Gros et al. (2009b) where we have two chemical reactions:

$$A + B \longrightarrow C \text{ and } B \longrightarrow D \tag{8.15}$$

where C is the product and D is the undesired side product. A is already presented in the reactor while B is fed during the batch. The goal is to maximize the difference between the amount of C and D at the end of the batch.The dynamics are given by:

$$\begin{aligned}\dot{c}_A &= -k_1 c_A c_B - c_A u/V \\ \dot{c}_B &= -k_1 c_A c_B - 2k_2 c_B - (c_B - c_{B_{in}})u/V \\ \dot{V} &= u,\end{aligned} \tag{8.16}$$

where c_A and c_B are the concentrations [mol/l] of A and B respectively, V [l] is the volume and u [l/min] is the inlet feed rate and $c_{B_{in}}$ is the inlet concentration [mol/l]. The initial conditions $c_A(0) = c_{A0}$, $c_B(0) = c_{B0}$ and $V(0) = V_0$. Additionally, the initial product concentration is zero.

Concentrations $c_C(t)$ and $c_D(t)$ are obtained from mass balance and are written as:

$$c_C(t) = \frac{1}{V}(c_{A0}V_0 - c_A(t)V(t)) \tag{8.17}$$

and

$$c_D(t) = \frac{1}{2V}[(c_A(t) + c_{B_{in}} - c_B(t))V(t) - (c_{A0} + c_{B_{in}} - c_{B0})V_0] \tag{8.18}$$

The optimization problem is thus formulated as:

$$\min_u J(t_f) = -(c_C(t_f) - c_D(t_f)) \tag{8.19}$$

subject to the dynamic model (8.16) and $u \leq u_{max}$ and $u \geq u_{min}$. The final time is fixed. All the problem parameters for the nominal conditions are summarized in Table 8.1.

8.3.1 Nominal optimal solution

The input and output trajectories for the nominal conditions are given in Fig. 8.2 and Fig. 8.3 respectively.

8.3.2 Disturbances and measurements

We consider here 20% disturbance on the kinetic parameters k_1 and k_2 ($d = [k_1,\ k_2]^T$). Because we consider two disturbances ($n_d = 2$) and we have one manipulated variable ($n_u = 1$), we will make use of thee measurements to satisfy the condition $n_y \geq n_u + n_d = 3$. We consider measurements of concentrations c_A and c_B in addition to the volume V. Thus, our measurement vector becomes

$$y = \begin{bmatrix} c_A & c_B & V \end{bmatrix}^T \tag{8.20}$$

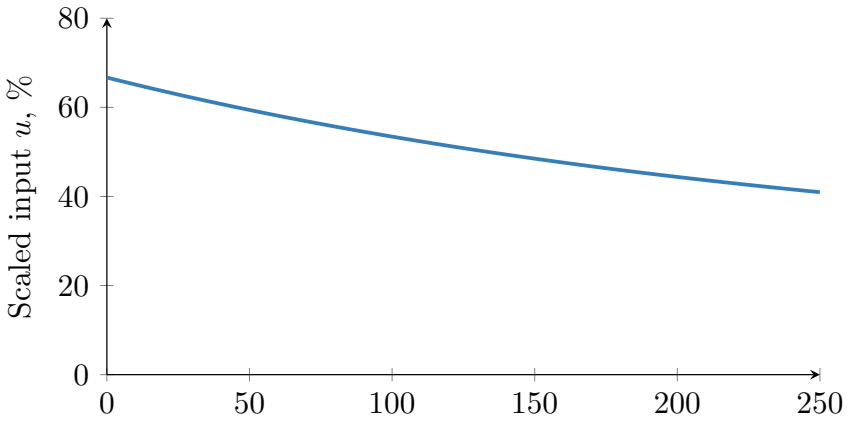

Figure 8.2: Scaled input for the nominal case (optimal solution for $d = d_0$)

8.3.3 Computing invariant trajectories

Once the important disturbances d and the measurement vector y have been defined the next step is to compute the optimal sensitivity $F(t)$. A simple practical method to obtain F is to use finite differences, where we recompute the optimal solution for a perturbed problem and approximate the sensitivities using the deviation from the nominal solution, that is

$$F(t) \approx \frac{y_{opt}^{d^*}(t) - y_0(t)}{d^* - d_0} \tag{8.21}$$

where d^* is the perturbed parameter vector and $y_{opt}^{d^*}$ is the optimized for the perturbed problem. Note that the deviation $\|d^* - d_0\|$ should be small to bound the approximation error. Nonetheless, this approach may be computationally demanding for large dimension problems with large number of disturbances. For such cases, we may use more efficient methods for calculations of the sensitivities as those provided by H. Pirnay and Biegler. (2011). In that approach, the basic strategy is based on the application of the Implicit Function Theorem to the KKT conditions of the NLP, where it can be shown that sensitivities can be obtained simply by solving a linearization of the KKT conditions. The main implementation idea is to take advantage of the exact second derivatives used in the intermediate steps of the NLP algorithm to computed exact parametric sensitivities with very little added computation (H. Pirnay and Biegler., 2011).

Finally, the final step is to compute the optimal invariant trajectory $c_0(t) = H(t)y_0(t)$ such that $F(t)H(t) = 0$. The optimal combination matrix

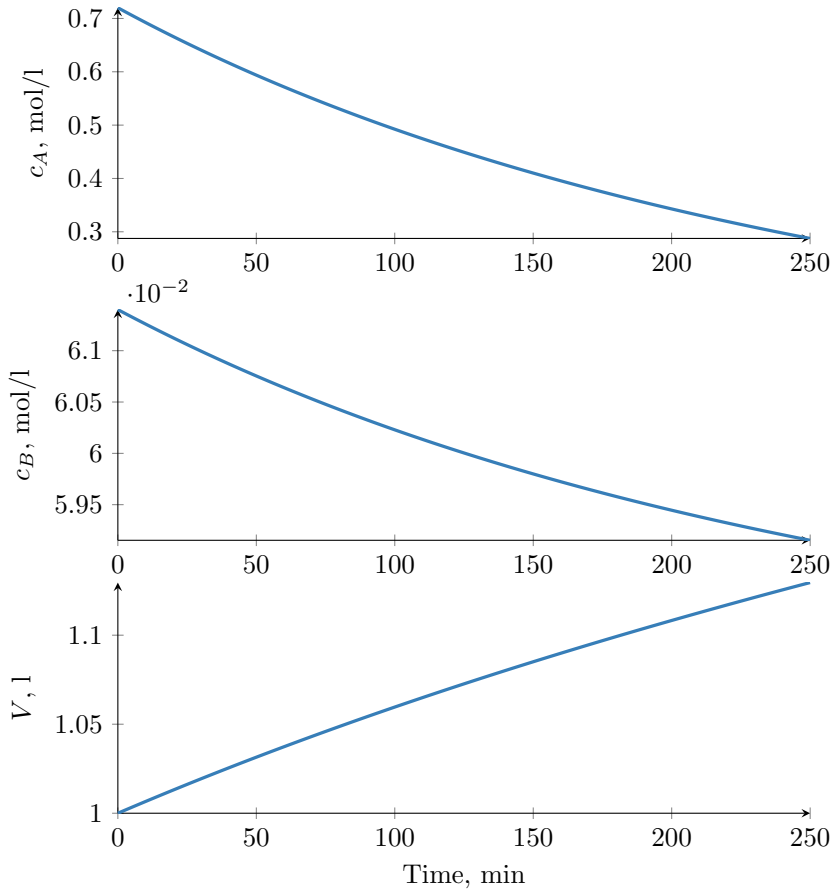

Figure 8.3: State variables for the nominal case (optimal solution for $d = d_0$)

$H(t) = [h_1(t) \quad h_2(t) \quad h_3(t)]$ for our problem is depicted in the bottom of Fig. 8.4. Note that the weights are fairly constant, a fact that may simplify the implementation tasks, such as the control tuning. Figure 8.4 also shows the invariant $c_0(t)$. The final step is the online implementation, where we design a feedback controller to track the reference $c_0(t)$. The controller used here is a simple PI.

8.3.4 Closed-loop evaluation

In this simulation study we consider four disturbance cases, which are summarized in Table 8.2. Figures 8.5 and 8.6 show the performance of the

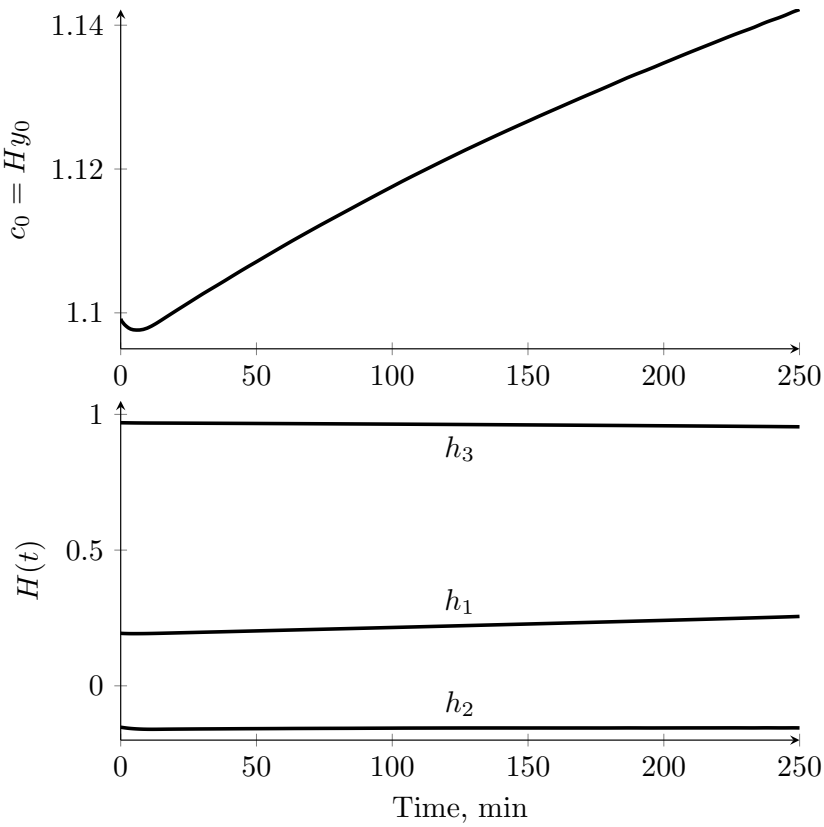

Figure 8.4: Nominal inputs

proposed method in comparison with the reoptimized solution and the open-loop nominal solution for the disturbance case 2 (see Table 8.2). Note in Fig. 8.5 that the optimal solution (red line) consists of a short boundary arc $u(t) = u_{min}$ of about $\Delta t = 2.5$ min followed by a sensitivity seeking arc. Interestingly, although the proposed controller starts with nominal values, it rapidly catches up with the optimal input trajectory. As a consequence, the state trajectories in the proposed method (shown in 8.6) are nearly identical to the optimal ones.

In Gros et al. (2009b) Neighbouring-Extremal (NE) controller for singular optimal control problems is proposed. The main idea of that NE consists in linearizing the necessary conditions of optimality around an optimal trajectory of the corresponding undisturbed problem leading to a state-feedback control law. The NE feedback law computes directly the updates

δu to the nominal control input u_n so that $u = \delta u + u_n$. We compare the proposed controller with the one presented in Gros et al. (2009b) for different disturbance scenarios. Table 8.3 summarizes the comparisons. As it can be seen, the self-optimizing controller and $NE(\theta)$ give very good results for all cases. Both methods are based on linearized conditions of optimality and should theoretically yield the same economic performance. However, the implementation philosophies of both cases are fundamentally different. In the NE approach the feedback law is derived directly from the linearized optimization problem and we have no control over important closed-loop dynamic properties, such as stability margins. In the proposed approach, the optimization and the control objectives are decoupled, that is, the design of feedback controller is an independent decision that can be made after the optimal invariant trajectories are obtained.

8.4 Discussion

A drawback of this approach is that it cannot explicitly handle constraints. Therefore, for a realistic implementation the proposed method should be combined with a periodic solution of the dynamic optimization where a new reference solution is obtained, and new invariant trajectories $c(t)$ are computed. The idea is to recompute the optimal sensitivities $F(t)$ online after solving the current NLP and then apply the approach shown in Fig 8.1 in between two successive optimizations. Similar idea has been published in Würth et al. (2009) where the authors proposed to use sensitivity based neighbouring-extremal updates combined with real-time optimization. In this way, the frequency of optimizations can be greatly reduced.

For simplicity, in this paper we have assumed a fixed final time in the dynamic optimization problem formulation. However, it is often necessary to consider a variable final time to handle uncertainties. In fact, many practical applications can be formulated as minimum time problems. The main complication here is the fact that nominal and disturbed trajectories may be misaligned in time. Thus, in order to apply our method in such cases we would need to synchronize the different trajectories using a new time variable (a 'warped-time' variable) that is comparable in all cases. An example of a typical candidate could be the distance between the current measured state and an end-point state active constraint.

8.5 Conclusion

In this paper we extend the concept of self-optimizing control to the dynamic optimization of batch processes. The main idea is to find a function of the measurements whose trajectory is optimally invariant to disturbances and then track the trajectory using standard feedback controllers. The invariant trajectory is computed as a time-varying linear combination of the measurements and the optimal combination is obtained from optimal sensitivities that are easily computed. The proposed method was tested in a semi-batch reactor case study, where near-optimal performance was achieved for various disturbances.

Table 8.1: Nominal parameters values

Symbol	Value	Unit
k_1	0.053	l/(mol×min)
k_2	0.128	l/(mol×min)
$c_{B_{in}}$	5	mol/l
t_f	250	min
u_{min}	0	l/min
u_{max}	0.001	l/min
c_{A0}	0.72	mol/l
c_{B0}	0.0614	mol/l
c_{C0}	0	mol/l
c_{D0}	0	mol/l
V_0	1	l

Table 8.2: Disturbances

Case	k_1	k_2
Nominal	0.0530	0.1280
Case 1	0.0424	0.1024
Case 2	0.0424	0.1536
Case 3	0.0636	0.1024
Case 4	0.0636	0.1536

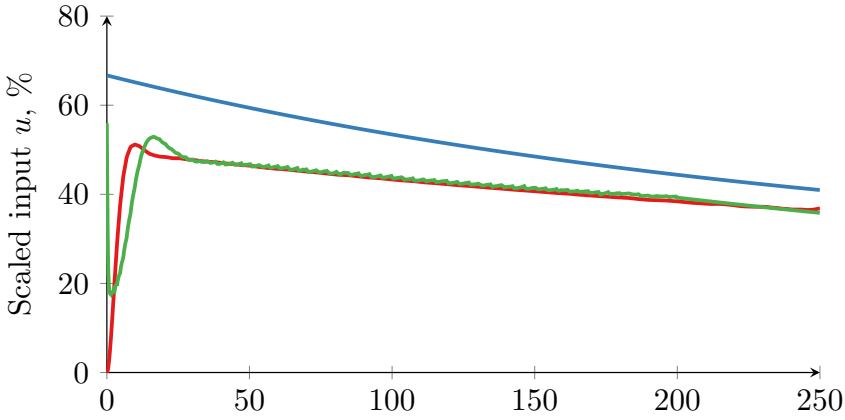

Figure 8.5: Case 2: Control input. Blue line: open-loop nominal input; red line: optimal solution; green line: proposed approach. Note that the input trajectory in our approach stays near the optimal solution without the need for re-optimization.

Table 8.3: Results for different disturbances on k_1 and k_2. J_{opt} is the optimal cost with the perturbed system, J_{soc} is the cost with the proposed approach, J_{OL} is the cost of the open-loop strategy, J_{NE}^{θ} is the cost of the NE controller proposed in Gros et al. (2009b) considering the parametric uncertainty and J_{NE} is the NE controller proposed in Gros et al. (2009b) ignoring the uncertainty.

Case	$-J_{opt}$	$-J_{soc}$	$-J_{OL}$	$-J_{NE}^{\theta}$	$-J_{NE}$
Case 1	0.2435	0.2434	0.2431	0.2435	0.2433
Case 2	0.1957	0.1957	0.1904	0.1956	0.1857
Case 3	0.3476	0.3474	0.3437	0.3475	0.3398
Case 4	0.2952	0.2952	0.2950	0.2952	0.2950

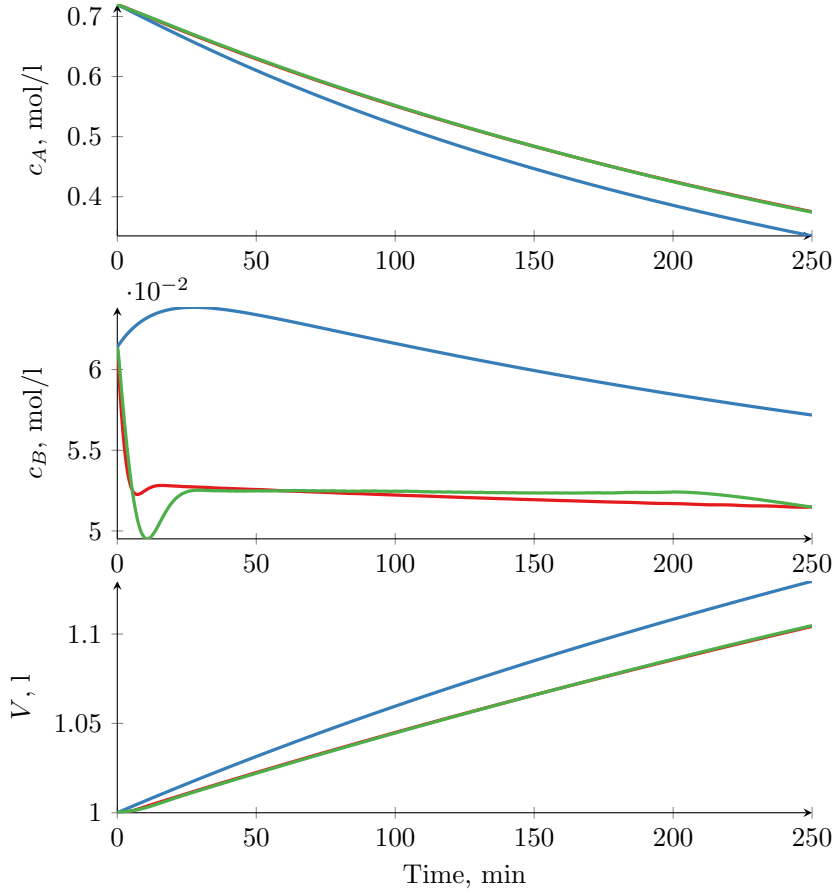

Figure 8.6: Case 2: Measurements. Blue lines: open-loop nominal input; red lines: optimal solution; green lines: proposed approach.

Chapter 9

Conclusion and further work

9.1 Conclusions

The focus of this thesis has been on processes where the dynamic behaviour is important in terms of economic performance, that is, its not sufficient to assume pseudo steady state. We have selected three main cases which have been treated in three different parts of this thesis.

Part I of the thesis was dedicated to the optimal operation of thermal energy storage systems, with focus on a domestic hot water system and a heating system. We presented a detailed problem formulation which may also be suitable similar problems. Many insights into the optimization problem formulation are given and guidelines on implementation strategies including feedback control structures are proposed. Next, we use the hot water system as an example to illustrate our proposed implementation strategy based on hierarchical decomposition of the optimization-control problem. In our approach, economic objectives and control objectives are decoupled using a two-layer cascade feedback structure. The main result here is that great economical benefits can be obtained at a very low computational cost and suitable for low cost embedded hardware.

In Part II of the thesis we presented our intelligent adaptive anti-slug control system for production maximization. Our complete control solution is composed of an autonomous supervisor that seeks to maximize production by manipulating a pressure setpoint and a robust adaptive controller that is able to quickly identify and adapt to changes in the plant. Our proposed solution has been tested in a experimental rig and the results are very encouraging. In fact, based on this work a patent application has been filed and dialogues with several companies are being carried out in order to bring this technology to the market. Other examples for which this approach

could be applicable include the control of compressors near surge and the operation of airfoil systems near the stability boundary to achieve greater power efficiency in aircraft.

In Part III of the thesis we presented contributions on the topic of finding near-optimal operating strategies using simple feedback control. First, we proposed a generalization of the neighbouring extremal control design for steady-state optimization to explicitly handle measurement noise and implementation errors. Finally, we present an extension of the previously published null-space method (Alstad and Skogestad, 2007) for near-optimal operation of transient processes. We showed that optimally invariant trajectories can be computed as linear combinations of the measurement vector, where the time-varying combination matrix is easily obtained from optimal sensitivities.

9.2 Further work

9.2.1 Implementation and evaluation of simple adaptive control rules

In Chapter 5 we presented an adaptive anti-slug control solution for production optimization. One of the most important components of our solution is the adaptive law. In this work, we have used some of the state-of-the-art techniques for adaptive control available in the literature. However, their design may require an in-depth expertise in control engineering, which may create some resistance for its acceptance by the practitioner. An alternative is to develop simple fit-for-purpose adaptive rules which give acceptable performance for this application. The main requirements for such rules is that they intuitive and have very few tuning knobs.

9.2.2 Extensions to dynamic self-optimizing control

In Chapter 8 we presented an extension of the null-space method for the operation of transient processes. A desirable improvement to our proposed method is to be able to handle measurement noise and implementation errors explicitly in the design. Another important issue is the time synchronization of the nominal reference trajectories. Since the reference signal and the combination matrix are time-varying, it is relevant to ensure that the 'computer time' and the 'process-time' are consistent to avoid implementation errors. More generally, we would like to find a variable (a 'warped-time' variable) which better describes the evolution of the process during transients to be used in the algorithm. The basic requirements for

a warped-time variable is that it should be strictly monotonic, easily measurable and should have known initial and final values. This would allow a straightforward application of the null-space method to cases where the final time is variable. For example, in our car problem presented in Chapter 1 a good candidate for a 'warped-time' would be the distance to the final position.

9.2.3 Study on the effect of end-consumer polices in the performance of the network

The first part of the thesis is dedicated to optimal policies for local energy storage systems subject to real-time electricity pricing, with focus on an individual end-consumers. An interesting question is what would be the effect on the electric network if such policies are deployed in large scale by many consumers. Because the entire system operates in a closed-loop, questions of optimality and stability of the entire network would need to be carefully analysed.

Bibliography

AI-Nimr, M. A., 1994. Temperature distributions inside electrical hot-water storage tanks. Applied Energy 48, 353–362.

Alstad, V., Skogestad, S., 2007. Null space method for selecting optimal measurement combinations as controlled variables. Industrial & Engineering Chemistry Research 46, 846–853.

Alstad, V., Skogestad, S., Hori, E. S., 2009. Optimal measurement combinations as controlled variables. Journal of Process Control 19 (1).

Åström, K., Hägglund, T., 2006. Advanced PID Control. ISA.

Avci, M., Erkoc, M., Rahmani, A., Asfour, S., 2013. Model predictive hvac load control in buildings using real-time electricity pricing. Energy and Buildings 60 (0), 199 – 209.
URL http://www.sciencedirect.com/science/article/pii/S037877881300025X

Baten, M. A., Kamil, A. A., 2011. Optimal Production Control in Stochastic Manufacturing Systems with Degenerate Demand. East Asian Journal on Applied Mathematics 1 (1), 89–96.
URL http://www.global-sci.org/eajam/readabs.php?vol=1&no=1&doc=89&year=2011&ppage=96

Biegler, L. T., 1984. Solution of dynamic optimization problems by successive quadratic programming and orthogonal collocation. Computers & chemical engineering 8 (3), 243–247.

Biegler, L. T., 2010. Nonlinear Programming: Concepts, Algorithms, and Applications to Chemical Processes, 1st Edition. MOS-SIAM Series on Optimization.

Borenstein, S., 2005. The long-run efficiency of real-time electricity pricing. The Energy Journal 26 (3), 93 – 161.

Boukas, E. K., Shi, P., Andijani, A., 1999. Robust inventory-production control problem with sthocastic demand. Optimal Control Applications and Methods 20 (February 1998), 1–20.

Bryson, A. E., HO, Y.-C., 1975. Applied Optimal Control: Optimization, Estimation and Control, 1st Edition. Taylor & Francis.

Campos, M., Takahashi, T., Ashikawa, F., Simoes, F., Stender, A., Meien, O., May 2015. Advanced anti-slug control for offshore production plants. In: Preprints of the 2nd IFAC Workshop on Automatic Control in Offsshore Oil and Gas Production. Florianopolis, Brazil.

Capolei, A., Foss, B., Jórgensen, J. B., 2015. Profit and risk measures in oil production optimization. In: 2nd IFAC Workshop on Automatic Control in Offshore Oil and Gas Production. Florianopolis, Brazil.

de Oliveira, V., Jäschke, J., Skogestad, S., 2015. Optimal operation of energy storage in buildings: Use of the hot water system. Journal of Energy Storage.

de Oliveira, V., Jäschke, J., Skogestad, S., 2016. Hierarchical control for dynamic optimization of energy storage systems. in preparation.

Di Meglio, F., Kaasa, G.-O., Petit, N., Alstad, V., 2010. Model-based control of slugging flow: an experimental case study. In: American Control Conference. Baltimore, USA, pp. 2995–3002.

Doyle, J., Glover, K., Khargonekar, P., Francis, B., aug 1989. State-space solutions to standard $\mathcal{H}_2$ and $\mathcal{H}_\infty$ control problems. IEEE Transactions on Automatic Control 34 (8), 831–847.

Ellis, M., Christofides, P. D., 2014. Integrating dynamic economic optimization and model predictive control for optimal operation of nonlinear process systems. Control Engineering Practice 22, 242 – 251.
URL http://www.sciencedirect.com/science/article/pii/S0967066113000348

Ellis, M., Durand, H., Christofides, P. D., 2014. A tutorial review of economic model predictive control methods. Journal of Process Control 24 (8), 1156 – 1178, economic nonlinear model predictive control.
URL http://www.sciencedirect.com/science/article/pii/S0959152414000900

Ericson, T., 2009. Direct load control of residential water heaters. Energy Policy 37, 3502–3512.

Faruqui, A., Sergici, S., 2010. Household response to dynamic pricing of electricity: A survey of 15 experiments. Journal of Regulatory Economics 38 (2), 193–225.

François, G., Srinivasan, B., Bonvin, D., 2014. Equivalence between neighboring-extremal control and self-optimizing control for the steady-state optimization of dynamical systems. Industrial & Engineering Chemistry Research 53 (18), 7470–7478.

Gallego, G., Hu, H., 2004. Optimal Policies for Production / Inventory Systems with Finite Capacity and Markov-Modulated Demand and Supply Processes. Annals of Operations Research 126 (1-4), 21–41.

Ghadrdan, M., Grimholt, C., Skogestad, S., 2013. A new class of model-based static estimators. Industrial & Engineering Chemistry Research 52 (35), 12451–12462.

Gill, P. E., Murray, W., Saunders, M. A., 2002. SNOPT: an SQP algorithm for large-scale constrained optimization. SIAM Journal on Optimization 12 (4), 979–1006.

Gill, P. E., Murray, W., Sunders, M. A., 2005. SNOPT: An SQP Algorithm for Large-Scale Constrained Optimization. SIAM Journal on Optimization 47 (1), 99–131.

Glover, K., Doyle, J. C., 1988. State-space formulae for all stabilizing controllers that satisfy an $\mathcal{H}_\infty$-norm bound and relations to relations to risk sensitivity. Systems and Control Letters 11 (3), 167–172.

Glover, K., McFarlane, D., 1989. Robust stabilization of normalized coprime factor plant descriptions with h_∞-bounded uncertainty. IEEE Transactions on Automatic Control 34 (8), 821–830.

Godhavn, J.-M., Fard, M. P., Fuchs, P. H., 2005. New slug control strategies, tuning rules and experimental results. Journal of Process Control 15, 547?–557.

Goudarzi, H., Hatami, S., Pedram, M., 2011. Demand-Side Load Scheduling Incentivized by Dynamic Energy Prices. In: IEEE International Conference on Smart Grid Communications. pp. 351–356.

Grema, A. S., Landa, A. C., Cao, Y., 2015. Dynamic self-optimizing control for oil reservoir waterflooding. In: 2nd IFAC Workshop on Automatic Control in Offshore Oil and Gas Production, Florianpolis, Brazil.

Grimholt, C., Skogestad, S., 2012. Optimal PI-control and verification of the SIMC tuning rules. In: IFAC Conference on Advances in PID Control. Brescia, Italy.

Gros, S., Srinivasan, B., Bonvin, D., 2009a. Optimizing control based on output feedback. Computers & Chemical Engineering 33 (1), 191–198.

Gros, S., Srinivasan, B., Chachuat, B., Bonvin, D., 2009b. Neighboring-extremal control for singular dynamic optimization problems. I-single-input systems. International Journal of Control 82 (6), 1099–1112.

H. Pirnay, R. L.-N., Biegler., L. T., 2011. Optimal sensitivity based on ipopt.

Hammerstrom, D., 2007. Pacific Northwest GridWise Testbed Demonstration Projects Part I . Olympic Peninsula Project. Tech. rep.

Havre, K., Stornes, K., Stray, H., 2000. Taming slug flow in pipelines. ABB Review 4, 55–63.

Henze, G. P., Felsmann, C., Knabe, G., 2004. Evaluation of optimal control for active and passive building thermal storage. International Journal of Thermal Sciences 43 (2), 173 – 183.
URL http://www.sciencedirect.com/science/article/pii/S1290072903001327

Institutt, M., 2012. Yr.
URL www.yr.no

Jahanshahi, E., 2013. Control Solutions for Multiphase Flow. Ph.D. thesis, Norwegian University of Science and Technology.

Jahanshahi, E., de Oliveira, V., Grimholt, C., Skogestad, S., August 2014. A comparison between internal model control, optimal PIDF and robust controllers for unstable flow in risers. In: Preprints of the 19th IFAC World Congress. Cape Town, South Africa.

Jahanshahi, E., Skogestad, S., Auguest 2011. Simplified dynamical models for control of severe slugging in multiphase risers. In: 18th IFAC World Congress. Milan, Italy, pp. 1634–1639.

Jahanshahi, E., Skogestad, S., 2013a. Closed-loop model identification and pid/pi tuning for robust anti-slug control. In: 10th IFAC International Symposium on Dynamics and Control of Process Systems. Mumbai, India.

Jahanshahi, E., Skogestad, S., 2013b. Comparison between nonlinear modelbased controllers and gain-scheduling internal model control based on identified model. In: 52nd IEEE Conference on Decision and Control. Florence, Italy.

Jahanshahi, E., Skogestad, S., Lieungh, M., July 2013. Subsea solution for anti-slug control of multiphase risers. In: Control Conference (ECC), 2013 European. pp. 4094–4099.

Jaschke, J., Fikar, M., Skogestad, S., Dec 2011. Self-optimizing invariants in dynamic optimization. In: Decision and Control and European Control Conference (CDC-ECC), 2011 50th IEEE Conference on. pp. 7753–7758.

Jäschke, J., Skogestad, S., 2012. Optimal controlled variables for polynomial systems. Journal of Process Control 22 (1).

Jordan, U., Vajen, K., 2001. Realistic domestic hot-water profiles in different time scales. IEA SHC. Task 26: Solar combisystems.

Khalifa, A. J., Mustafa, A., Khammas, F., 2009. Experimental study of temperature stratification ina thermal storage tank in the static mode for different aspect ratios. ARPN Journal of Engineering and Applied Sciences 6 (2).

Lavretsky, E., June 2012. Adaptive output feedback design using asymptotic properties of LQG/LTR controllers. IEEE Transactions on Automatic Control 57 (6), 1587–1591.

Lavretsky, E., Wise, K., 2013. Robust and Adaptive Control with Aerospace Applications. Springer.

Lee, Y., Park, S., Lee, M., January 2006. Consider the generalized imc-pid method for pid controller tuning of time-delay processes. Hybrocarbon Processing 6, 87–91.

Li, P., Arellano-Garcia, H., Wozny, G., Jan. 2008. Chance constrained programming approach to process optimization under uncertainty. Computers & Chemical Engineering 32 (1-2), 25–45.

Mardavij Roozbehani, M. D., Mitter, S., 2010. Dynamic Pricing and Stabilization of Supply and Demand in Modern Electric Power Grids. In: IEEE International Conference on Smart Grid Communications. pp. 543–548.

Misra, P., December 1992. A computational algorithm for squaring-up linear sysetms, part i: zero input output matrix. In: Proceedings of the 1992 IEEE CDC. Tucson, AZ.

Molderink, A., Bakker, V., Bosman, M. G., Hurink, J. L., Smit, G. J., Jun. 2009. Domestic energy management methodology for optimizing efficiency in Smart Grids. 2009 IEEE Bucharest PowerTech, 1–7.

Morari, M., Zafiriou, E., 1989. Robust Process Control. Prentice Hall, Englewood Cliffs, New Jersey.

Nocedal, J., Wright, S., 2006. Numerical Optimization, 2nd Edition. Springer.

NordPoolSpot, Jan. 2014. Nord pool spot: Historical market data. URL `http://www.nordpoolspot.com/`

Pomet, J.-B., Praly, L., Jun 1992. Adaptive nonlinear regulation: estimation from the lyapunov equation. Automatic Control, IEEE Transactions on 37 (6), 729–740.

Rao, A. S., Chidambaram, M., 2006. Control of unstable processes with two rhp poles, a zero and time delay. Asia-Pacific Journal of Chemical Engineering 1 (1-2), 63–69.

Skogestad, S., 2000. Plantwide control: The search for the self-optimizing control structure. Journal of Process Control 10, 487–507.

Skogestad, S., 2009. Chemical and Energy Process Engineering. CRC Press.

Skogestad, S., Postlethwaite, I., 2005a. Multivariable feedback control - analysis and design, 2nd Edition. Wiley, Chichester.

Skogestad, S., Postlethwaite, I., 2005b. Multivariable Feedback Control: Analysis and Design. Wiley & Sons, Chichester, West Sussex, UK.

Srinivasan, B., Palanki, S., Bonvin, D., 2003. Dynamic optimization of batch processes: I. characterization of the nominal solution. Computers and Chemical Engineering 27, 1–26.

van de Ven, P. M., Hegde, N., Massoulié, L., Salonidis, T., 2012. Optimal control of end-user energy storage. CoRR abs/1203.1891.

Wilson, D., Robinett, R., Sep. 3 2013. Nonlinear power flow feedback control for improved stability and performance of airfoil sections. US Patent 8,527,247.
URL https://www.google.com/patents/US8527247

Wuhua Hu, Jianfeng Mao, G. X. V. K., 2012. Selection of self-optimizing controlled variables for dynamic processes. In: 8th IFAC Symposium on Advanced Control of Chemical Processes, Furama Riverfront, Singapore.

Würth, L., Hannemann, R., Marquardt, W., Sep. 2009. Neighboring-extremal updates for nonlinear model-predictive control and dynamic real-time optimization. Journal of Process Control 19 (8), 1277–1288.

Zavala, V. M., Biegler, L. T., Jan. 2009. The advanced-step NMPC controller: Optimality, stability and robustness. Automatica 45 (1), 86–93.

Zhou, D., Zhao, C., Tian, Y., 2012. Review on thermal energy storage with phase change materials (pcms) in building applications. Applied Energy 92 (0), 593 – 605.
URL http://www.sciencedirect.com/science/article/pii/S0306261911005216

Appendix A

Derivation of the alternative energy balance

The energy balance of the overall system is

$$\frac{dH}{dt} = H_{in} + H_{cw} - H_{hw} + Q - Q_{loss} \tag{A.1}$$

For sake of simplicity, we will use the notation $RHS \triangleq H_{in} + H_{cw} - H_{hw} + Q - Q_{loss}$ and $LHS \triangleq \frac{dH}{dt}$.

The left hand side can be expanded as

$$\frac{1}{\rho c_p} LHS = (T - T_{ref})\frac{dV}{dt} + V\frac{dT}{dt} \tag{A.2}$$

By adding and subtracting $(T_{cw}\frac{dV}{dt} + V\frac{dT_{cw}}{dt})$ to the right hand side of (A.2) we obtain

$$\frac{1}{\rho c_p} LHS = \underbrace{(T - T_{cw})\frac{dV}{dt} + V\frac{d(T - T_{cw})}{dt}}_{\frac{1}{\rho c_p} dE/dt} + (T_{cw} - T_{ref})\frac{dV}{dt} + V\frac{dT_{cw}}{dt} \tag{A.3}$$

The right hand side of (A.1) is written as

$$\frac{1}{\rho c_p}(RHS) = q_{in}(T_{cw} - T_{ref}) + q_{cw}(T_{cw} - T_{ref}) - q_{hw}(T_{cw} - T_{ref}) + \frac{Q - Q_{loss}}{\rho c_p} \tag{A.4}$$

Adding and subtracting $q_{hw}(T_{cw} - T_{ref})$ to the right hand side of (A.4), after some rearrangements yields

$$\frac{1}{\rho c_p}(RHS) = (T_{cw} - T_{ref})\overbrace{(q_{in} + q_{cw} - q_{hw})}^{dV/dt} - \overbrace{q_{hw}(T_{hw} - T_{cw})}^{Q_{\text{demand}}/\rho c_p} + \frac{Q - Q_{loss}}{\rho c_p} \tag{A.5}$$

where we have introduced the mass balance:

$$\frac{dV}{dt} = q_{in} + q_{cw} - q_{hw} \tag{A.6}$$

Finally, be equating (A.5) and (A.3) we get the alternative form of the energy balance:

$$\frac{dE}{dt} = Q - Q_{\text{demand}} - Q_{loss} - \rho V c_p \frac{dT_{cw}}{dt} \tag{A.7}$$

Appendix B

Observer-based model reference design procedure

Open-loop dynamics

First step is to define the open-loop plan dynamics:

$$\begin{aligned} \dot{x}_p &= A_p x_p + B_p u \\ y_p &= C_p x_p, \quad z = C_{z,p} x_p \end{aligned} \tag{B.1}$$

where $A_p \in R^{n_p \times n_p}$, $B_p \in R^{n_p \times n_u}$, $C_p \in R^{n_y \times n_p}$ and $C_{z,p} \in R^{n_u \times n_p}$ are known matrices. y_p are the measured outputs and z are the regulated outputs. Next, we augment the state vector x to include the integral of the control error $e = z_{sp} - z$ and form the extended model

$$\begin{aligned} \dot{x} &= Ax + Bu + B_{sp} z_{sp} \\ y_m &= Cx, \quad z = C_z x \end{aligned} \tag{B.2}$$

where

$$x = \begin{bmatrix} \int e \\ x_p \end{bmatrix}, \quad C = \begin{bmatrix} I_{m \times m} & C_p \end{bmatrix}, \quad C_z = \begin{bmatrix} 0_{m \times m} & C_{z,p} \end{bmatrix} \tag{B.3}$$

$$A = \begin{bmatrix} 0_{m \times m} & -C_{z,p} \\ 0_{n_p \times m} & A_p \end{bmatrix}, \quad B = \begin{bmatrix} 0_{m \times m} \\ B_p \end{bmatrix}, \quad B_{sp} = \begin{bmatrix} I_{m \times m} \\ 0_{n_p \times m} \end{bmatrix} \tag{B.4}$$

The main requirement here is to have $\dim(y_m) > \dim(u)$. In addition, we must restrict the pair (A, B) to be controllable and the (A, C) to be observable.

Reference dynamics based on state feedback

Based on the extended dynamics we proceed to design a linear quadratic regulator (LQR) controller and form the desired closed-loop dynamics. The LQR design entails choosing weighting matrices (Q, R) and solving the algebraic Riccati equation

$$PA + A^T P + Q - PB^{-1}B^T P = 0 \tag{B.5}$$

to finally obtain the optimal state feedback gain $K_{lqr} = R^{-1}B^T P$. The LQR design step should include a trade study where robustness, performance and actuator constraints are well balanced. From the achieved state feedback design we form the closed-loop reference dynamics

$$\dot{x}_{ref} = \underbrace{A - BK_{lqr}^T}_{A_{ref}} x_{ref} + B_{sp} z_{sp} \tag{B.6}$$

Observer-based reference model design

Our observer-based reference model is defined by

$$\begin{aligned} \dot{x}_{ref} &= A_{ref} x_{ref} + L_v(y - y_{ref}) + B_{sp} z_{sp} \\ z_{ref} &= C_z x_{ref} \end{aligned} \tag{B.7}$$

The observer gain L_v is given by

$$L_v = P_v C^T R_v^{-1} \tag{B.8}$$

where P_v is the solution to the Riccati equation

$$P_v A^T + A P_v + Q - P_v C^T R_v^{-1} C P_v + Q_v = 0 \tag{B.9}$$

The process and measurement noise covariance matrices are parametrized using a positive scalar v:

$$Q_v = Q_0 + \left(\frac{v+1}{v}\right)\bar{B}\bar{B}^T, \quad R_v = \frac{v}{v+1}R_0 \tag{B.10}$$

where $\bar{B}$ is a matrix formed by adding "fictitious" columns to B, to make $\bar{B} = \begin{bmatrix} B & X \end{bmatrix}$ (this is called 'square-up step') have its column rank equal to the row rank of C, such that $C\bar{B}$ becomes invertible and the corresponding extended system $C(sI - A)^{-1}\bar{B}$ is minimum phase. and letting $v \to 0$ we can show that the system asymptotically approaches strict positive realness (SPR), which is a highly desired property.

Squaring-up and transmission zero placement

The effect of the matrix Q_v is to shape the zeros of the feedback loop. In fact, the observer transmission zeros are defined by

$$C(sI - A)^{-1}L \tag{B.11}$$

where $Q_v = L^T L$. Placing the zeros in a desirable location is key to achieving a robust design because the eigenvalues of the observer $\lambda(A - L_v C)$ will approach the observers finite zeros as $v \to 0$.

Misra (1992) showed that squaring-up problem can be transformed into a state feedback problem in which we may place the transmission zeros at desired locations. The idea is outlined in the following. Assume the original system (A, B, C) has been transformed by means of orthogonal state coordinate transformed to the form:

$$R(\lambda) = \begin{bmatrix} A_{11} - \lambda I_{n_y} & A_{12} & B_{11} \\ A_{21} & A_{22} - \lambda I_{n_x - n_y} & B_{21} \\ C_1 & 0 & 0_{n_y \times n_u} \end{bmatrix} \tag{B.12}$$

We would like to add columns to B to square the plant up.

$$R(\lambda) = \begin{bmatrix} A_{11} - \lambda I_{n_y} & A_{12} & B_{11} & \hat{B}_{12} \\ A_{21} & A_{22} - \lambda I_{n_x - n_y} & B_{21} & \hat{B}_{22} \\ C_1 & 0 & & 0_{n_y \times n_y} \end{bmatrix} \tag{B.13}$$

Defining $B_1 = \begin{bmatrix} B_{11} & \hat{B}_{12} \end{bmatrix}_{n_y \times n_y}$ and $B_2 = \begin{bmatrix} B_{21} & \hat{B}_{22} \end{bmatrix}$ it can be shown that the rank of the Rosenbrock matrix $R(\lambda)$ is

$$rank(R(\lambda)) = 2n_y + rank(\lambda I_{n_x - n_y} - A_{22}^T + A_{12}^T B_1^{-T} B_2^T) \tag{B.14}$$

where we see that the matrix $R(\lambda)$ loses rank at all the eigenvalues of $A_{22}^T - A_{12}^T B_1^{-T} B_2^T$ and thus are transmission zeros of the original system. Therefore, the problem reduces to finding B_1 and B_2 such that $A_{22}^T - A_{12}^T B_1^{-T} B_2^T$ has desired eigenvalues. LQR or pole placement techniques are readily available to solve such problem.

Appendix C

Robustification of adaptive laws

Dead-zone modification

To improve robustness of adaptive laws in the presence of unmatched disturbance such as process and measurement noise dead-zone modification is advised. The idea is to stop the adaptation process when the norm of the observation error $e_y = y_m - \hat{y}$ is small. This will prevent the adaptive parameters from drifting due to noise. Let Θ be the adaptive parameter and assume for simplicity an adaptive law in the form

$$\dot{\Theta} = \Gamma_\Theta \Phi(x) e_y F \tag{C.1}$$

where F is a constant matrix, $\Phi(x)$ is a known regressor and Γ_Θ is the adaptation gain. The modified adaptive law using dead-zone is

$$\dot{\Theta} = \begin{cases} \Gamma_\Theta \Phi(x) e_y F, & \text{if} \quad \|e_y\| > e_0 \\ 0, & \text{if} \quad \|e_y\| \leq e_0 \end{cases} \tag{C.2}$$

This dead-zone modification however is not Lipschitz and it may cause undesirable effects such as chattering when the error is near the dead-zone boundary. A smooth version of the dead-zone is then used. Choosing a constant $0 < \delta < 1$ we construct a modulation function in the form

$$\mu(\|e_y\|) = \max\left(0, \min\left(1, \frac{\|e_y\| - \delta e_0}{(1-\delta)e_0}\right)\right) \tag{C.3}$$

The adaptive law becomes

$$\dot{\Theta} = \Gamma_\Theta \Phi(x) \mu(\|e_y\|) e_y F \tag{C.4}$$

The projection operator

The projection operator is essential to achieve robustness against parametric and nonparametric uncertainty and to ensure boundedness of adaptive parameters. The projection operator is defined as

$$\text{Proj}(\theta, y) = \begin{cases} y - \frac{\nabla f (\nabla f)^T}{(\nabla f)^T I \nabla f} y f, & \text{if}[f > 0 \text{ and } (y^T \nabla f) > 0] \\ y, & \text{otherwise} \end{cases} \tag{C.5}$$

where f is a convex function of the form

$$f(\theta) = \frac{(1+\epsilon)\|\theta\|^2 - \theta_{max}^2}{\epsilon \theta_{max}^2} \tag{C.6}$$

with θ_{max} being the bound for the parameter θ and ϵ the projection tolerance. Note that

$$f(\theta) \leq 0 \qquad \text{if } \|\theta\| \leq \frac{\theta_{max}}{\sqrt{1+\epsilon}} \tag{C.7}$$

$$f(\theta) \leq 1 \qquad \text{if } \|\theta\| \leq \theta_{max} \tag{C.8}$$

Thus, by defining the parameter dynamics as

$$\dot{\theta} = \text{Proj}(\theta, y) \tag{C.9}$$

we can ensure $\|\theta\| \leq \theta_{max}$ is always true as long as θ initially lies within tighter bounds defined by $\frac{\theta_{max}}{\sqrt{1+\epsilon}}$. The projection operator does not alter the vector field y if $\|\theta\| \leq \frac{\theta_{max}}{\sqrt{1+\epsilon}}$. For $\frac{\theta_{max}}{\sqrt{1+\epsilon}} \leq \|\theta\| \leq \theta_{max}$ the projection operator results in a smooth transformation that ensures boundedness of the parameters.

The adaptive laws that are implemented in practice should always include both modifications: smooth dead-zone and projection operator. The resulting adaptive law takes the form

$$\dot{\Theta} = \text{Proj}(\Theta, \Gamma_\Theta \Phi(x) \mu(\|e_y\|) e_y F) \tag{C.10}$$

Additional details and information regarding other modifications be found in Lavretsky and Wise (2013).